STRUCTURAL AND FUNCTIONAL CHARACTERISATION OF APOPTOTIC CELL-DERIVED EXTRACELLULAR VESICLES

Annaïg Jeanne Orlane Rozo

Doctor of Philosophy

Aston University

September 2022

This project has received funding from the EU'S Horizon 2020 research and innovation programme under MSC grant agreement N°847419.

Abstract

Persistent and uncontrolled inflammation promotes the development of numerous chronic pathologies. During efferocytosis, apoptotic cells (AC) are recognized and engulfed by professional phagocytes. This phagocytic event is guided by the release of “find-me” signals creating a chemotactic gradient that aids the recruitment of macrophages. AC also release extracellular vesicles (ACdEVs) in the environment, and although this subset of EVs has not yet been extensively characterized, evidence highlights their role as key mediators of efferocytosis. This study aims to understand the complex mechanisms of the resolution of inflammation mediated by ACdEVs.

AC (UV induced) were shown to continuously release highly heterogeneous EVs, as observed by their various structures/shapes (Cryo-TEM), and polydisperse size distribution (resistive pulse sensing). ACdEVs were shown to have a similar membrane fluidity as their parent cells as measured by laurdan fluorescence. Interestingly, comparing early and late ACdEVs revealed differences in lipid composition, which may reflect different biogenesis pathways. ACdEVs samples depleted of soluble factors lose the ability to recruit macrophages whereas their uptake remained unchanged. Depleting the membrane of cholesterol resulted in an increased membrane rigidity and surface charges which was found to promote the ACdEVs uptake. Early and late apoptosis timepoints were defined by the kinetic study of UV-induced apoptosis as 6h and 18h, respectively. Early ACdEVs were more efficiently engulfed but less chemo attractive than the late ACdEVs, which may result in different immunomodulatory functions. The characterization of EV subtypes in different contexts is extremely challenging. Here, an alternative passive microfluidic method was shown to continuously separate EVs (above 500 nm) based on their size, while retaining soluble factors.

Altogether, these data suggest that ACdEVs are complex mediators of efferocytosis and also highlights the importance of eat-me and find-me signals in ACdEV’s functions. Lipidomics should support a new and fundamental way of discriminating between different EV subtypes and, indeed, the lipid composition of the membrane is likely vital in tuning the activity of these subtypes.

Keywords: *Extracellular vesicles, apoptosis, ACdEV, inflammation, efferocytosis, microfluidics*

Acknowledgments

Personal acknowledgements

I would like to dedicate this work to my family, especially my mom and dad. You have always been very supportive of me throughout my studies, even if we are far away you have helped immensely, and I will not be where I am now if it wasn't for you. To my brothers also, for your love and support, you may now only call me by my title: Dr.

To my other half Mark, for always being there for me through all the ups and downs of this PhD. You have always shared my excitements when I had good results, without understanding what it is that I really do. Thank you for keeping me motivated when I had doubts, you truly made my PhD a much better experience. I can not mention Mark, without mentioning his family and especially Carol and Ian for your love and support, it did not go unnoticed.

Finally, I would like to dedicate this work to all my friends, near or far. To all the good and the bad times that we shared and to all the memories that we yet have to make, cheers ! Thank you all (Marie, Millie, Lauren, Gwendoline, Julien, Daniel, Luke, Leah, Raine, Sam, Heather, Elliott, Cristina, and more).

Professional acknowledgments

First of all, I would like to thank my main supervisor Dr. Alan Goddard for his continuous support and guidance throughout my PhD, and especially during the pandemic. You have showed me that research can be challenging but the "good science days" make it all worth it! Thank you for sharing your enthusiasm and knowledge, I will be forever grateful for this opportunity.

To my co supervisor Prof. Andrew Devitt and his lab, for their training and guidance on EV related matters. A special thanks to Rachel for your help and friendship, I only wish you started sooner!

To Alexis, I would not want to think what these past three years would have been like without you. I am so grateful for our friendship and to have had this insane opportunity to do a PhD with you, sharing the same lab and office. Thank you for everything.

To Peer, Afroditi, Thanos, and Ellen for being the first friendly faces I met at the start of my PhD and for the three years of friendship that followed. I would also like to acknowledge the second MemTrain cohort. To the lab MB 331 for making such a great work environment as well as the AMPL team for all the support and constructive feedback.

We acknowledge Dr Saiska Bakker and the university of Warwick Advanced Bioimaging Research Technology Platform supported by BBSRC ALERT14 award BB/M01228X/1, for the use of the Jeol 2200FS/DiSPIM/Cryo-ultramicrotome. I am grateful for Dr Megan Cox and Meritics Ltd for the use of the nCS1 supported by a Knowledge Transfer Partnership between Aston University and Meritics Ltd (KTP 11605). My industrial partner uFraction8, and more specifically Brian Miller and Monika Tomecka, for providing me with the microfluidic chips and HPLC pumps.

List of figures and tables

List of figures

Unless stated otherwise, figures were made using BioRender.com.

List of Tables

List of abbreviations

AA	Arachidonic Acid
AC	Apoptotic Cell
ACdEV	Apoptotic Cell-Derived Extracellular Vesicle
APAF1	Apoptotic Peptidase Activating Factor 1
APC	Antigen Presenting Cell
ApoBD	Apoptotic Body
ApoMV	Apoptotic Microvesicle
AnV	Annexin V
BCL	B Cell Lymphoma
bFGF	Basic Fibroblast Growth Factor
BODIPY	BoronDipyrromethene
BSA	Bovine Serum Albumin
CDE	Clathrin Dependent Endocytosis
CIE	Clathrin Independent Endocytosis
DC	Dendritic Cell
DUFA	Diunsaturated Fatty Acid
DLS	Dynamic Light Scattering
ECM	Extracellular Matrix
ESCRT	Endosomal Sorting Complex Required for Transport
EV	Extracellular Vesicle
EVs	Extracellular Vesicles

EXO	Exosome
FA	Fatty Acid
FADD	Fas-Associated Death Domain
FCM	Flow Cytometry/Cytometer
GF	Growth Factor
GP	Generalized Polarisation
HR-FCM	High Resolution - FCM
IL	Interleukin
ILM	Interferometric Light Microscopy
ILV	Intraluminal Vesicle
LBPA	Lysobisphosphatidic Acid
LO	Large Outlet
LOC	Lab-On-A-Chip
LT	Leukotriene
MFI	Mean Fluorescence Intensity
MHC	Major Histocompatibility Complex
MMP	Matrix Metallo Proteinase
MOMP	Mitochondrial Outer Membrane Permeabilization
MPD	Mean Particle Diameter
mRNA	Messenger RNA
MRPS	Microfluidic Resistive Pulse Sensing
MUFA	Monounsaturated Fatty Acid
MV	Microvesicle

MVB	Multivesicular Bodies
NSAID	Non-Steroidal Anti-Inflammatory Drug
NTA	Nanoparticle Tracking Analysis
PBS	Phosphate Buffer Solution
PDGF	Platelet-Derived Growth Factor
PEG	Polyethylene Glycol
PES	Polyethersulfone
PG	Prostaglandin
PI	Propidium Iodide
PMMA	Polymethyl Methacrylate
POPC	1-Palmitoyl-2-Oleoyl-sn-Glycero-3-Phosphocholine
PRR	Pattern Recognition Receptors
PS	Phosphatidylserine
PSD	Particle Size Distribution
PUFA	Polyunsaturated Fatty Acid
RNA	Ribonucleic Acid
SEC	Size Exclusion Chromatography
SFA	Saturated Fatty Acid
SO	Small Outlet
TGF	Transforming Growth Factor
TNF	Tumour Necrosis Factor
TNFR	Tumour Necrosis Factor Receptor
TRAIL	Tumour Necrosis Factor-related Apoptosis-Inducing Ligand

tRNA	Total RNA
TRPS	Tunable Resistive Pulse Sensing
UC	Ultracentrifugation
VD3	Vitamin D3
VEGF	Vascular Endothelial Growth Factor

Table of content

1. Introduction

1.1 Inflammation

Descriptions of inflammation date back to the ancient Egyptian and Greek cultures with terms like Edema. The four cardinal signs of inflammation, still relevant to this day, were introduced by Aulus Cornelius Celsus in the first century AD: redness (rubor), pain (dolor), heat (calor), and swelling (tumour) (Granger and Senchenkova, 2010). Over the centuries, advances in technologies allowed scientists to investigate the inflammatory response in more depth.

Inflammation is now referred to as a complex and coordinated biological protective response against pathogens, damaged cells, injury, and other trauma. It consists in a vascular and cellular response. During the **short-term acute** response, many mediators of the immune response will work to restore a physiological state, such as endothelial cells, immune cells, fibroblasts, soluble factors, etc. An immune system out of balance can cause a **long-lasting chronic** inflammation that can lead to severe inflammatory disorders.

1.1.1 Acute Inflammation

When a tissue injury occurs, resident cells (tissue macrophages, dendritic cells and epithelial cells), through pattern recognition receptors (PRRs), recognize damage/pathogen-associated molecular patterns (D/PAMP) derived from damaged cells or pathogens (Takeuchi and Akira, 2010). This leads to the rapid production and secretion of soluble pro-inflammatory factors, also known as cytokines, that will stimulate the migration and recruitment of leukocytes. These include interleukin (IL)-1α, IL-1β, IL-6, IL-8, tumour necrosis factor (TNF)-α, platelet-derived growth factor (PDGF) and transforming growth factor (TGF)-β (Zhang and An, 2007).

Chemical mediators such as amines, peptides, and eicosanoids are also released by immune cells. Amines include histamine and serotonin, peptides include bradykinin, whereas eicosanoids include prostaglandins (PGs), leukotrienes (LTs), and thromboxanes. These vasoactive mediators target local vascular endothelial cells promoting vascular permeability and a decreased blood flow (**Figure 1.1.a**) (Abdulkhaleq *et al.*, 2018). This facilitates the extravasation of recruited leukocytes to the site of infection/injury by allowing them to bind to specific adhesion molecules (selectins and integrins) on endothelial cells surfaces (van Steen *et al.*, 2020).

Neutrophils are the first to be recruited to the inflamed tissue. They secrete proteolytic enzymes such as serine proteases and matrix metalloproteinases (MMP) -2 and –9 that break down nonhealthy tissue. Additionally, they phagocytose extracellular matrix (ECM) debris (Xue and Jackson, 2015) (**Figure 1.1.b**).

Following neutrophils, monocytes are the next to infiltrate the site of injury. Blood circulating monocytes extravasate into the inflamed tissue through rolling, adhesion and transmigration of the endothelial cells (Ley et al., 2007). Once in the tissue, monocytes then mature into active M1 macrophages where they will ingest apoptotic neutrophils and remaining debris (**Figure 1.1.c)** (Yang et al., 2014). Due to their own production of nitric oxide (NO), M1 macrophages undergo cell death, resulting in an increase of resolution-phase M2 like macrophages (Mills, 2012). In more details, NO production results in oxidative stress which eventually lead to irreversible cellular damages and cell death. M2 macrophages produce and release anti-inflammatory cytokines and growth factors (GF) that will inhibit neutrophil migration and tissue infiltration, including TGF-α, TGF-β, basic fibroblast growth factor (bFGF), PDGF, and vascular endothelial growth factor (VEGF). These soluble mediators will also recruit and activate fibroblasts and endothelial cells for tissue proliferation and repair (**Figure 1.1.d**) (Watanabe et al., 2019). When the stable physiological equilibrium has been restored, both tissue resident- and monocyte-derive macrophages maintain an M2-like phenotype and stay in the tissue, possibly becoming trained memory macrophages, or exit the tissue through the lymphatic system (**Figure 1.1.e**) (Italiani and Boraschi, 2014).

It should be noted that macrophages exhibit a complex plasticity depending on the environmental cues. Here, M1 and M2 represent a simplified taxonomy of two extreme macrophages activation states (Sica and Mantovani, 2012; Xue *et al.*, 2014).

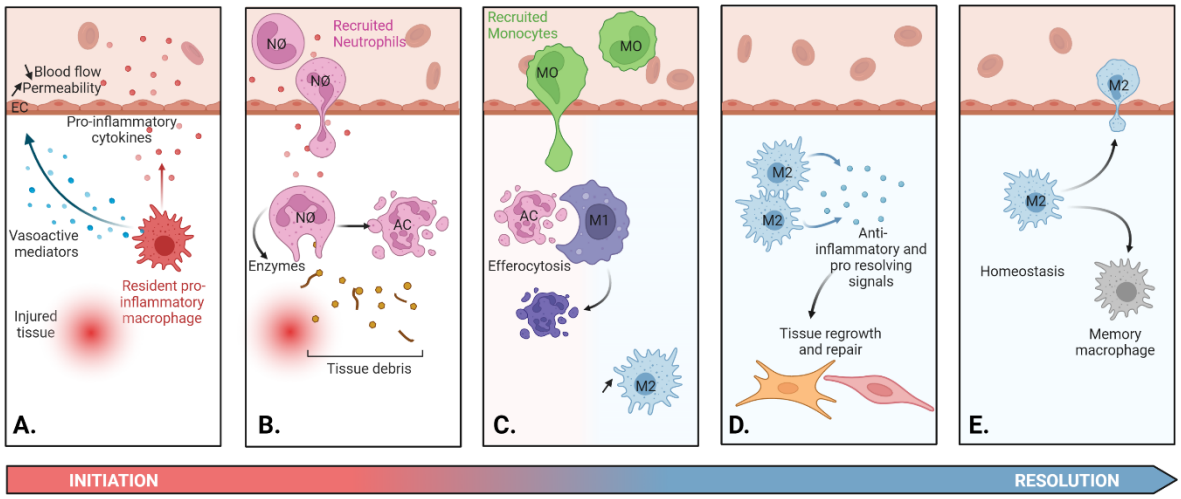

Figure 1.1: Summary of the mediators involved in the resolution of the inflammatory response. ***(a)*** *Tissue injury leads to the release of vasoactive mediators that promote the dilatation and increase the leakiness of blood vessels.* ***(b)*** *Pro-inflammatory cytokines recruit leukocytes to the site of injury that phagocytose pathogens, damaged cells and debris.* ***(c)*** *Recruited monocytes differentiate into M1 inflammatory MØ that engulf apoptotic leukocytes. Surviving M1 MØ eventually die due to their own NO production, increasing the level of M2 MØ.* ***(d)*** *Pro-resolving M2 MØ stimulate tissue regrowth and repair to return to the state of homeostasis.* ***(e)*** *M2 MØ then either exit or stay in the tissue as a M2-like resident MØ or memory MØ. NØ: Neutrophils; EC: Endothelial cell; AC: Apoptotic Cell; MO: Monocyte; MØ: Macrophage.*

Due to the complexity and the number of mediators involved in the inflammatory response, various imbalances or defects can lead to a long lasting excessive or deficient immune response known as chronic inflammation.

1.1.2 Chronic inflammation

Long lasting inflammation or chronic inflammation can last for months up to several years (Pahwa, Goyal and Jialal, 2022). This long-term response is caused by the immune system failure to restore tissue homeostasis following acute inflammation caused by an infection, injury, etc. Additionally, chronic inflammation can be caused by autoimmune disorders which consist in immune cells attacking healthy tissues/cells (rheumatoid arthritis, systemic lupus erythematosus), and long-term exposure to chemical irritants (silica dust) (Furman *et al.*, 2019). Chronic inflammation can lead to severe tissue damages and remodelling, promoting

cell mutation and proliferation. This harmful environment is prone to many pathologies such as, but not limited to: cardiovascular diseases (Mozos *et al.*, 2017; Qi, Yang and Zhang, 2017), development and progression of cancer (Singh and Baby, 2019), diabetes (Clark, Kroger and Tisch, 2017; Purohit *et al.*, 2018), arthritis, Alzheimer's disease, autoimmune diseases and pulmonary diseases (Vroman, Hendriks and Kool, 2017) (**Figure 1.2**).

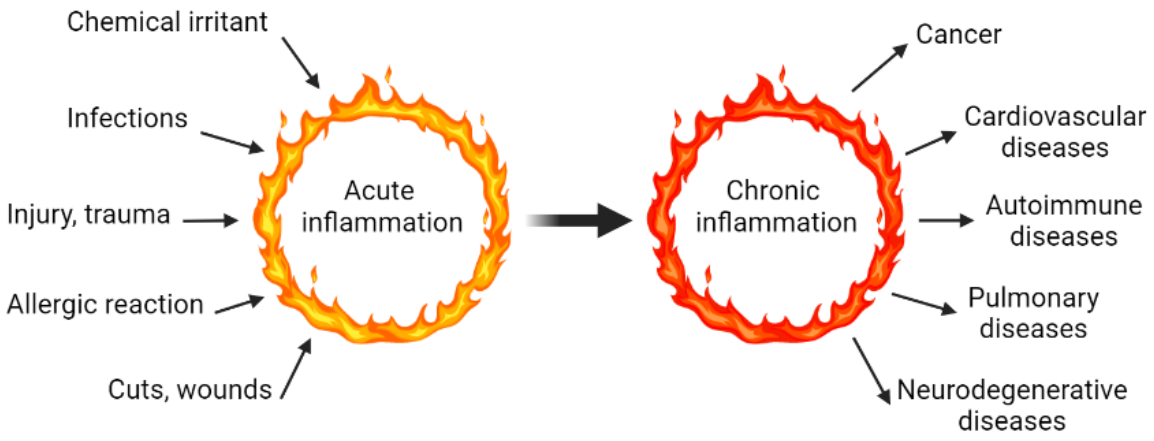

Figure 1.2: Overview of causes and consequences of acute and chronic inflammation. *Acute inflammation is caused by exogeneous inflammogens, and if prolonged, leads to chronic inflammation and numerous pathologies.*

1.1.3 Inhibition of pro-inflammatory signalling

The first treatment against fever and inflammation was discovered by the Greek physician Hippocrates who used an extract of willow tree, about 3,500 years ago. The active compound of this extract was then identified as salicylic acid in the 17th century and led to the commercialization of aspirin in 1869. Since then, not much improvement has been made to the anti-inflammatory drug discovery development. Anti-inflammatory drugs still work in a very similar way by targeting the eicosanoids synthesis pathway such as cyclooxygenase, lipoxygenase, and corticoid receptor (**Figure 1.3**).

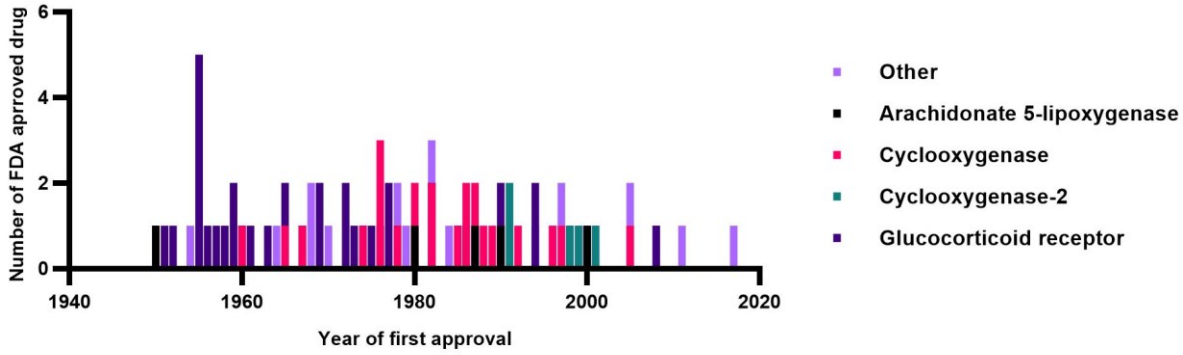

Figure 1.3: Anti-inflammatory drug targets over the years. *Data originated from chEMBL online database. Graph shows the number of food and drug administration (FDA)-approved drugs to treat inflammation from 1940 to 2020.*

Eicosanoid synthesis pathways, such as those of prostaglandins (PGs) and leukotrienes (LTs), generate key inflammatory mediators and are thus of great interest in the development of anti-inflammatory drugs (**Figure 1.4**). Indeed, PGs and LTs promote vascular permeability and leukocytes accumulation. Activated by an inflammatory stimulus, a 20-carbon fatty acid with four double bonds e.g., arachidonic acid (AA), gets released from the plasma membrane by the action of phospholipase A2 (PLA-2). AA can then get oxygenated by cyclooxygenase (COX) and lipoxygenase (LOX) enzymes to generate PGs and LTs. PGE2 is a crucial inflammatory mediator, and reducing its level using up-stream targets of its biosynthetic pathway has been extensively explored over the years by either inhibiting PLA-2 using corticosteroids, or by inhibiting COX-1 and COX-2 using non-steroidal anti-inflammatory drugs (NSAIDs). Corticosteroids and NSAIDs drugs (such as aspirin), have been widely used to manage inflammation. Additionally, LOX inhibitors and COX/LOX dual inhibitors drugs have been developed to target LTs formed via the 5-lipoxygenase pathway. However, these drugs can cause side effects such as gastrointestinal toxicity, hematologic toxicity, and nephrotoxicity; and do not target the inflammatory stimulus.

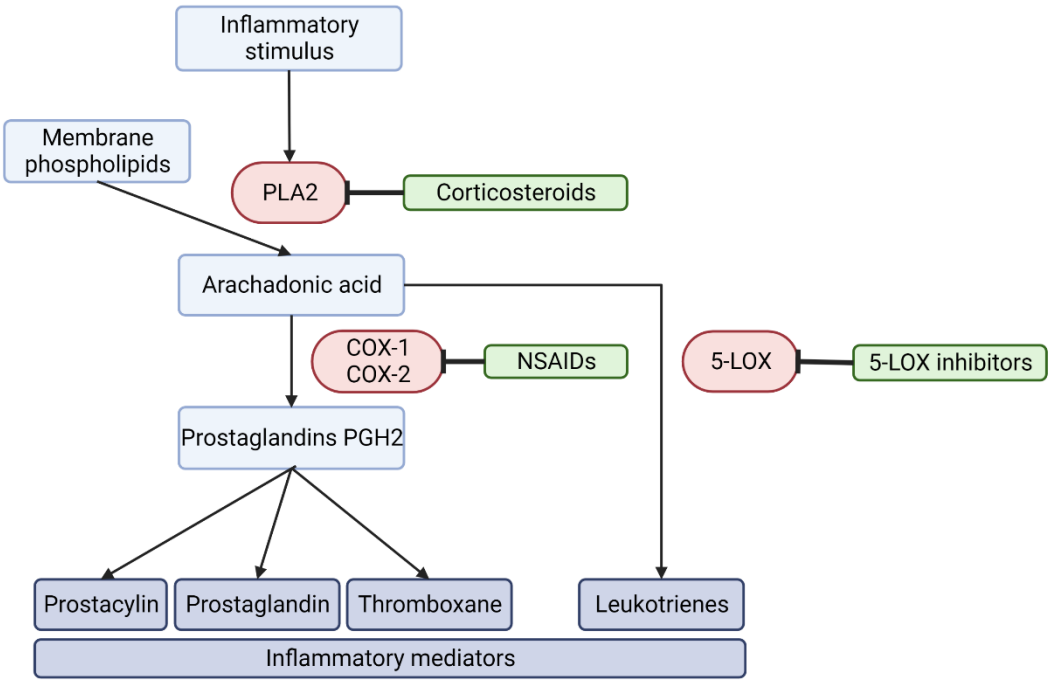

Figure 1.4: Overview of the cyclooxygenase and lipoxygenase pathways of the arachidonate cascade and current anti-inflammatory targets. *Red boxes represent the targeted enzymes: Phospholipase A2 (PLA2), Cyclooxygenase-1 and -2 (COX-1 and COX-2), and 5-Lipooxygenase (5-LOX). Green boxes represent the main three inflammatory drugs: corticosteroids, non-steroidal anti-inflammatory drugs (NSAIDs), and 5-LOX inhibitors.*

Recently, more disease modifying drugs have been developed such as immune cell anti-proliferative, anti-inflammatory cytokines, or inflammasomes inhibitors (Dinarello, 2013). Nevertheless, as inflammation is crucial for our everyday survival by protecting ourselves from pathogens, research should focus on immunoresolvent therapies instead of immunosuppressive therapies. Indeed, improving the understanding of the mechanisms that control the resolution of inflammation and the role of pro resolving mediators will undoubtably lead to important breakthrough in the treatment of various diseases.

Specialized pro resolving mediators (SPMs) are derived from n-3 (omega-3) long chain poly-unsaturated fatty acids (n-3PUFA) and produced across various cell types (Serhan, Chiang and Van Dyke, 2008). SPMs comprise resolvins, protectins, maresins, and lipoxins (Serhan and Levy, 2018). SPMs are active mediators of the resolution of inflammation and play important roles in the downregulation of pro inflammatory mediators, the promotion of

efferocytosis, the clearance of pathogens, the inhibition of neutrophils infiltration, and the increase of the M2 macrophage's pool.

Even though chronic inflammation has multifactorial causes, using a computational modelling approach, it was shown that the main critical factor was the macrophages influx and efflux rates (Nagaraja *et al.*, 2014). Indeed, macrophages play a significant role in the resolution of inflammation by phagocyting apoptotic immune cells in the inflamed tissue, also known as efferocytosis.

1.2 Resolving acute inflammation: Efferocytosis

Apoptosis plays an important role in regulating the inflammatory response (Yang *et al.*, 2015). Following the initial elimination of inflammogens, neutrophils undergo apoptosis. Efferocytosis is the controlled recognition and removal of apoptotic cells by macrophages. This anti-inflammatory mechanism occurs in three steps: the sensing of apoptotic cells, the recognition of eat-me / keep-out signals, and finally its engulfment. Efficient efferocytosis prevents apoptotic neutrophils from undergoing secondary necrosis further releasing toxic DAMPs in the surrounding tissue, as well as promoting a pro-resolving phenotype in efferocytotic macrophages. Subsequently, efferocytosis is a key step of the resolution of inflammation.

1.2.1 Cell death

The Nomenclature Committee on Cell Death (NCCD) has unveiled and classified multiple types of cell death over the past decades from which three different forms emerge: apoptosis (Type I), autophagy (Type II), and necrosis (Type III) (Galluzzi *et al.*, 2018).

Type I cell death or apoptosis, first observed by Carl Vogt in 1842 (Vogt, C. and Vogt, 1842), is a type of controlled programmed cell death necessary for the growth and development of any organism as well as the maintenance of tissue homeostasis (Ke *et al.*, 2018). It is different from senescence which is the biological process of ageing where the cells stop dividing but do not die, and to necrosis which is a traumatic version of cell death. Major hallmarks of apoptosis include membrane blebbing, cell shrinkage, nuclear fragmentation, chromatin condensation, DNA fragmentation and mRNA decay (Saraste and Pulkki, 2000; Gheibi Hayat *et al.*, 2019). There are two major pathways leading to apoptosis: the extrinsic and the intrinsic pathways (**Figure 1.5**). Ultimately, both pathways converge towards the activation of

caspases (serine proteases) that cleave critical cellular components such as polymerases and lamins leading to morphological changes observed during cell death (M. COHEN, 1997).

The extrinsic pathway is initiated by the binding of a death ligand, commonly Fas and tumour necrosis factor-related apoptosis-inducing ligand (TRAIL), to a TNFR family death receptor. This leads to conformational changes in the intracellular death domain of the receptor, activating the Fas-associated death domain (FADD) protein. Activated FADD will then cleave the pro-caspases-8 and -10 resulting in their activation and cleavage of the effectors caspases-3 and -7.

The intrinsic pathway, occurring in UV-induced apoptosis, can be caused by stress or damage to the cell (genotoxic damage, hypoxia, metabolic and ER stress, and other cytotoxic cues), and is mediated by the irreversible mitochondrial outer membrane permeabilization (MOMP). MOMP is controlled by apoptotic regulators part of the B-cell lymphoma (BCL)-2 protein family (Singh, Letai and Sarosiek, 2020), which can be either pro- or anti- apoptotic proteins. In the intrinsic signalling cascade, pro-apoptotic members of the BCL-2 family, also known as BH3-only proteins, are activated in response to stress signalling (Pihán, Carreras-Sureda and Hetz, 2017) (Bouillet *et al.*, 2002). These includes BAX and BAK, that switch the equilibrium against anti-apoptotic proteins (BCL-2, BCL-X, MCL-1) towards apoptosis (Czabotar, Lessene and Strasser, 2014). BH3-only proteins are responsible for the pore's formation in the mitochondrial outer membrane leading to the release of cytochrome *c* into the cytoplasm (Shamas-Din *et al.*, 2013; Aluvila *et al.*, 2014; Salvador-Gallego *et al.*, 2016). Together with apoptotic peptidase activating factor 1 (APAF1), these apoptotic signalling molecules will assemble to form the apoptosome complex, whose role is to cleave and activate the pro caspase-9, in terms activating the effectors caspase-3 and -7 (Li *et al.*, 1997).

Both intrinsic and extrinsic pathways converge at the activation of pro-apoptotic molecules BAX and BAK. Indeed, in the extrinsic pathway, the proteolytic cleavage of BID into its truncated form tBID by both capase-8 and -10. tBID then acts as a BH3-only protein and mediate the BAX/BAK dependant MOMP (Li *et al.*, 1998). Ultimately, both extrinsic and intrinsic apoptotic pathways lead to cell death and the release of apoptotic vesicles, ACdEVs.

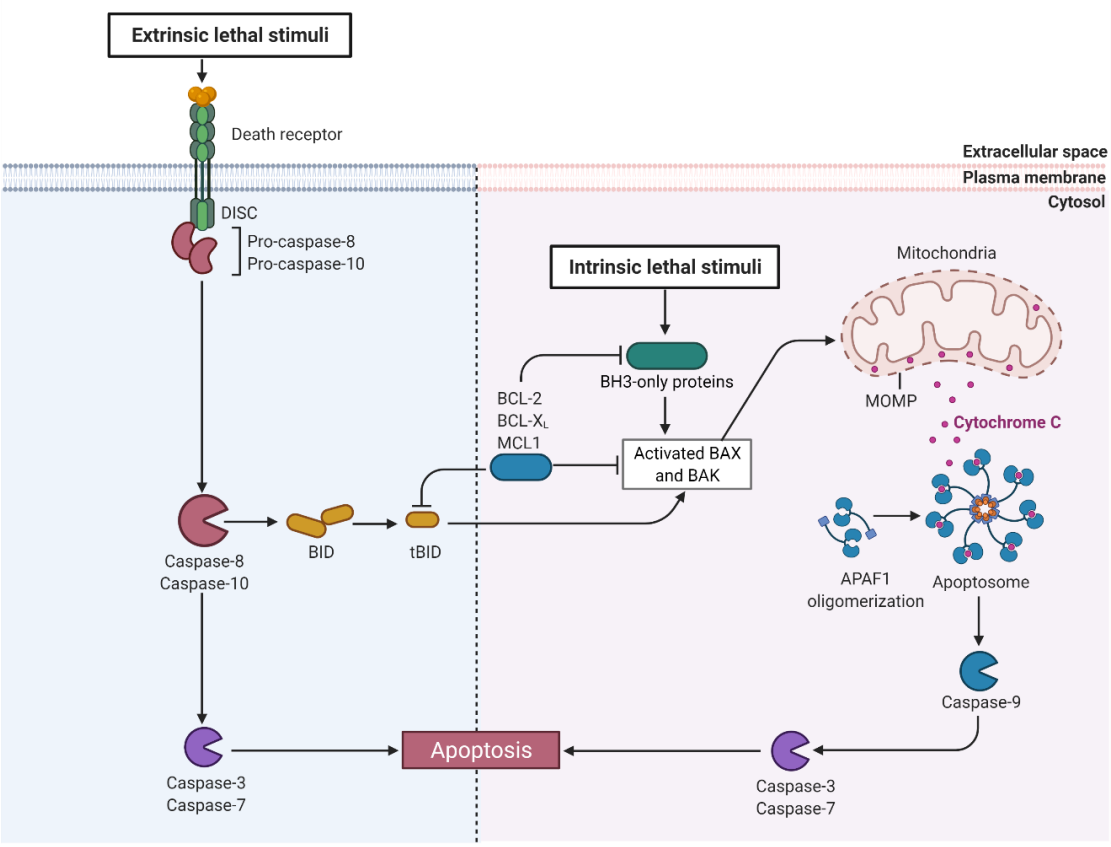

Figure 1.5: Overview of the apoptosis extrinsic and intrinsic pathways. *The extrinsic pathway is activated by an external lethal stimulus and leads to a signalling cascade. The intrinsic pathway is activated by an intrinsic lethal stimulus and is mainly characterized by mitochondrial outer membrane permeabilization (MOMP). Both processes result in the activation of the execution caspases-3 and -7.*

1.2.2 Macrophage recruitment to the site of cell death

For efferocytosis to be efficient, macrophages need to be rapidly mobilized to the site of cell death. During apoptosis, cells release a multitude of signals in the environment that form a chemotactic gradient, aiding macrophage's direction. Those signals are called "find-me" signals and include nucleotides, lipids, chemokines, and ACdEVs (**Figure 1.6**).

Adenosine triphosphate (ATP) and uridine-5′-triphosphate (UTP) are released in the extracellular environment through the plasma membrane channel pannexin 1 (PANX1), as an effector of caspase-3 and -7 (Chekeni *et al.*, 2010). Extracellular nucleotides interact with macrophages via the ATP/UTP receptor P2Y(2). However, the precise downstream signalling from P2Y(2) leading to the macrophage migration remains unknown. Interestingly, extracellular nucleotides can also upregulate the release of pro resolving factors (Köröskényi *et al.*, 2011; Lin, Niparko and Ferrucci, 2014).

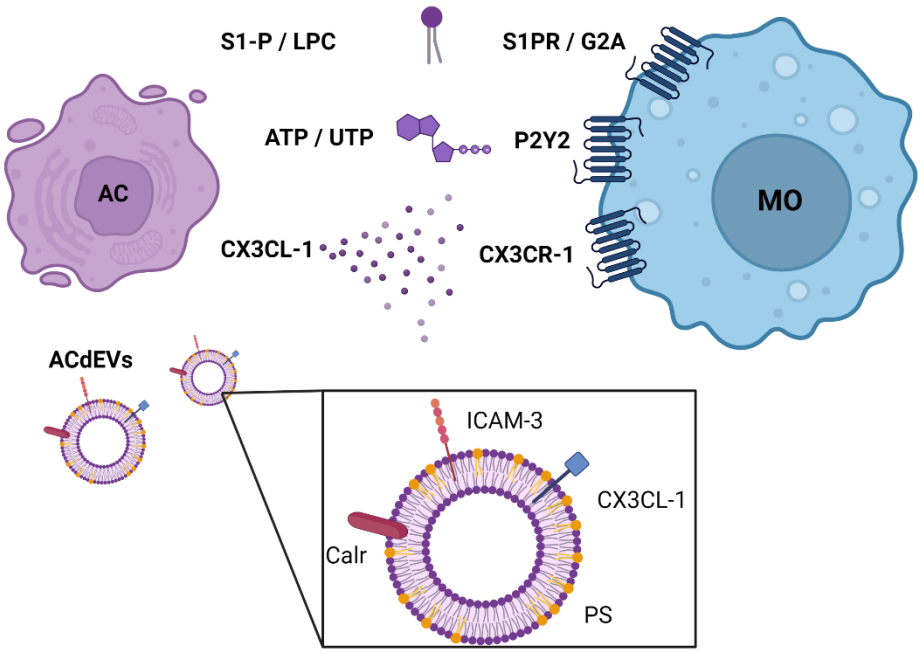

Figure 1.6: Apoptotic cells release find-me signals attracting macrophages. *Apoptotic cells (AC) release lipids (S1-P, LPC), nucleotides (ATP, UTP), chemokines (CX3CL-1), and ACdEVs. These soluble find me signals are recognized by macrophages (MO) through membrane receptors (S1PR, G2A, P2Y2, and CX3CR-1). Molecules involved in ACdEVs recognition by macrophages remain unknown.*

Lipid attraction signals include lyso-phosphatidylcholine (LPC), and sphingosine-1-phosphate (S1P) (Lauber *et al.*, 2003; Gude *et al.*, 2008). LPC is generated in a caspase 3 dependent manner, where upon activation of calcium independent phospholipase A2 (iPLA-2), plasma membrane PC is cleaved into two products: LPC and arachidonic acid. LPC engages with the G protein coupled receptor G2A on macrophages surfaces (Radu *et al.*, 2004). Additionally, S1P is produced and secreted by apoptotic cells upon upregulation of sphingosine kinases and is sensed by macrophages through the S1P receptor (S1PR). The C-X3-C motif chemokine ligand 1 (CX3CL1) chemokine was also identified as a find-me signal (Truman *et al.*, 2008). CX3CL1 stimulates the chemotaxis of CX3CR1 positive phagocytes. Furthermore, CX3CL1 – CX3CR1 signalling decreases pro inflammatory cytokines release.

The release of ACdEVs promotes apoptotic cell clearance by exhibiting chemo attractive properties (Segundo *et al.*, 1999). However, the identified molecules involved in ACdEVs mediated macrophages recruitment are limited. The adhesion molecule ICAM-3 was identified as one of these molecules. Indeed, ICAM-3 positive ACdEVs were found to be more efficient

at attracting macrophages than ICAM-3 negative ACdEVs (Torr *et al.*, 2012). ICAM-3 positive ACdEVs were also found to promote the chemoattraction of phagocytes (Torr *et al.*, 2012). Nevertheless, the interactions and signalling pathways behind ACdEVs mediated phagocyte's recruitment are poorly understood. Investigating the ACdEVs immunomodulatory functions is crucial to better characterize efferocytosis and the resolution of inflammation, which could lead to potential new therapeutic target for the treatment of inflammatory diseases.

Once nearby phagocytes have sensed the numerous soluble factors released during early apoptosis, the tethering of apoptotic cells begins. Interestingly, ACdEVs, in addition to acting as a find-me signal, also harbour eat-me signalling molecules. Those ACdEVs associated eat-me signals are also found on apoptotic cells surface suggesting that ACdEVs have the potential to be engulfed by professional phagocytes.

1.2.3 Viable and apoptotic cells discrimination

Interactions between eat-me or keep-out signals with macrophages are crucial for the discrimination of viable cells and apoptotic cells (**Figure 1.7**). Eat-me signals include ICAM-3, calreticulin, CX3CL1, phosphatidylserine (PS) and will induce the engulfment of the dying cells. Whereas keep-out signals include CD47 and CD31 and will promote the detachment from the viable cell.

PS is a negatively charged phospholipid composed of a hydrophobic tail (two fatty acids) and a hydrophilic head group (a glycerol and phosphate group to which is attached a serine residue). The increased PS exposure in the outer leaflet of the plasma is known as the main marker of apoptosis and a well characterized eat-me signal (Leventis and Grinstein, 2010; Segawa and Nagata, 2015). It is caused by the caspase-dependent inactivation of flippases and the activation of scramblase by caspases. Flippases comprise a family of proteins that translocate phospholipid, here PS, from the outer to the inner leaflet of the membrane (Sharom, 2011). Whereas the scramblase family comprises proteins that translocate phospholipids from the inner to the outer leaflet of the membrane (Suzuki et al., 2010; Brunner et al., 2014). During efferocytosis, PS is recognized by phagocytes through scavenger receptors either directly (TIM-4, BAI-1, stabilin) or indirectly (Gas-6, protein S, MFGEA) (Penberthy and Ravichandran, 2016). Additionally, there is evidence in the literature of the importance of PS in the clearance of certain viruses by macropinocytosis (Mercer and Helenius, 2008). The adhesion molecule ICAM-3, only expressed by leukocytes, was found to facilitate the synapsing and engulfing of apoptotic cells. This attachment could be mediated

by the binding of phagocytes CD14 to ICAM-3 (Ravichandran, 2010). However, ICAM-3 level decreases with time in apoptotic cells as it is loaded in ACdEVs. Another candidate “eat-me” signal is calreticulin (Calr). In ER-stress induced apoptotic cells, Calr is translocated from the ER membrane to the plasma membrane through exocytosis (Panaretakis et al., 2009). Calr is sensed by macrophages through low-density lipoprotein receptor LRP1 (Gardai et al., 2005). Additionally, Calr binds to C1q (Ogden et al., 2001), a component of the complement system that opsonizes pathogens to aid the immune response by acting like a molecular tag to facilitate their elimination by phagocytes. Membrane bound CX3CL-1 also play a role in the selective clearance of dying cells through interaction with CX2CR-1 receptor on macrophages surface.

While the binding to apoptotic cell ligands triggers the engulfment of the corpse, keep out signals repel phagocytes efferocytosis. Signals like CD47 and CD31 ensure that healthy cells are not wrongly engulfed by macrophages (Oldenborg, 2000). CD47 binds to SIRPα which causes a cytoskeletal rearrangements in macrophages downregulating phagocytosis (Oldenborg, Gresham and Lindberg, 2001). Apoptotic cells still display CD47 on their surface but at a much lower level which allows them to be phagocyted. Similarly, the binding of CD31 on viable cells to macrophages promotes their detachment, whereas in apoptotic cells this CD31 mediated detachment is disabled (Brown *et al.*, 2002).

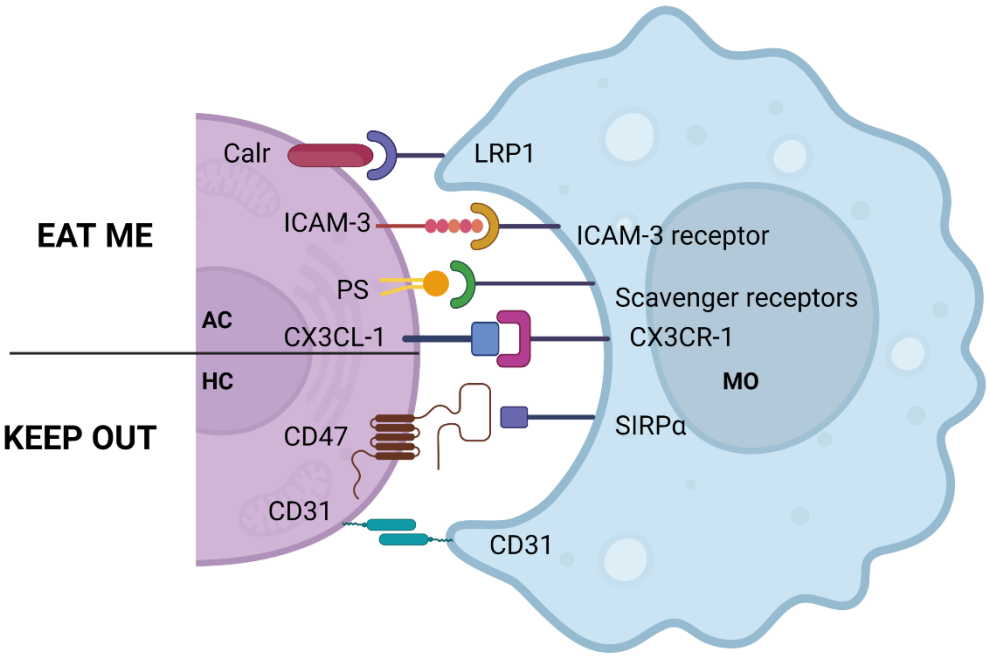

Figure 1.7: Macrophages discriminate healthy and apoptotic cells through eat me and keep out signals. *Healthy cells (HC) carry keep out signals on their surface such as CD47 and CD31. Macrophages (MO) recognize apoptotic cells (AC) via surface molecules such as calreticulin (Calr), ICAM-3, PS, and membrane bound CX3CL-1. The balance between eat me and keep out signals will determine the fate of the cell.*

The tethering of macrophages to apoptotic cell ligands triggers intracellular signalling cascades needed for the initiation of phagocytosis and the degradation of apoptotic cells.

1.2.4 Clearance of apoptotic cells

Firstly, apoptotic corpse internalisation by macrophages is mediated by a major cytoskeletal reorganization. Downstream of eat-me signalling cascades, RAC1 dependent actin polymerisation is essential to form protrusions needed for the engulfment (Evans *et al.*, 2013). The plasma membrane derived vacuole containing the engulfed and sealed AC or large apoptotic bodies is referred to as efferosome (Kinchen and Ravichandran, 2008). The fate of the efferosome in the efferocytes has been described as either canonical or microtubule-associated protein 1 light chain 3 alpha (LC3)-associated efferocytosis (Yin and Heit, 2021).

The canonical efferocytosis, or endo-lysosomal maturation pathway, is characterized by the sequential fusion of the efferosome with the endosome and lysosome. The fusion of the engulfed AC with the early endosome is mediated by the Rab5 GTPase, which then fuse with the late endosome and lysosome through Rab7 interaction (Roberts *et al.*, 2000; Harrison *et al.*, 2003). The acidification of the maturating efferosome allow the degradation of the AC by hydrolytic enzymes.

The non-canonical pathway is the LC3-associated efferocytosis that recruits the autophagy machinery (Martinez *et al.*, 2011). The autophagy pathway is normally activated through nutrient starvation or growth factors depletion, whereas during efferocytosis, autophagy proteins are recruited upon ligation of PS with scavenger receptors of the efferocyte. Afterward, the rapid degradation of the efferosome is mediated by autophagy related proteins such as ATG5 and ATG7 (Heckmann and Green, 2019). However, the exact mechanisms behind this LC3-associated phagocytosis remain unknown.

Effective ingestion and degradation of apoptotic cells leads to a change in macrophage polarisation towards an anti-inflammatory phenotype, with an increased production of anti-inflammatory mediators such as SPMs in the environment, crucial to restore homeostasis (Dalli and Serhan, 2012; Cai *et al.*, 2016). Additionally, both efferocytosis pathways prevent AC antigens presentation by efferocytes, resulting in an immunologically silent AC clearance (Yin *et al.*, 2016; Wan, 2020).

ACdEVs act as a “find-me” signal to attract phagocytic cells, and express “eat-me” signals (phosphatidylserine, ICAM-3, CX3CL-1, and calreticulin) to aid the uptake of AC by phagocytes (Ravichandran, 2010). ACdEVs also have the ability to deliver their cargo and increase the production of pro resolving mediators. Not much is known about ACdEVs functions in efferocytosis, but they are already of great interest in intercellular communication and modulation of activity to mediate inflammation’s resolution. Indeed, further understanding of ACdEVs in AC clearance could lead to the development of new therapy for inflammatory disorders.

1.3 Apoptotic cell derived extracellular vesicles

As highlighted in the previous sections, apoptosis plays an important role in the regulation of inflammation. Most importantly, the rapid clearance of apoptotic cells promotes tissue homeostasis, and this process is mediated by soluble factors released by apoptotic cells. Although various chemotactic factors are released, this study focuses on ACdEVs due to their ability to carry various cargo and affect the recipient cells.

1.3.1 Extracellular vesicles

Extracellular vesicles (EVs) derived from plasma platelets were first observed in 1967 using electron microscopy and were referred to as “platelet dust” (Wolf, 1967). EVs are now defined as nanoscale lipid bilayer encapsulated particles secreted by cells. They are highly heterogeneous as they can vary in size, content, and mechanism of formation (Caruso and Poon, 2018a) (**Figure 1.9, 1.10**). They carry cargo such as proteins, lipids, nucleic acids, metabolites, etc, and play a key role in intercellular communication.

The principal forms of soluble intercellular communication (IC) include hormones, cytokines and growth factors, acting as signalosomes. Dysregulation of IC leads to various pathologies such as cancer and autoimmune diseases. IC can also be mediated by EVs encompassing exosomes, microvesicles, oncosomes, matrix vesicles, ACdEVs, etc. A sizeable percentage of EV proteins seem to be involved in cell communication or signal transduction which correlates with the role of EVs as mediators of intercellular communication (**Figure 1.8**). Other processes associated with EV proteins were identified such as metabolism, energy pathways, cell growth, transport, etc (**Figure 1.8**).

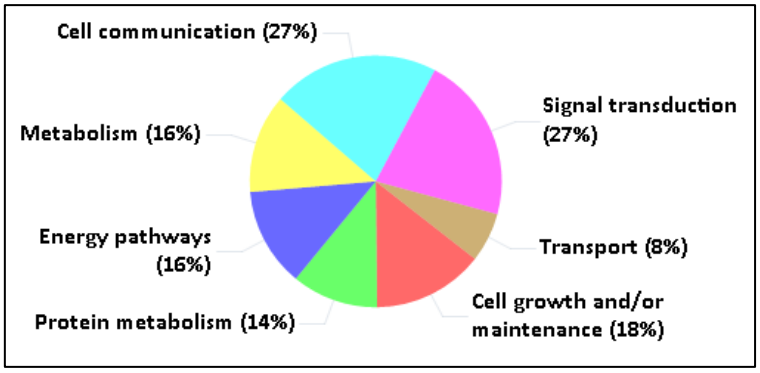

Figure 1.8: Biological process associated with EV proteins. *The top 100 EV proteins list published on Vesiclepedia was used to determine the main biological processes EV proteins are involved in based on Gene Ontology terms. The FunRich analysis tool was used to generate this chart.*

In innate immunity, inflammation can be enhanced by different cargo inside EVs such as proinflammatory cytokines (IL-1β (MacKenzie *et al.*, 2001)) or DAMPs than can lead to chronic inflammatory diseases. EVs also play a role in adaptive immunity, through antigen presentation, influencing the immune response and tolerance. Indeed, EV being a source of antigens, they can be taken up by antigen presenting cells (APC) e.g., dendritic cell (DC), MØ, B cells, leading to stimulatory or down regulatory signals in APCs. Additionally, APCs release EVs than can carry major histocompatibility complex (MHC) peptides and costimulatory molecules (Raposo *et al.*, 1996), resulting in the direct presentation of antigen that can activate CD4+ helper T cells (Giri and Schorey, 2008). Cross antigen presentation is mediated by the transport of the antigen by the EVs to the APC. This cross talk was observed in infected macrophages releasing EVs that delivered mycobacterial antigen to APCs in turn activating CD8+ cytotoxic T cells (Schaible *et al.*, 2003).

Other physio pathological functions of EVs include: vascular system and coagulation, pregnancy, bone calcification, etc (Yáñez-Mó *et al.*, 2015). Through all their involvement in pathological and biological processes, EVs therapeutic and pharmaceutical applications have widened to clinical therapy (Akers *et al.*, 2013), gene vector delivery, biomarker, drug delivery (Alvarez-Erviti *et al.*, 2011; Tian *et al.*, 2014; Haney *et al.*, 2015; Vader *et al.*, 2016), regenerative medicine (Lai *et al.*, 2010), tissue engineering, amongst others.

EVs can be divided into three main subtypes which are exosomes (EXOs), microvesicles (MVs) and apoptotic cell derived EVs (ACdEVs). However, different terms can be found in the

literature as there is no standard nomenclature e.g. microparticles, ectosomes, etc (Lötvall *et al.*, 2014).

1.3.1.1 Biogenesis and release of extracellular vesicles

1.4.1.1.1 Exosomes

In 1987, Rose Johnstone proposed the name “exosome” to refer to secreted membrane vesicles derived from multivesicular bodies (Johnstone *et al.*, 1987). Exosomes represent a heterogeneous population with a size ranging from 30 to 120 nm in diameter. Exosomes are released through the exocytic intracellular pathway (Denzer *et al.*, 2000), and are initially formed inside the endosome. The endosome can be divided in three major compartments: the early endosome, the late endosome, and the recycling endosome. This organelle’s function is to sort and deliver intracellular material to its specific destination. Intraluminal vesicle (ILV) formation in the early endosome is mediated by protein-protein interactions in tetraspanin enriched microdomains of the endosome membrane (e.g. CD63) (Pols and Klumperman, 2009). Additionally, endosomal sorting complexes required for transport (ESCRTs) are necessary for an efficient ILVs formation. Four different complexes are involved in this biogenesis mechanism: ESCRT 0 clusters the cargo, ESCRT 1 and 2 mediate the inward budding of the endosomal membrane and the cargo confinement, and finally ESCRT 3 cleaves the neck of the bud (Wollert and Hurley, 2010). The early endosome matures into the late endosome containing multiple vesicles in its lumen, this structure is referred to as multivesicular bodies (MVBs) (SOTELO and PORTER, 1959). Lysobisphosphatidic acid (LBPA) was found to be enriched in the endosome membrane and is involved in MVBs formation (Kobayashi *et al.*, 1998). Degradative MVB fuses with the lysosome for the degradation of its content while exocytic MVB fuses with the plasma membrane to release exosomes in the extracellular environment.

1.4.1.1.2 Microvesicles

Microvesicles, by their name, are larger vesicles and their size usually varies from 50 nm to 1 µm. They are formed by budding off the plasma membrane. The localization of the cellular machinery to the membrane initiates the outward budding of the plasma membrane. This recruitment of MVs cargo and machinery happens at specific membrane domain enriched in lipid raft (Cocucci, Racchetti and Meldolesi, 2009). Some key mediators involve tethering molecules (SNARE), molecular motors (kinesins, myosins), and actin (Willms *et al.*, 2018). To allow the membrane to bend to form a vesicle, the lipids present in the membrane are redistributed to change the membrane curvature and rigidity (Kozlov *et al.*, 2014; McMahon

and Boucrot, 2015). This alteration in lipid composition is mediated by flippase, translocase, and scramblase. The main key mediators of MVs biogenesis are ADP-ribosylation factor 6 (ARF6) and Ras homolog gene family member A (RhoA). ARF6 mediates the myosin localization and regulation whereas RhoA mediates the recruitment and activation of actin, both comprising the contractile machinery at the neck of the budding vesicle (Wickman *et al.*, 2013a). Finally, the vesicle is cleaved and released in the extracellular environment. However, this mechanism of microvesicle release is poorly understood.

1.4.1.1.3 Apoptotic cell-derived extracellular vesicles (ACdEVs)

Subtypes of ACdEVs include large apoptotic bodies (ApoBDs) of 1 to 5 µm, smaller apoptotic microvesicles (ApoMVs) under 1µm, and apoptotic exosome-like vesicles around 100 nm. This type of programmed cell death induces morphological changes starting with membrane blebbing that will lead to thin membrane protrusions, which in turn form apoptotic bodies. These membrane protrusions can be generated through microtubule spikes, apoptopodia, beaded apoptopodia or non-beaded apoptopodia (Atkin-Smith *et al.*, 2015). Unlike ApoBDs, ApoMVs are formed by the outward budding and fission of the plasma membrane. It remains unclear what mechanism of biogenesis is involved for smaller apoptotic exosome-like EVs.

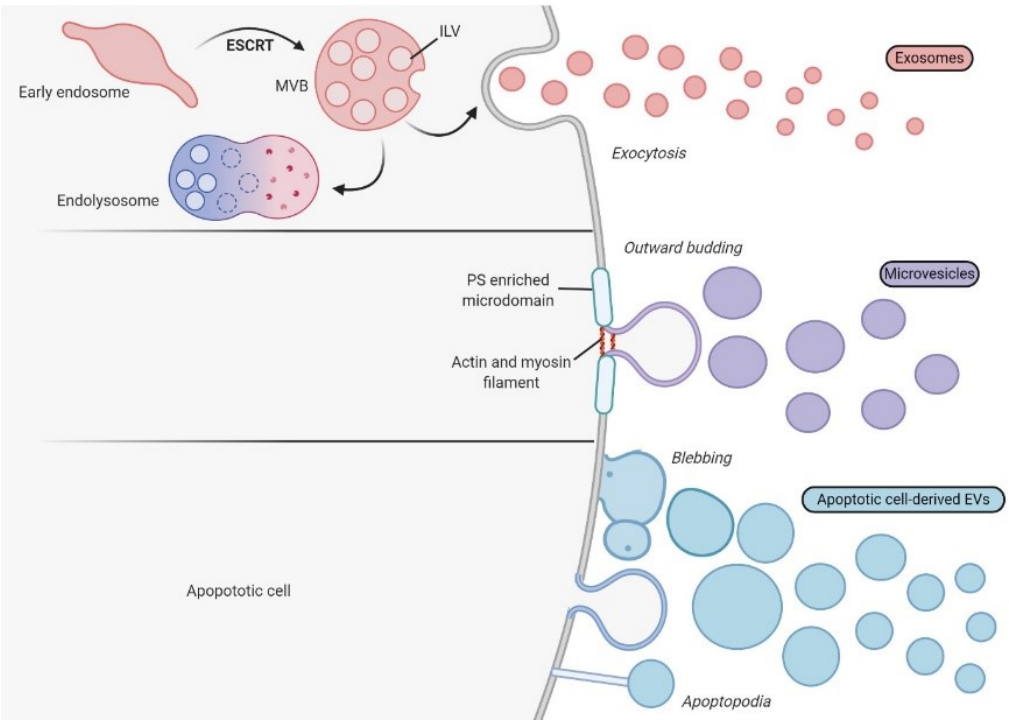

Figure 1.9: Biogenesis of the 3 main EV subtypes. *Exosome formation in the early endosome is mediated by the ESCRTs proteins. The endosome matures into MVBs containing ILVs. MVBs either fuse with lysosomes for the degradation of its content or fuse with the plasma membrane to release exosomes by exocytosis. Microvesicles (MVs) are formed in membrane microdomains enriched in PS and the outward budding will then release MVs via the contraction of actin and myosin filaments. Apoptotic cell releases EVs via membrane blebbing, outward budding or via the formation of apoptopodia.*

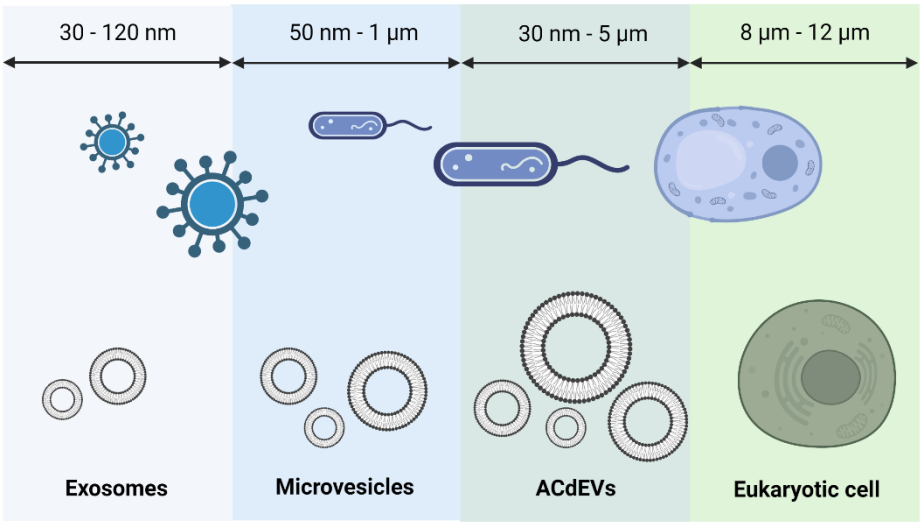

Figure 1.10: Size overlap of EV subtypes. *Exosomes range from 30 to 120 nm, microvesicles from 50 nm to 1 µm, ACdEVs from 30 nm to 5 µm, and are released by cells ranging from 8 to 12 µm. Graphical representation of (left to right) viruses, bacteria and yeast was added as a visual aid.*

1.3.1.2 Composition of EVs

EVs were first believed to carry random cellular components, mostly cell debris. However, as the interest in the EVs field grew, research demonstrated that EVs harbour a specific subset of proteins, mRNAs, miRNAs, enzymes and lipids (Skog *et al.*, 2008; Théry, Ostrowski and Segura, 2009) (**Figure 1.11**). These specific cargoes derive from the secreting cell providing valuable information about the cell state and its surrounding environment. Thus, EVs carry biomarkers that could help with early diagnosis, prognosis and therapeutic solutions as they are found in all body fluids i.e. blood, plasma, breast milk, urine, etc (Keller *et al.*, 2011; Lässer *et al.*, 2011).

The proteomic composition of EVs varies between the different EV subtypes and the parent cells they derive from. Broadly, proteomic composition has been determined by a combination

of western blotting, ELISAs and mass spectrometry approaches. The protein cargo of exosomes includes membrane proteins of endocytic origin and is enriched with tetraspanin, integrins and membrane trafficking proteins. As ESCRT proteins play a leading role in the biogenesis of exosomes, they are also found to be enriched in this EV subset. Specific proteins identified as exosome markers (e.g. Flotillin-1, heat-shock 70-kDa proteins, MHC I and II) have recently been detected in other EV subtypes such as microvesicles (Kowal *et al.*, 2016). MVs mainly contain cytosolic and plasma membrane proteins as a result of their biogenesis process. MMP-2, an enzyme involved in vascularization and invasiveness, was found to be enriched in MVs (Muralidharan-Chari *et al.*, 2010). Additionally, so were glycoproteins and integrins such as P-Selectin and Mac-1 (Falati *et al.*, 2003; Pluskota *et al.*, 2008). However, protein markers seem to be less specific for this EV subtype as they are mainly cell specific since they bud off the plasma membrane thus expressing the same surface marker as the cell they derived from. Nonetheless, a small number of proteins were found to be enriched in microvesicles and larger EVs derived from human DC, isolated by sedimentation speed followed by density gradient or immune-isolation (Kowal *et al.*, 2016). These enriched proteins were identified using both western blot and quantitative proteomic comparison and comprise actinin-4 and 1, glycoprotein 96, Mitofilin, major vault protein, and eEF2. For ACdEVs, there is a lack of knowledge as they were thought to be formed randomly.

Several studies demonstrate that genetic material such as RNA can be transferred from the donor cell to the recipient cell through EVs (Skog *et al.*, 2008; Mittelbrunn *et al.*, 2011). Functional RNA in EVs, first observed in 2007 (Valadi *et al.*, 2007), can affect the recipient cell's activity as the EV-mRNA can be translated, and the EV-miRNA can regulate the translation of the recipient cell's mRNA. Additionally, EV are enriched in mRNA fragment with increased 3' UTR regions including multiple regulatory miRNA binding sites. These fragmented EV-mRNA are actively delivered to the recipient cell and can compete with the host cellular mRNA for miRNA regulation. In comparison to EV-RNA, the DNA content of EV remains less explored despite the fact that both single and double stranded DNA have been observed in EVs (Thakur *et al.*, 2014). EV-DNA reflects the donor cell's DNA, as studies showed that cancer cell mutation such as BRAF and KRAS were also found in EVs released from melanoma and pancreatic cells (Kahlert *et al.*, 2014). Furthermore, DNA was successfully transferred to recipient cells as labelled EV-DNA was seen in their cytosol and even in their nucleus (Waldenström *et al.*, 2012). Finally, mitochondrial elements from astrocytes and glioblastoma cells can also be released through exosomes (Guescini *et al.*, 2010).

The lipidomic profile of EVs can be different to that of the donor cell with a specific enrichment of lipids (Llorente *et al.*, 2013). EVs are generally enriched in glycosphingolipids, ceramide, sphingomyelin and PS (Trajkovic *et al.*, 2008; Record *et al.*, 2014). Other studies also state that there is an increase of cholesterol in exosomes relative to the donor cell's membrane (Llorente *et al.*, 2013). EV's membranes being enriched in sphingomyelin and cholesterol agrees with the evidence that lipid raft-like domains are enriched in exosomes. Like apoptotic cells, ACdEVs harbour increased levels of PS in the outer leaflet of the membrane. ACdEVs also carry lipid mediators of inflammation and the level of pro- versus anti- inflammatory mediators contained in ACdEV might balance the fate of the resolution of inflammation (Devitt, Griffiths and Milic, 2018). Calreticulin and ICAM-3 were previously detected by protein mass spectrometry on the ACdEVs studied in this research (Dr Ivana Millic, personal communication).

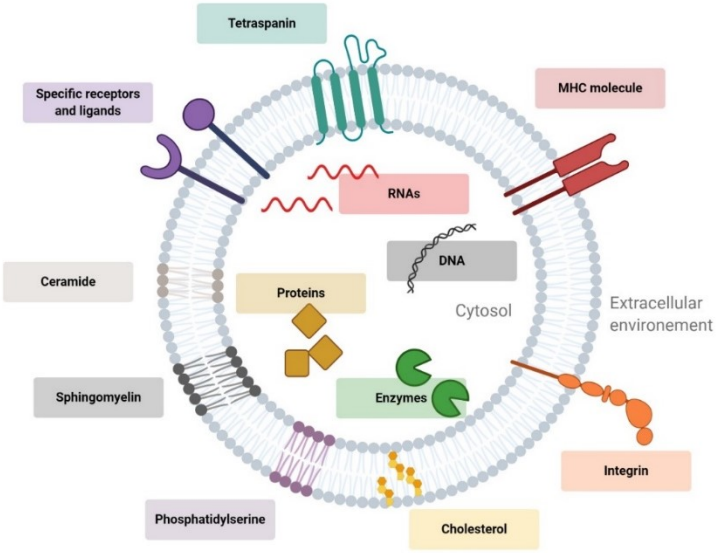

Figure 1.11: Overall composition of extracellular vesicles. *Schematic representation of the composition of EVs: nucleic acids, proteins, and lipids. Some components are present in specific EV subtypes.*

Taken together, the cargo of ACdEVs is highly variable and dependent on the physiological context, the donor cell, and the EV subtypes. However, the membrane composition of EVs is highly important in regard to its physical properties such as the lipid packing order, fluidity and curvature that could dictate the preferred uptake route of EVs by recipient cells.

1.3.1.3 EV uptake by recipient cells

As previously described, the composition of EVs plays a significant role in intercellular communication (IC) as they can generate various responses in the recipient cells, affecting their behaviour. This short and long range signalling can be mediated through direct receptor-ligand interaction e.g. PS binding scavenger receptors on macrophages surfaces (Miyanishi *et al.*, 2007), or through internalization of the vesicle contents (CLAYTON *et al.*, 2004; Valadi *et al.*, 2007). Respectively, this results in an induced intracellular signalling, or the transfer of molecules. In order to release their content in the recipient cell, EVs either fuse with the plasma membrane or are taken up by endocytosis. There is evidence that this uptake is energy-dependent, as the uptake of exosomes is inhibited at 4˚C (Morelli *et al.*, 2004; Escrevente *et al.*, 2011). However, at such temperature, membrane properties important for the uptake of vesicles such as fluidity can be modified. The internalization of EV content can be mediated through different routes (Mulcahy, Pink and Carter, 2014) i.e. endocytosis and cell surface membrane fusion (**Figure 1.12**).

Endocytosis comprises several uptake mechanisms: phagocytosis and pinocytosis. Phagocytosis is the engulfment of large particles by a professional phagocyte whereas pinocytosis is performed by all cells and can be divided into three subtypes: clathrin-dependant endocytosis (CDE), clathrin-independent endocytosis (CIE) (e.g. caveolin- and lipid raft-mediated endocytosis) and macropinocytosis. Macropinocytosis and phagocytosis are quite similar in a way that these endocytic mechanisms generate large intracellular vacuoles.

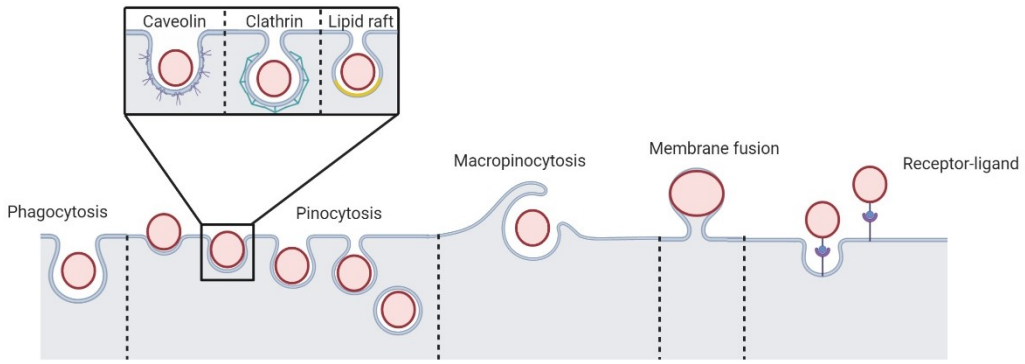

Figure 1.12: The main routes of EV uptake by recipient cells. *EV signalling can be direct through specific receptor-ligand interaction leading to intracellular signal transduction. EV can also signal*

indirectly to the recipient cells through internalization via different routes. The main uptake mechanisms are endocytosis and membrane fusion. Endocytosis can be further divided into phagocytosis that eat up large vesicles, pinocytosis (CDE and CIE), and macropinocytosis.

Phagocytosis involves specialized recipient cells taking up particles in the extracellular environment resulting in the formation of large vacuoles called phagosomes. This uptake process is more specific to macrophages and dendritic cells than other recipient cells, and is mainly mediated by PS that acts as a ligand between ACdEVs and scavenger receptors of phagocytes (Kourtzelis, Hajishengallis and Chavakis, 2020).

Pinocytosis, also called fluid endocytosis, is the uptake of small vesicles and extracellular fluid. This type of endocytosis can be receptor mediated generating caveolin- and clathrin-coated pits. CDE is the formation of the inward budding of the plasma membrane following specific receptor-ligand interaction at the cell surface. These buddings are coated with clathrin and will mediate the vesicle formation from the plasma membrane. The clathrin molecules will then detach and be recycled to the plasma membrane while the content of the vesicle is released in the endosome for further sorting. CIE such as caveolin-mediated endocytosis is very similar to this mechanism as vesicular buds from the plasma membrane are formed in caveolin-rich domains also enriched in cholesterol (Anderson, 1998). Another type of CIE is lipid raft-mediated endocytosis. Lipid rafts are microdomains that are enriched in sphingomyelin, ceramide, and cholesterol (Anchisi *et al.*, 2013; Sezgin *et al.*, 2017). These lipid microdomains are less fluid than the plasma membrane and can move freely within the plasma membrane. The colocalization of EVs with lipid rafts of recipient cells suggests lipid raft-mediated endocytosis (Svensson *et al.*, 2013). Moreover, lipid rafts within EV membranes seems to facilitate the binding and uptake of EVs by recipient cells (Izquierdo-Useros *et al.*, 2009).

Macropinocytosis can be described as protrusions that loop over particles being engulfed, and fuse back with the plasma membrane (**Figure 1.12**). This uptake route is triggered via the activation of growth factors (GF) signalling pathways (EGFR, PDGFR). This GF signalling results in an increase of actin polymerization at the cell surface in turn forming membrane protrusions referred to as ruffles (Kerr and Teasdale, 2009). Actin-mediated ruffles engulf the particles producing macropinosomes (Fitzner *et al.*, 2011). The macropinosome organelle's fate tend to be cell type dependent but mainly end up fusing with the late endosome or lysosome. This actin-dependent macropinocytic mechanism is mediated by Rac1 GTPase, Na^+/H^+ exchangers, dynamin as well as phosphoinositide-3-kinase activity (Kerr and Teasdale, 2009; Mercer and Helenius, 2009; Costa Verdera *et al.*, 2017).

Membrane fusion is the merger of vesicles with the plasma membrane, this process is stabilized via various proteins interactions involving SNAREs, Rab, etc (Jahn and Scheller, 2006). The fusion of the vesicle allows the content of the EV to be mixed with the recipient cell cytosol. This uptake route of EVs can be observed by fluorescent lipid quenching (Franzen *et al.*, 2014). The direct fusion between the EV membrane and the plasma membrane requires the same membrane fluidity (Chang and Cheng, 2006; Kima *et al.*, 2017). Regulatory lipids play an important role in creating microdomains that serve as fusion site, mainly by modulating the membrane curvature and fluidity (Lang, Halemani and Rammner, 2008; Zhukovsky *et al.*, 2019).

As phagocytosis is aimed at larger particles, it is more likely that macrophages are taking up ACdEVs via a different route, perhaps pinocytosis for smaller vesicles or membrane fusion. Feng *et al*., 2010, showed that most of the exosomes were actively internalized via phagocytosis, however a small portion were taken up by non-phagocytic cells meaning that this specificity is only partial (Feng *et al.*, 2010). Whether this process is cell type specific, or EV subtype specific remains unclear. The specificity of the EV uptake route could be affected by their size, surface molecules, membrane fluidity, etc.

1.4 EV isolation methods

As EVs are of great interest in diagnosis and biomarkers research, it is crucial to isolate EVs from non-EV proteins and non-EV particles to validate EV-related discoveries. Indeed, blood derived samples or supplemented culture media samples, often contain serum derived proteins and lipoproteins which can interfere with the particle counts and further analysis (Liangsupree, Multia and Riekkola, 2021). However, it can be challenging to discriminate between EV cargo and soluble contaminants (complement component, immune complexes, protein aggregates, etc.) present in the extracellular environment from which EVs are harvested (Webber and Clayton, 2013). Various isolation techniques can therefore be used to isolate EVs based on their size, charges, affinity, density, and other properties.

1.4.1 Conventional methods

Conventional isolation methods can be divided into external field (centrifugal force), sieving (physical holes or barrier) and colloidal stability (size-selective precipitation or solvent addition). The choice of the method is mostly based on the EV subtype of interest and the experimental design.

Ultracentrifugation (UC) based techniques include differential UC and density gradient UC. Differential UC is the most commonly used method for EV isolation (Gardiner *et al.*, 2016). This isolation principle is based on a series of increasing centrifugal forces and time based on the size, density and shape of the vesicles (Théry *et al.*, 2006). The series of sedimentation cycles is as followed: cells are pelleted first at 300 x g, then the apoptotic bodies and larger debris at 1000 x g, the MVs at 2000 x g and finally, exosomes at 100,000 x g. This protocol can be modified by adding filtration steps to increase the purity. Additionally, the choice of the rotor, g-force, and centrifugation time can affect the yield and purity of the sample by, for example, altering the sedimentation path (Cvjetkovic, Lötvall and Lässer, 2014).
The other type of UC, density gradient, can be further divided into isopycnic UC or rate zonal UC. The key difference between the two is that isopycnic UC separates particles that differ in density but not in size, whereas rate zonal UC separates particles that differ in size but not in density. In general, it consists in a predetermined density gradient on the top of which the sample is added. Upon centrifugal force, the different sedimentation rate of the particles will separate them and the different fractions can be collected (Cantin *et al.*, 2008).

Size-based techniques include ultrafiltration and size exclusion chromatography (SEC). Different EV subtypes are isolated based on their size difference. Ultrafiltration uses membrane filters with specific size exclusion limits based on the size and molecular weight of the vesicles. The SEC principle is based on the different elution rate of particles where larger vesicles move faster and elute first while smaller vesicles elute later. The sample is loaded onto a chromatography column which contains a porous stationary phase that will retain the smaller particles while the larger ones are eluted (Böing *et al.*, 2014).

Precipitation techniques can also be used for EV isolation. The main precipitation experiments involve either polyethylene glycol (PEG) or lectin. PEG-mediated precipitation relies on PEG's water excluding properties in order to change the solubility of the EVs, forcing them to precipitate out of the solution. As for the use of lectin, it binds to carbohydrates on the surface of the vesicles and causes them to agglutinate. For both precipitation methods, low speed centrifugation or filtration can be used afterwards to collect the isolated vesicles.

Lastly, immunoaffinity based capture techniques use antibodies to capture EVs based on specific surface markers. The antibodies can be attached to a plate, beads, and more recently, to microfluidic devices. This requires a high expression of the biomarker of interest in order to increase the capture and recovery of EVs. This technique is particularly relevant for EVs

derived from a specific cell type such as hepatocyte-derived EVs carrying asialoglycoprotein receptor 1 on their surface (Conde-Vancells *et al.*, 2008).

Techniques	Examples	Advantages	Disadvantages
UC-based	Differential UC Density gradient	Large sample capacity. Mostly used.	Lowest number of particles/mL. Limited resolution. Sample loss. Aggregation. Time consuming. Multistep.
Size-based	SEC Ultrafiltration Isolation kits	Fast. Reproducibility. Moderate sample capacity. Low cost.	Clogging and vesicle trapping. Sample loss.
Precipitation	PEG Lectin	Large capacity. Scalable.	Contaminant precipitation. No EV subtype specificity. Moderately time consuming. Low purity.
Immunoaffinity	Immunocapture ELISA	High specificity. High purity. High recovery.	Few specific surface markers. High cost.

Table 1.1: Comparison of EV conventional isolation methods*. ELISA (*enzyme-linked immunoassay).

EV isolation remains a challenge as each technique shows disadvantages (**Table 1.1**). Due to the size overlap of the different EV subtypes, size-based techniques fail to purify specific EV subtypes to homogeneity. Moreover, immunoaffinity based techniques are challenging due to the lack of specific membrane bound biomarkers for each EV subtype, and especially ACdEVs. In order to increase the specificity and purity of EV isolation, it is recommended to use complementary approaches such as UC followed by SEC. Current conventional isolation methods only enrich the subtype of interest and might damage the cargo and membrane of EVs (Taylor and Shah, 2015). The need for novel isolation methods is crucial and one of the potential alternatives is microfluidic isolation.

1.4.2 Microfluidics and EV isolation

Microfluidics is the science of manipulating and controlling fluids in a network of channels in a small device usually with dimensions from 10 to 100 μm. The size of the channels will define whether it is microfluidic or nanofluidic. However, they have similar physical properties and often come under the same terminology: “Microfluidics”. In opposition to passive microfluidics, active microfluidics refers to the fluid handling made by active components such as microfluidic pumps or valves. Pressure driven flows use a pressure gradient to drive the fluid through the channels. Different parameters can affect the fluid dynamics such as the height of the channel, the pressure, the density, and gravity. However, when working on such smaller scales, like the microfluidic device used in this study, most of those forces are nullified leading to what is known as a fully developed flow. In more details, a fully developed flow’s velocity do not change with the increased distance along the microfluidic channels, ensuring a continuous and homogeneous isolation of nanoparticles.

The behaviours of the fluid inside the microfluidic channels define the type of flow based on the Reynolds number Re, a measure of flow turbulences (Nguyen and Wereley, 2006). There are two major types of flow in fluid dynamics: laminar and turbulent. Laminar flow is when the fluid particles move along smooth paths in layers whereas turbulent flow is when the fluid particles move along irregular paths. There are two types of fluids: Newtonian and non-Newtonian fluids (Ong *et al.*, 2008). When working with a Newtonian fluid and based on its linear relationship, the liquid density and the viscosity are constants. The only two parameters left that are considered are the velocity and the geometric parameter known as the hydraulic diameter. This is relevant when isolating ACdEVs in said fluids solely based on their size and the flow rate at which it is perfused through the microfluidic channels.

In the microfluidic field, novel devices known as lab-on-a-chip (LOC) offer promising applications for EV isolation (Haeberle and Zengerle, 2007). A LOC is a microfluidic chip that has a set of micro-channels moulded into a material. Fluids enter the channel network and are separated or manipulated depending on the desired function and design of the chip. Usually, LOCs integrate one or multiple laboratory functions. Various LOC techniques have been recently developed in microfluidics for nanoparticle isolation (Salafi, Zeming and Zhang, 2017). The main active and passive separations techniques are listed below (**Table 1.2**).

	Techniques	References
Active separations	Field Flow Fractionation	(De Momi and Lead, 2008; Dayanand and Widomska Justyna, 2018; Drexel *et al.*, 2020)
	Centrifugal Microfluidic	(Arosio *et al.*, 2014)
	Optical	(Statsenko, Inami and Kawata, 2017)
	Magnetophoresis	(Lee, Hatton and Khan, 2011; Munir *et al.*, 2014)
	Acoustophoresis	(Lee *et al.*, 2015)
	Affinity Based Sieving	(Ebara *et al.*, 2013)
	Electrophoresis	(Ban, Yoo and Song, 2015; Jeon, Kim and Lim, 2016)
	Dielectrophoresis	(Kazemi and Darabi, 2018)
	Ion Concentration Polarization	(Jeon *et al.*, 2013)
	Electrohydrodynamic vortices	(Boettcher *et al.*, 2011)
Passive separations	Deterministic Lateral Displacement	(McGrath, Jimenez and Bridle, 2014; Tottori, Hatsuzawa and Nisisako, 2017; Naotomo Tottori, Yasuhiko Muramoto, Hiraku Sakai, 2020)
	Inertial Microfluidics	(Bhagat, Kuntaegowdanahalli and Papautsky, 2009; Zhang *et al.*, 2016)
	Filtration	(Amato *et al.*, 2012; Davies *et al.*, 2012)
	Electrostatic Sieving	(Krishnan *et al.*, 2010; Regtmeier *et al.*, 2011)
	Cell Actuation	(Traore and Behkam, 2013; Suh, Traore and Behkam, 2016)

***Table 1.2: Current microfluidics techniques for nanoparticles separation**. Separation techniques can be divided into active separations, which require an external field, and passive separations, which do not.*

Similarly to some conventional EV isolation techniques, active microfluidic separation techniques can damage EV samples such as electric fields, acoustic waves, optical beams, etc. In opposition, label-free and external field-free passive microfluidic separation techniques offer a less damaging approach for EV isolation. Among them, the microfluidic filtration-based separation can be further defined by the specificity of the separation forces such as hydrodynamic-, hydrophoretic-, size-exclusion- and crossflow filtration.

Microfluidics for EV isolation offers many advantages compared to conventional approaches. The main advantage of microfluidic devices is the miniaturization of conventional techniques with decreased materials and samples consumptions especially for small biological sample volume as well as reagents. Additionally, this method has a lower power budget enabling high throughput capabilities at a lower cost (Streets and Huang, 2013). Most importantly, microfluidics is able to separate nanoparticles continuously unlike most conventional isolation methods used in the EV field where multiple preparation steps are required.

1.5 Knowledge gap and objectives

Inflammation is a crucial protective response against pathogens. When impaired, inflammation can lead to a harmful environment prone to cellular mutation and proliferation leading to various pathologies. Current therapeutic targets focus on immune-suppressive strategies putting the patient at greater risks of side effects and infections. Instead, improving the understanding of the mechanisms that control the resolution of inflammation and the role of pro-resolving mediators will undoubtably lead to important breakthrough in the treatment of various diseases.

In this study we focus on a major pro-resolving process: efferocytosis. This phagocytic event is defined as the controlled recognition and removal of apoptotic leukocytes by macrophages. For this, macrophages are recruited to the site of cell death through a chemotactic gradient created by apoptotic cells derived extracellular vesicles (ACdEVs). Little is known about the structure and functions of this extracellular vesicle population as they were long thought to be cellular debris.

The aim of this thesis is to characterize the structure and function of ACdEVs to gain knowledge on the mechanisms that control the resolution of inflammation. To achieve this, several objectives were set:

(1) Compare the particle size distribution and basic characteristics of early and late ACdEVs, discussed in chapter 1 and chapter 2, p. 75.
(2) Investigate the composition of ACdEVs (protein, cholesterol, lipid content), discussed in chapter 2, p.88.
(3) Investigate the membrane properties of ACdEVs throughout apoptosis, discussed in chapter 2, p. 85.
(4) Determine the bioactivity of different ACdEVs subpopulation (macrophages recruitment and EV uptake), discussed in chapter 3.
(5) Develop a novel microfluidic strategy to isolate ACdEVs based on their size, discussed in chapter 4.

2. Material and methods

2.1 Materials

Reagents, equipments and antibodies used in this study are listed below.

2.1.1 Reagents

Reagents	Manufacturer
RPMI-1640 cell culture medium (phenol red supplemented and phenol red-free)	Sigma Aldrich
L-glutamine	Sigma Aldrich
Penicillin/Streptomycin	Sigma Aldrich
Dulbecco's phosphate buffered saline (PBS)	Sigma Aldrich
Foetal calf serum of South American origin	Gibco (Thermo Fisher Scientific)
1α,25-Dihydroxyvitamin D3 (VD3)	Enzo Life Sciences
Apoptosis detection kit FITC/APC	eBioscience™ (Thermo Fisher Scientific)
BODIPY™ FL N-(2-Aminoethyl)) Maleimide	Invitrogen (Thermo Fisher Scientific)
BODIPY™ TMR maleimide	Invitrogen (Thermo Fisher Scientific)
Megamix-Plus Forward Scatter and Side Scatter beads	Biocytex

2.1.2 Equipment

- EVOS™ FL Digital Inverted Microscope (Invitrogen, UK)
- Multiskan™ GO Microplate Spectrophotometer (Fisher Scientific, UK)
- qNano - Tunable Resistive Pulse Sensing (IZON Science, New Zealand)
- nCs1 – Microfluidic Resistive Pulse Sensing (Spectradyne)
- CytoFLEX S, Beckman Coulter, USA
- Videodrop particle analyser (Myriade, France)
- Nanodrop 1000 (ThermoFisher, UK)
- UVP chromato-vue C71 light box cabinet and UVX radiometer (UV-P Inc, Uplands, CA, USA)

- Mithras plate reader (Berthold technologies, Germany)
- Cytation 5 automated cell imaging reader (Biotek, USA)
- Ultrospec 2000 spectrophotometer (Pharmacia Biotech, USA)
- ZetaView PMX120 NTA (Particle Metrix GmbH, Meerbusch, Germany)

2.1.3 Antibodies

Antibody	Manufacturer
Mouse anti-human CD11b PE	eBioscience™ (Thermo Fisher Scientific)
Mouse anti-human CD14 PE	Invitrogen (Thermo Fisher Scientific)
Mouse IgG1kappa isotype control PE	eBioscience™ (Thermo Fisher Scientific)
Mouse IgG2a isotype control PE	Invitrogen (Thermo Fisher Scientific)

2.2 Methods

2.2.1 Cell lines and culture

THP-1 monocytes and Jurkat T lymphocytes (ATCC, VA, USA), were cultured at a density of $5x10^5$ cells/mL in RPMI1640 medium supplemented with 10 % foetal bovine serum, 100 µg/mL penicillin/streptomycin, and 2 mM L-glutamine. Cells were passaged every two to three days and kept in the incubator at 37 °C, with 5 % carbon dioxide (CO_2). Prior to induction of apoptosis, cells were transferred to serum-free (SF) and phenol free (PF) RPMI1640 supplemented with 1 % L-glutamine, and 100 µg/mL penicillin/streptomycin. When needed, THP-1 cells were differentiated into THP-derived macrophages over 48 hours via addition of 100 nM Vitamin D3.

2.2.2 Induction of apoptosis

Cells were washed with D-phosphate buffer solution (PBS) and resuspended in serum-free and phenol red-free RPMI 1640 at a density of $4x10^6$ cells/ml. Cells were then exposed to a UV-B dose of 30 mJ/cm² using the UVP chromato-vue C71 light box cabinet and UVX radiometer. Apoptotic cells were collected at different time points after irradiation (0-, 2-, 6- and 18-hours) and observed under the microscope (EVOS FL, Invitrogen) for morphological signs of apoptosis (shrinking and blebbing).

2.2.3 EV isolation and purification

After induction of apoptosis and incubation for 6 hours or 18 hours, apoptotic cells were first centrifuged at 300 x g for 5 min/4°C to remove cells, and the supernatant was collected to be

further centrifuged at 2000 x g for 20 min/4°C to remove larger cellular debris. The 2000 x g supernatant containing the cell secretome including the EVs, was then collected for further analysis. When required, the 2000 x g supernatant was first concentrated down using 30 KDa cut off Amicon spin filter to a volume ≤ 1mL. 500 µL was then transferred to a 70 nm qEV original column (Izon, France), previously washed with 20 mL PBS. Following the manufacturer instructions, a void volume of 3 mL was discarded before collecting a 3.5 mL purified EV fraction.

2.2.4 Flow cytometry

All flow cytometry measurements were realised using the CytoFLEX S (Beckman Coulter, USA). Data were analysed using CytExpert version 2.2 (Beckman Coulter, USA). For cells measurements, a 488 nm laser was used, whereas for EV measurements, the violet side scatter laser of 509 nm was used.

2.2.4.1 Cell staining

$5x10^5$ cells were washed with PBS containing 0.1 % bovine serum albumin (BSA), twice, and stained with anti-mouse CD14 followed by anti-mouse IgG FITC (Sigma-Aldrich) and then incubated in PBS supplemented with 10 % human serum for 30 minutes on ice. Samples were then washed twice with PBS and resuspended in a final volume of 250 µL PBS. Antigen expression was determined by flow cytometry using the CytoFLEX (Beckman Coulter, USA) by looking at the percentage of positive cells for the antigens as well as the mean fluorescence intensity (MFI).

2.2.4.2 Apoptosis assay

Quantification of apoptosis was performed using annexin V-FITC and propidium iodide (PI) staining kit according to the manufacturer's instructions. Briefly, samples were washed and resuspended in annexin V-binding buffer (10 mM HEPES, 150 mM NaCl and 2.5 mM $CaCl_2$ in water) and stained with annexin V (5 µL) on ice for 10 minutes. For double stained samples, propidium iodide (PI) (10 µL) was added directly. The stained samples were detected by flow cytometry (cytoFLEX S, Beckman Coulter, USA). Distinct stages of cell apoptosis were studied with this assay where early apoptotic cells are AnV positive and PI negative (AnV-FITC +/PI-), whereas late apoptotic cells are AnV/PI-double-positive (AnV-FITC+/PI+.) Viable cells are unstained (AnV-FITC-/PI-).

2.2.4.3 Extracellular vesicles

Typically, a volume of 10 mL of 2000 x g ACdEVs were concentrated down to 1 mL and stained with 5 μM Bodipy FL or TMR for one hour on ice. The samples were then washed in PBS and purified by SEC using the qEV 70 nm original columns (Izon, France). EVs were then measured by flow cytometry by gating on FIT-C or PE positive events, 50,000 events were recorded per measurement. MegaMix forward and side scatter fluorescent beads were used to determine relative sizes of the particles after gating using FIT-C fluorescence.

For measuring the level of surface phosphatidylserine (PS), SEC purified ACdEVs were stained with annexin V (AnV)-FITC for 15 minutes on ice. EVs were gated against the unstained samples using violet side scatter for size and FIT-C channel for fluorescence. Violet side scatter (VSSC) was used as a trigger for EVs detection.

2.2.4.4 EV uptake assay

10 mL of 2000 x g supernatant of Jurkat T cell culture from 6h or 18h post-UV was concentrated down to < 1 mL with a 10 KDa molecular weight Amicon filter tube and stained with BODIPY™ TMR at 5 μM and incubated for up to 1 hour on ice in the dark. Stained or unstained ACdEVs were purified, and the excess dye was removed by SEC using qEV 70 nm columns (Izon). Labelled EVs were then incubated with VD3 treated THP-1 monocytes for up to 4 hours. Before flow cytometry analysis, macrophages were washed with PBS to remove unbound EVs to measure the level of EV uptake. Samples were recorded at an event rate of <10,000/second.

2.2.5 Cryo-transmission electron microscopy

Early or late ACdEVs samples for cryo-EM were stored at 4 °C for less than 24 hours before being processed. Carbon grids were made hydrophilic using a glow discharger. 5 μL of samples were loaded on a glow-discharged 300 mesh EM grid with lacey carbon (EM Resolutions – LC300Cu100) and vitrified using a Leica EM GP2 (Leica, Germany). Excess sample was removed by blotting once between 1 and 2 seconds with filter paper. Grids were mounted in a cryo-holder for cryo-EM imaging. Imaging was performed on a JEOL2200FS TEM operated at 200 kV. Images were recorded on a Gatan K2 Summit camera. Images were recorded at 15,000 x magnification (pixel size 0,25 nm) and analysed on ImageJ.

2.2.6 EVs particle size distribution measurement

2.2.6.1 Microfluidic resistive pulse sensing (MRPS)

ACdEVs size distribution and concentration was measured with the nCS1 (Spectradyne, USA) using TS-400 and TS-2K single use cartridges. These cartridges are suitable for the detection of particles between 65- to 400 nm, and 250- to 2000 nm, respectively. Samples were diluted in 1% Tween-20 or 0.1 % BSA and 3 µL was loaded onto the microfluidic device to be measured.

2.2.6.2 Tuneable Resistive Pulse Sensing (TRPS)

Tuneable resistive pulse sensing using the qNano (iZON Science, Oxford, UK) platform was used to establish size and concentration of vesicles in suspension. Manufacturer's instructions were followed for all measurements, and particles were measured using NP-200 nanopore and calibration particles CPC100 beads (Izon). Samples were analysed until 500 particles were counted, with an optimal size detection ranging from 60 to 400 nm. Following parameters were maintained constant between samples and calibration while measuring size and concentration: stretch of 47.02 mm, Voltage of 0.66 nA, and a pressure of 7 mbar.

2.2.7 Liposomes

Liposomes were prepared using POPC lipids (Avanti Polar). Lipids in chloroform were dried down in a round-bottom flask with nitrogen. Resulting lipid films were stored at -20 °C under nitrogen to prevent oxidisation. Lipid films were rehydrated in liposome buffer (50 mM Tris, 50 mM NaCl, pH 7.4). This was done through vortexing, resulting in large, multilamellar vesicles (LMV). Following this, LMVs were extruded using 1 mL Hamilton syringes to produce smaller unilamellar liposomes at a size of 200 nm. For laurdan assays, extruded liposomes were incubated with 2.5 µM laurdan for at least 1h at 180 RPM at 37 °C, in the dark.

2.2.8 Membrane fluidity assay

Cells were washed and resuspended in PBS at an OD_{600} of 0.4 prior to adding the laurdan fluorescent probe at 5 µM. For EVs, laurdan was added at 2.5 µM. Samples were incubated at 37°C for 1 hour at 180 RPM in the dark. After excitation at 355 nm, fluorescence was measured at both 435 nm and 500 nm using the Mithras plate reader (Berthold technologies, Germany). The GP was then calculated as:

$$GP = \frac{I_{435} - I_{500}}{I_{435} + I_{500}}$$ ***(Equation 1)***

Where I435 stands for the fluorescence intensity measured using a 485 nm emission filter, while I490 is the fluorescence intensity measured using a 535 nm emission filter. The closer the GP is to 1, the more rigid the lipidic bilayer is, and vice versa.

2.2.9 Total cholesterol quantification

Cholesterol was quantified using the colorimetric cholesterol quantification assay kit (Sigma-Aldrich) according to the manufacturer's instructions. The absorbance at 570 nm was measured using the Multiskan FC photometer plate reader (ThermoFisher Scientific, USA). Prior to this assay, the concentration in particles/mL of each sample was measured using the Videodrop (Myriade, France).

2.2.10 Total protein quantification

The total protein content of purified early and late ACdEVs was determined using a colorimetric micro bicinchoninic acid (BCA) protein assay kit (ThermoFisher, UK) according to the manufacturer's instructions. BSA was used as a protein standard. The absorbance at 562 nm was measured with the Nanodrop 1000 (ThermoFisher, UK). Prior to this assay, the concentration in particles/mL of each sample was measured using the Videodrop (Myriade, France).

2.2.11 Lipid Mass Spectrometry
2.2.11.1 Lipid extraction for mass spectrometry lipidomics

Mass spectrometry-based lipid analysis was performed by Lipotype GmbH (Dresden, Germany) as described (Sampaio et al. 2011). Lipids were extracted using a two-step chloroform/methanol procedure (Ejsing et al. 2009). Samples were spiked with internal lipid standard mixture containing: cardiolipin 14:0/14:0/14:0/14:0 (CL), ceramide 18:1;2/17:0 (Cer), diacylglycerol 17:0/17:0 (DAG), hexosylceramide 18:1;2/12:0 (HexCer), lyso-phosphatidate 17:0 (LPA), lyso-phosphatidylcholine 12:0 (LPC), lyso-phosphatidylethanolamine 17:1 (LPE), lyso-phosphatidylglycerol 17:1 (LPG), lyso-phosphatidylinositol 17:1 (LPI), lyso-phosphatidylserine 17:1 (LPS), phosphatidate 17:0/17:0 (PA), phosphatidylcholine 17:0/17:0 (PC), phosphatidylethanolamine 17:0/17:0 (PE), phosphatidylglycerol 17:0/17:0 (PG), phosphatidylinositol 16:0/16:0 (PI), phosphatidylserine 17:0/17:0 (PS), cholesterol ester 20:0

(CE), sphingomyelin 18:1;2/12:0;0 (SM), triacylglycerol 17:0/17:0/17:0 (TAG). After extraction, the organic phase was transferred to an infusion plate and dried in a speed vacuum concentrator. The first step dry extract was re-suspended in 7.5 mM ammonium acetate in chloroform/methanol/propanol (1:2:4, V:V:V) and the second step dry extract in 33 % ethanol solution of methylamine in chloroform/methanol (0.003:5:1; V:V:V). All liquid handling steps were performed using Hamilton Robotics STARlet robotic platform with the Anti Droplet Control feature for organic solvents pipetting.

2.2.11.2 MS data acquisition

Samples were analysed by direct infusion on a QExactive mass spectrometer (Thermo Scientific) equipped with a TriVersa NanoMate ion source (Advion Biosciences). Samples were analysed in both positive and negative ion modes with a resolution of Rm/z=200=280000 for MS and Rm/z=200=17500 for MSMS experiments, in a single acquisition. MSMS was triggered by an inclusion list encompassing corresponding MS mass ranges scanned in 1 Da increments (Surma et al. 2015). Both MS and MSMS data were combined to monitor CE, DAG and TAG ions as ammonium adducts; PC, PC O-, as acetate adducts; and CL, PA, PE, PE O-, PG, PI and PS as deprotonated anions. MS only was used to monitor LPA, LPE, LPE O-, LPI and LPS as deprotonated anions; Cer, HexCer, SM, LPC and LPC O- as acetate adducts.

2.2.11.3 Data analysis and post-processing

Data were analysed with in-house developed lipid identification software based on LipidXplorer (Herzog et al. 2011; Herzog et al. 2012). Data post-processing and normalization were performed using an in-house developed data management system. Only lipid identifications with a signal-to-noise ratio >5, and a signal intensity 5-fold higher than in corresponding blank samples were considered for further data analysis.

2.2.12 Migration assay

Vertical transwell assay migration of macrophages was assessed using the Cytation 5 automated cell imaging reader (Biotek, USA). 700 µL of chemoattractants (~$1x10^9$ ACdEV/mL) was seeded per well on a 24-well plate. Using PVP-free polycarbonate membrane inserts (8.0 µm pore; Corning®, USA), each upper transwell chamber was loaded with 300 µL of THP-1 derived macrophages at a density of $8x10^4$ cells. The 24-well plate was then loaded in the Cytation 5 instrument, and the cell migration was measured by automated imaging of pre-selected fixed positions every 30 minutes over 12 hours (4 positions per well, with 3 technical

replicates per condition). For analysis, the Gen 5 software was used to count the migrated cells at the bottom of each well.

2.2.13 Luciferase-based ATP assay

Jurkat cells were starved for 24h in serum-free and phenol-free RPMI medium before UV treatment to decrease variability of the readouts as phenol can interfere with the luminescence signal. Early or late ACdEV were isolated by differential and ultracentrifugation at 300 x g/5 min, 2000 x g/20 min, or further by ultracentrifugation 100,000 x g/90 minutes. The EVs were then resuspended in SF PF RPMI and incubated for 1 hour at 37 °C with or without detergent. Quantitative amount of ATP present in AC secretome or released by EVs was measured using a luminescent ATP detection assay kit (ab113849: Abcam, Cambridge, MA, USA). EV samples and ATP standards were incubated with D-Luciferin and firefly luciferase reagents. Relative luminescent intensity (RLU) from luciferase activity was recorded using the Omega Plate reader. A standard curve was plotted and luminescent units from each sample were interpolated to calculate the quantitative ATP levels in µM.

2.2.15 Cholesterol depletion

Methyl-β-cyclodextrin (MBCD) (Sigma Aldrich) was used to deplete Jurkat ACdEVs of membrane cholesterol. SEC purified ACdEVs were treated with MBCD in the 10 - 20 mM range and incubated for 30 minutes at room temperature. Cholesterol extraction at 20 mM was used for further experiments.

2.2.16 Zeta potential measurements

Surface charges of non-treated and MBCD-treated 18H ACdEVs were quantified using zeta potential measurements by TRPS with the Exoid (Izon Science). Samples were diluted in PBS and measured with NP-200 nanopores with a 49.9 mm stretch and an applied voltage of 300 mV. 500 particles were measured, and the samples were calibrated with CPC200 standards particles (Izon Science).

2.2.17 Microfluidic isolation of particles

Using the chip SE-015-02-NA-C (µFraction8, Scotland), samples were perfused following manufacturer's instructions. Briefly, a HPLC 515 pump (WatersTM, UK) was used to perfuse the samples at a flow rate of 0.6 mL/min through the input of the microfluidic chip. Calculation of flow rate is part of proprietary data. Samples from the small outlet (SO) and large outlet

(LO) were then collected for further analysis. The flangeless fittings system (XLT-111 - FIngls Sys PEEK 10-32 for 1/16in) was used to connect the chips to tubing.

2.2.18 Characterisation of the microfluidic chip

Nanosphere™ size standards (ThermoScientific, USA) were used for the characterization of the microfluidic chip (SE-015-02-NA-C) designed to separate particles in the desired size range. They were resuspended in PBS solution with 1 % Tween-20 and filtered at 0.22 µm using a PES syringe filter. The polydisperse mixture of nanospheres standard of size 60-, 100-, 150-, 202-, 303- and 1000-nm was of a final concentration of ~$2.52x10^9$ particles/mL. The samples were measured before and after collection at either the small outlet (SO) or large outlet (LO). To do so, 3 µL was loaded onto both TS-400 and TS-2K microfluidic cartridges in order to visualize the different sized nanospheres using the nCS1. Similarly, 18H ACdEVs were resuspended in 0.1 % BSA for accurate characterisation of the microfluidic chip size cut-off.

2.2.19 BSA assay

BSA was diluted in dH_2O to a concentration of 0.1-, 0.2-, 0.3-, 0.4-, and 0.5-% (w/v). The absorbance intensity at 280 nm was measured using the Ultrospec 2000 spectrophotometer (Pharmacia Biotech, USA), and the results were used to draw a standard curve. A 0.2 % BSA solution was made and the absorbance at 280 nm of the collected fractions from both SO and LO were measured. The equation of the linear regression of the standard curve was then used to determine the accurate BSA concentration of the SO and LO fractions.

2.2.20 Statistical analysis

For data analysis, GraphPad Prism v.8. was used. Statistical test used are detailed in the legend of the figures. The probability *p*-values < 0.05 were considered statistically significant (*$p < 0.05$, **$p < 0.01$ and ***$p < 0.001$).

3. Chapter 1: Apoptotic cell-derived extracellular vesicles production

3.1 Introduction

In vitro, apoptosis can be induced biologically by using death ligands such as an anti-Fas antibody (Matsumoto *et al.*, 1995; Yi *et al.*, 2000), or chemically by using cellular damaging agents e.g., doxorubicin hydrochloride (Thakur *et al.*, 2020), staurosporine (Lotsberg *et al.*, 2020), etoposide (Sola *et al.*, 2020), etc. Additionally, as demonstrated across several cell types, ultraviolet (UV) radiation can be used as an apoptotic trigger (Salucci *et al.*, 2013). The kinetics of UV-induced apoptosis are specific to the cell type and the inducer of apoptosis (Wolbers *et al.*, 2004). UV irradiation can induce apoptosis via many different pathways (Kulms and Schwarz, 2000). UV induces nuclear DNA damage which activates the tumour suppressor p53 ultimately leading to oxidative stress. Additionally, UV induces the release or upregulation of death ligands which activates death receptors expressed on the cell. Furthermore, UV directly activates death receptors in a ligand-independent way by inducing receptor clustering. Activated death receptors trimerize and transduce the apoptotic signal via their intracytoplasmic death domain (DD). Finally, UV induces the release of cytochrome *c* from the mitochondria. Several studies have linked UV induced cell death to ROS production (de Jager, Cockrell and Du Plessis, 2017; Xie *et al.*, 2021).

Apoptotic cell death progression starts with internal changes such as chromatin condensation and rapidly the membrane starts to bleb. Towards the end of apoptosis, larger membrane enclosed vesicles, or apoptotic bodies are released. Various phases of apoptosis exist releasing multiple waves of ACdEVs in the extracellular environment. Indeed, apoptotic cell blebbing has been divided into two phases: early and late blebbing. The early phase is restricted to adherent cells only. The late blebbing is characterized by the engulfment of derived endoplasmic reticulum surrounding condensed chromatin. This mechanism is dependent on actin and microtubule activity that drives chromatin towards the periphery of the cell (Lane, Allan and Woodman, 2005). Altogether this suggests that different EV population are released during early and late apoptosis phases.

When studying ACdEVs, and more generally EVs, it is crucial to first confirm their presence. As mentioned previously, EVs can be mixed up with non-EV contaminants that would share the same characteristic used for their isolation (size, density, affinity, etc). Here, EVs are isolated by differential centrifugation followed by size exclusion chromatography.

3.2 Aims and objectives

The aim of this chapter is to validate a model for *in vitro* apoptosis induction and release of ACdEVs in mammalian cells. Due to a more extensive characterization of apoptotic bodies (Xu, Lai and Hua, 2019), this study will focus on smaller vesicles populations looking at both early and late AC derived EVs. This chapter also aims to define the kinetics of UV induced cell death in Jurkats and confirm the presence of EVs in AC secretome using a variety of techniques including flow cytometry and cryogenic transmission electron microscopy (Cryo-TEM).

3.3. Results

3.3.1 UV irradiation induces apoptosis in Jurkats

To study apoptotic cell clearance, various cell lines can be used. Jurkat cells are an immortalized line of T lymphocyte cells originally obtained from the peripheral blood of a 14-year-old boy with T cell Leukaemia. Previously, the Jurkat cell line has been used to model and characterize infection and immunity (Montano, 2014) as well as inflammation and apoptotic EVs (Gholijani *et al.*, 2015; Oh *et al.*, 2016; Németh *et al.*, 2017; Poon *et al.*, 2019). For the purpose of this study, the cells were treated with an intermediate UV-B dose of 30mJ/cm² (Dr Lois Grant, personal communication), as lower doses lead to a non-inflammatory response which would not be relevant for the study of inflammation (Masuda, Kimura and Morita, 2019). *In vitro* markers commonly used for the detection of apoptosis include morphological changes and PS exposure on the outer leaflet of the cell membrane.

To establish the kinetic of UV-induced apoptosis, the irradiated cells were analysed by flow cytometry at different time points (0-, 2-, 6- and 18-hours post UV treatment). Cell death and viability were measured using annexin V/propidium iodide staining. Phosphatidylserine (PS) is restricted to the inner monolayer of the plasma membrane in viable cells whereas, during the early stage of apoptosis, PS is externalised to the outer monolayer while the plasma membrane retains its integrity. In the presence of calcium, annexin V (AnV) binds to PS with high affinity. Coupled to a FIT-C fluorophore, An-V is used as an indicator of early apoptosis.

Propidium iodide (PI) is a membrane impermeable dye that stains nucleic acids. When the plasma membrane integrity is lost during the later stage of apoptosis, PI can enter the cells and bind to nucleic acids. Distinct stages of cell apoptosis were observed with this assay, where early apoptotic cells are AnV positive and PI negative (AnV-FITC +/PI-), late apoptotic/necrotic cells are AnV/PI-double-positive (AnV-FITC+/PI+), and viable cells are double negative (AnV-FITC-/PI-) as shown in (**Figure 3.1)**.

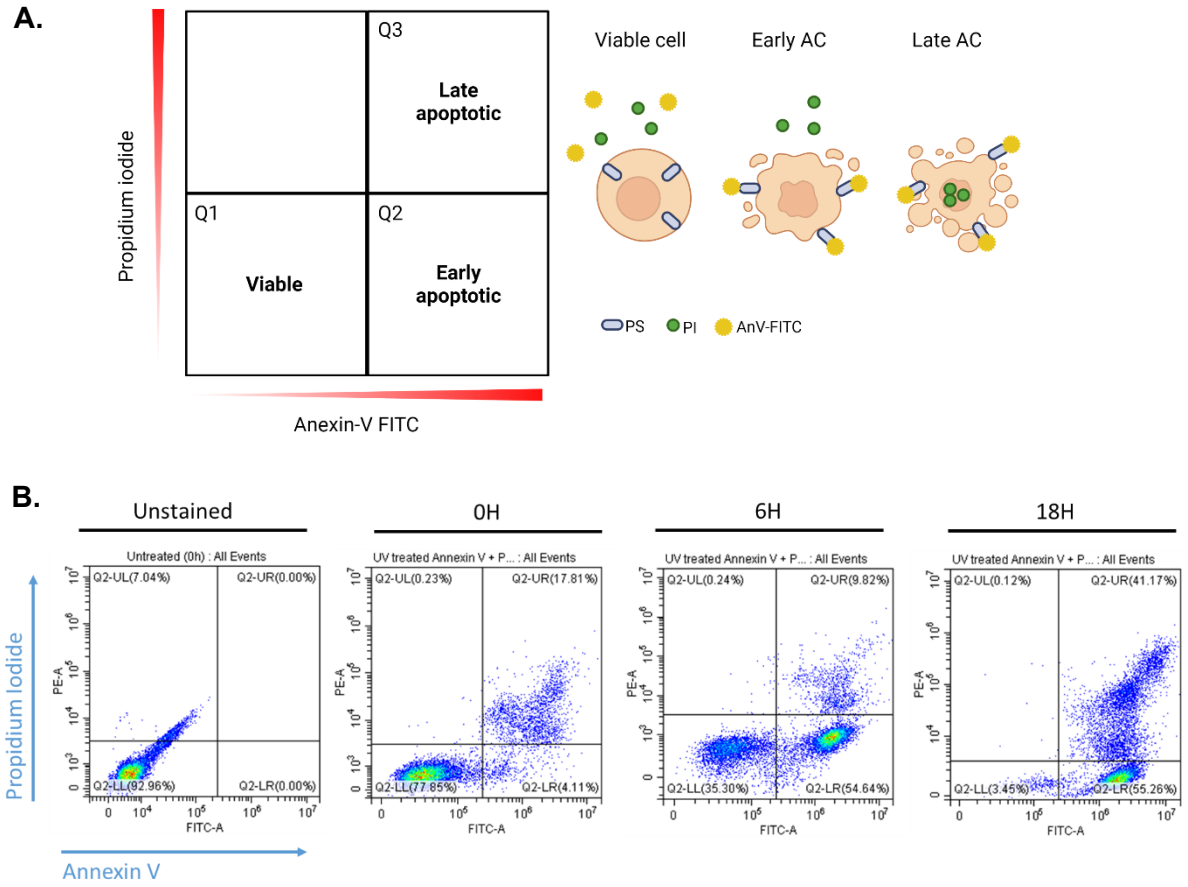

Figure 3.1: Annexin V / propidium iodide assay for the detection of apoptosis. (a) *Schematic representation of the principle of the assay. Viable cells can be detected in the first quadrant (Q1), early apoptotic cells in the second quadrant (Q2), and late apoptotic cells in the third quadrant (Q3). Viable cells are unstained, early apoptotic cells (AC) are stained with AnV-FITC binding to the externalised phosphatidylserine (PS), and late AC are stained with both AnV-FITC and propidium iodide (PI) binding to the accessible cellular DNA.* ***(b)*** *Representative flow cytometry plots of the assay showing cell viability through time gated against the unstained cell population.*

Additionally, UV-induced apoptosis was observed by light microscopy (**Figure 3.2.a**). The non-induced Jurkat cells (untreated) appear spherical and healthy looking, whereas 18H irradiated cells display membrane blebbing and budding, releasing apoptotic bodies, as well as cell shrinkage resulting in a denser cytoplasm. These microscopic characteristics are major morphological hallmarks of apoptosis (Salucci *et al.*, 2013), and thus support the cell viability assay data.

Healthy cell cultures are characterized by 80-95 % cell viability, which may vary due to the growth conditions such as the temperature, pH, CO_2 and O_2 levels, confluency, and medium composition (Segeritz and Vallier, 2017). From the flow cytometry data (**Figure 3.2.b**), the live culture showed an average of 77.7 % viable Jurkat cells prior to UV treatment, this could be explained by the several factors stated above. The percentage of viable cells was deemed reasonable to qualify as a healthy cell culture. After 18H-post UV this percentage decreases, with only 2.04 % viable cells remaining. This shift in cell viability over time also reveals that the significant distinction between early and late apoptosis starts at 6H post UV treatment, which will be the time point chosen for further analysis of early apoptosis (**Figure 3.2.b**).

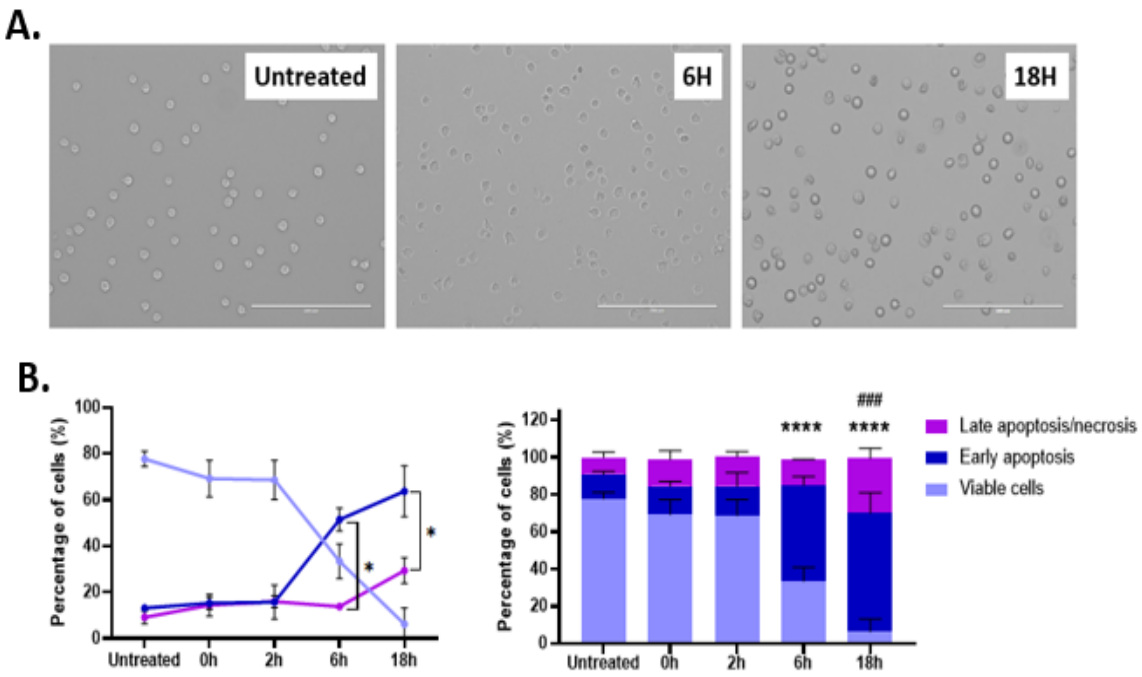

Figure 3.2: UV irradiation induces cell death in Jurkat cells after 18 hours incubation. (a) *Microscopic signs of apoptosis in Jurkat cells. Untreated, early and late apoptotic cells were imaged by bright field microscopy at 20X magnification. Scale bar = 200 µm.* ***(b)*** *On the* ***left****, the cell viability is represented as the progression of cell death with time. 2-way anova with Tukey's multiple comparison test showing the significant difference between early and late apoptosis from 6H and 18H. On the* ***right****,*

the apoptosis assay is represented as the percentage of cells in each condition. 2-way anova with Dunnett's multiple comparison test showing the significant mean difference between pre-treatment with 6H and/or 18H for early apoptosis (asterisk) and late apoptosis (hashtag). Samples were measured in three independent biological repeats (N=3). Error bars represent +/- SD and + SD.

The variability between biological repeats, and the 6.24 % of live cells present in the samples 18h post UV irradiation can be explained by the fact that cells are not previously synchronized and might thus undergo apoptosis at various times. Additionally, cells can take up to 24 hours to fully undergo apoptosis. 18 hours was judged adequate to obtain an acceptable percentage of late apoptotic cells for further experiments. Because some cells remain viable up to 18h after induction of apoptosis, it should be noted that EVs that do not classify as ACdEVs are also released. However, as commonly known, dying cells release much more EVs than viable cells, which is sufficient to say that the AC secretome is highly enriched in ACdEVs rather than viable cells derived EVs (Distler *et al.*, 2005; Baxter *et al.*, 2019).

Altogether, these results show that the UV-B dose of 30 mJ/cm^2 used is sufficient to induce nearly total cell death after 18 hours of incubation as observed by their loss of membrane integrity and morphological changes. This model of cell death will be used to further study ACdEVs collected at either 6 hours or 18 hours post UV irradiation as a model of early and late apoptosis, respectively. To avoid artefactual measurements of ACdEVs due to storage conditions, ACdEVs were always processed from fresh samples to avoid particle loss, purity reduction and particle fusion (Gelibter *et al.*, 2022).

Even though the mechanisms are largely conserved across all cells, broad observations unravelled in this chapter would have to be validated in other cell lines. Although no different methods for inducing apoptosis were tested in this study, it was shown that UV-B exposure was sufficient to induce apoptosis in Jurkat cells. Other types of cell death such as necrosis, ferroptosis or pyroptosis can also expose PS on the outer leaflet of the membrane, the Annexin V/ PI assay alone is not sufficient to validate our *in vitro* apoptosis model. The inactive pro-caspase 3 is present in viable cells, and activated during both intrinsic and extrinsic apoptotic pathways, ultimately executing cell death. To be activated, caspase 3 is cleaved by caspase 9 into individual units forming an active tetrameric effector caspase 3 (Asadi *et al.*, 2022). A western blot against active cleaved caspase 3 level following UV irradiation in Jurkat cells would be sufficient to confidently state that apoptosis is the type of cell death induced.

3.3.2 Evidence of EVs

EVs were isolated from early or late apoptotic cells by differential centrifugation followed by size exclusion chromatography (SEC). In more detail, irradiated cells in serum free media were first centrifuged at 300 x g for 5 minutes to pellet the apoptotic cells, and the supernatant (SN) was then centrifuged at 2000 x g for 20 minutes to remove larger cellular debris and apoptotic bodies. The 2000 x g SN was then concentrated and loaded onto a qEV SEC column with a 70 nm cut off, purifying ACdEVs from small contaminants such as soluble proteins. To identify the particles secreted from early and late apoptotic cells, multiple techniques were combined such as nanoparticle tracking analysis (NTA), interferometric light microscopy (ILM), flow cytometry (FCM) and electron microscopy (EM). Firstly, the AC secretome or 2000 x g SN was measured by NTA and ILM.

Nanoparticle tracking analysis measures particle's hydrodynamic diameter and concentration based on their Brownian motion. The Brownian motion can be defined as the random movement of particles in a liquid caused by collision with molecules of the containing liquid, which can be affected by the liquid's viscosity. Using the ZetaView instrument, each individual particle in the field of view is counted and tracked in short video clips. Particles present in the 2000 x g SN can be seen by NTA (**Figure 3.3.a**). Based on a similar principle as NTA, interferometric light microscopy was also used to visualize particles (**Figure 3.3.b**). This technique involves an optic system coupled to a camera, which generates a movie based on real time displacement of the particles, allowing to define the size and number of observed particles based on their trajectories' speed and distance.

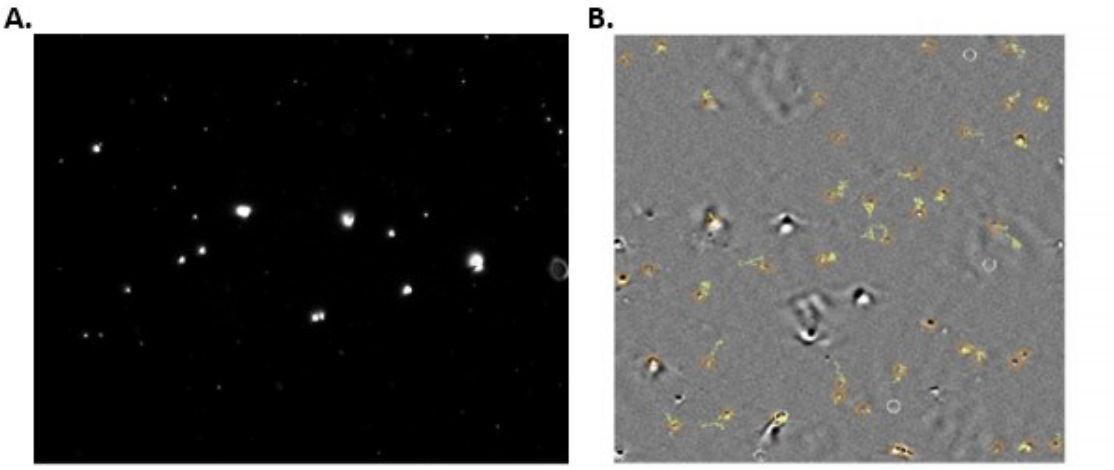

Figure 3.3: Evidence of nanoparticles in the apoptotic cell secretome. *2000 x g supernatant of 18h AC was measured by NTA and ILM.* ***(a)*** *Screenshot of the generated video with the ZetaView (ParticleMetrix).* ***(b)*** *Screenshot of the generated movie showing detected particles (circles) and tracked particles (orange circles) along with their displacement trajectories (yellow) observed with Videodrop (Myriade).*

Both these techniques confirmed the presence of particles in the apoptotic cells secretome. However, NTA and ILM cannot discriminate between EVs from nanobubbles, salt precipitates, soluble proteins, similar sized particles, and similar refractive index particles. This limited visualisation of particles was resolved by using a standard EV imaging technique: Cryo-TEM. It allows the visualization of the native morphology of EVs by giving information on the number of lipid bilayers, the internal structures, the size, and the shape of the vesicles. Additionally, Cryo-TEM can also be used to assess the purity of the samples. Cryo-TEM is the least invasive EM techniques to visualize samples, as the samples are plunge frozen avoiding the use of dehydration and fixation which can damage the samples and cause artifacts (Chernyshev *et al.*, 2015; Choi and Mun, 2017). An accelerated electron beams passes through the samples and the transmitted electrons are then collected to generate EM brightfield images.

SEC purified AC secretome from 6H and 18H post UV irradiation were imaged by cryo-TEM. The EM images confirmed the presence of EVs as distinct lipid bilayer encapsulated particles were observed in both samples (**Figure 3.4**). Due to the sparse number of images taken (<10 per condition), the accurate particle size distribution could not be estimated. Although not

representative of the samples, it can be noted that EVs varied in diameter from 108 to 678 nm and from 11 to 590 nm in early and late ACdEVs samples, respectively, already showing a high heterogeneity. Additionally, it shows that at by using a sedimentation speed of 2000 x g, particles with a diameter up to ~ 700 nm can be recovered from the supernatant of apoptotic cells. Furthermore, both samples showed an important diversity in structures, morphologies, and cargos.

Most vesicles were encapsulated by a single lipidic bilayer; however, some were classified as double membrane vesicles (**Figure 3.4.a.1,2**) as well as multilamellar vesicles when a smaller vesicle was found in the lumen of a larger vesicle (**Figure 3.4.b.1**). The diversity of vesicles was also observed based on their shape. Although most of the imaged vesicles were round shaped, some variants were cup shaped (**Figure 2.4.a.4, b.4**), oval (**Figure 3.4.a.5, b.3**), or elongated (**Figure 3.4.b.7**). The absence or presence of cargo was determined by the level of grey intensity within the vesicle lumen corresponding to a low- or high- electron density, respectively. The absence of cargo was observed when the lumen was smooth and light, whereas the presence of cargo was identified by a darker granular lumen. Vesicular cargo is often identified as proteins. Interestingly, some vesicles also displayed actin like filaments structures (**Figure 3.4.a.2**), possible vestige of their biogenesis pathway. Small spherical dense structures were also observed in vesicles (**Figure 3.4.a.4, b.2**). Some vesicles also seem to carry membrane bound cargo that could be glycosylation or protein corona (**Figure 3.4.b.1,3,5**), potentially useful for EV uptake and signalling. Interestingly, EV with compromised membrane integrity were identified, which could be a result of breakage during sample preparation (**Figure 3.4.b.4**). Other variants were shown to be surrounded by dark granular material similar to the one found in the vesicle lumen suggesting that it could be classified as secreted material (**Figure 3.4.a.3**).

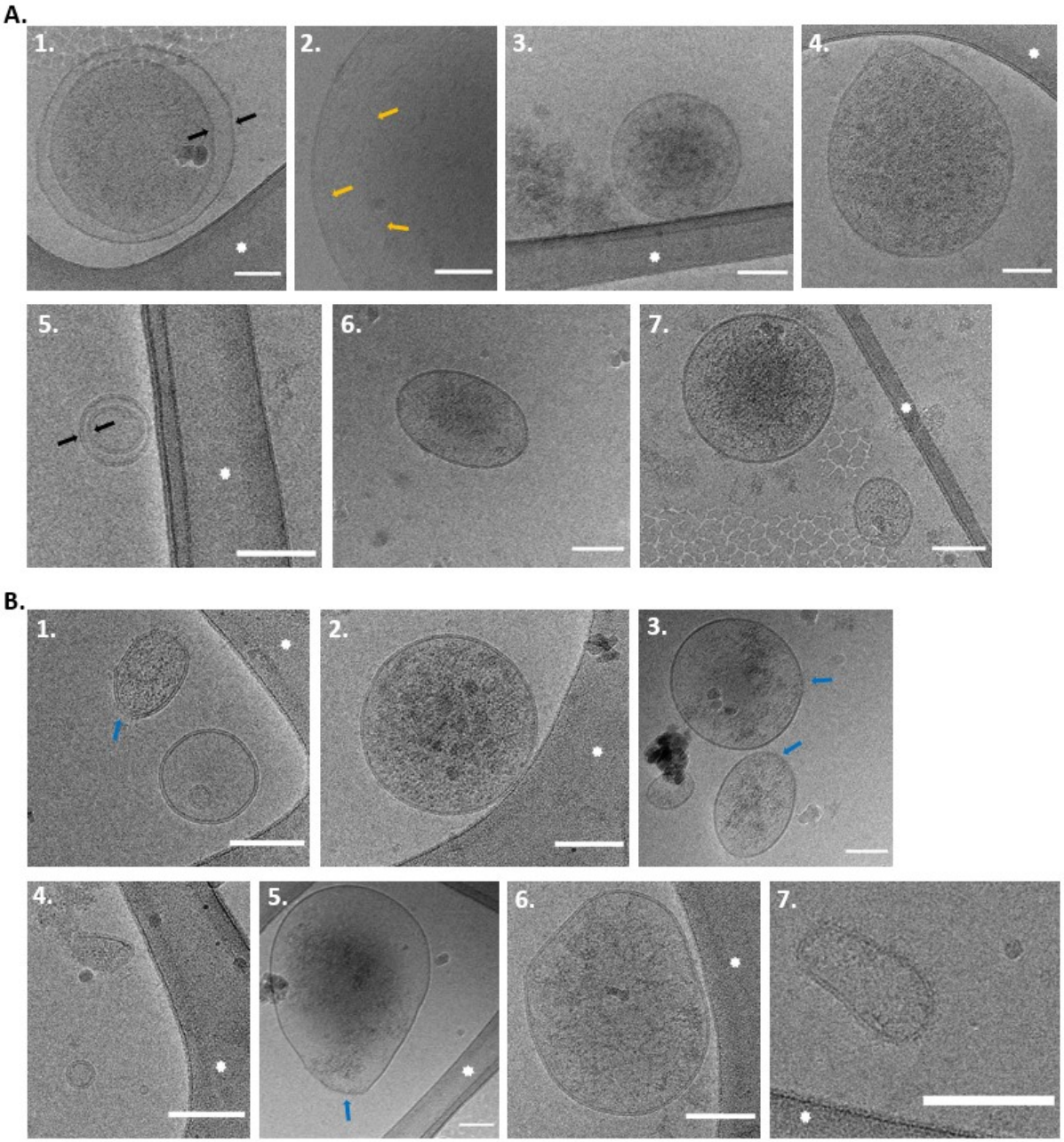

***Figure 3.4: Cryo-TEM images of isolated ACdEVs derived from Jurkat cells**. **(a)** Images of early ACdEVs. **(b)** Images of late ACdEVs. The black arrows point to vesicles with double membranes. The yellow arrows point to actin filament like structures. The blue arrows point to membrane bound EV cargo. The white asterisk shows the EM grid. Scale bar = 100 nm.*

For the Cryo-TEM imaging of EVs, the morphology of larger particles observed can be criticized. The ice layer is realistically under 200 nm thick to allow the beam of electron to go through, consequently any large particles are likely to be distorted exhibiting an altered morphology. Interestingly, some large EVs were cup shaped, which is usually a result of

dehydration of the samples as seen in previous studies. Here, the samples were plunge frozen which suggests that the morphology observed could indeed be the one of native state of the EVs. Specific packing of lipid could affect the curvature of membranes and could explain the non-spherical shapes of certain ACdEVs.

3.3.3 Labelling and detection of EVs by flow cytometry

Despite the precautions taken in washing the cells, depleting the media of serum, and purifying the EVs by SEC, some non-vesicular contaminants and debris remain, as seen by the cryo-TEM images (**Figure 3.4**). Labelling of EVs can shed light on the levels of non-vesicular contaminant present in the samples. Due to the lack of specific biomarkers on the surface of ACdEVs, a specific antibody could not be used. It was therefore more convenient to use a reactive dye to directly label membrane proteins within the EVs membrane. Here, Bodipy FLN-(2 aminoethyl)maleimide was used. As maleimide acts as a reactive probe, it irreversibly binds to free cysteine thiols present in membrane proteins thus labelling the EV membrane.

Due to a limitation on the filters available within the flow cytometer, it was important to validate the use of Bodipy for EV labelling. Bodipy and FITC fluorescence spectra are similar with a maximum excitation at 503 nm and 490 nm, and a maximum emission at 512 nm and 525 nm, respectively (**Figure 3.5**). This allows us to measure Bodipy fluorescence using a 488 nm excitation laser line and the common FITC filter to collect emissions from the Bodipy dye.

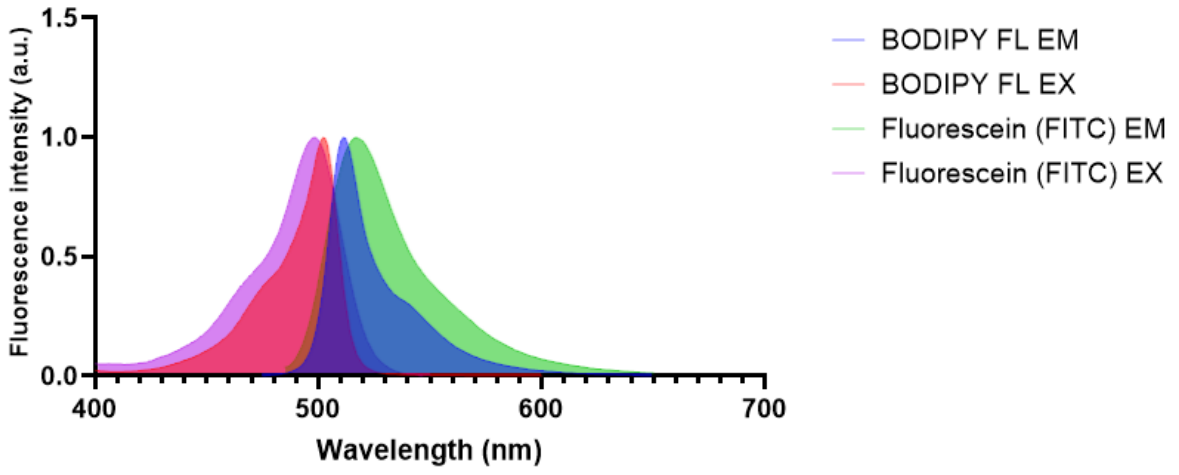

Figure 3.5: Fluorescence spectra of Bodipy and FITC dyes. *CSV data of Bodipy FL and Fluorescein FITC spectra were downloaded from www.FPbase.org. Arbitrary units (a.u.).*

The thiol reactive Bodipy maleimide dye was first titrated at 1-, 5-, and 10- μM to label ACdEVs (~1.5 $x10^9$ particles/mL) present in the 18h apoptotic cell secretome as shown in the representative flow cytometry plots (**Figure 3.6.a**). Analysis of the percentage of stained EVs showed a significant 1.3-fold increase in the number of stained EVs when using 1 μM and 5 μM of Bodipy, respectively (**Figure 3.6.b**). However, using 10 μM of Bodipy showed no significant difference in the percentage of FITC positive events from using 5 μM. Additionally, the mean fluorescence intensity (MFI) for FITC increased proportionally when Bodipy was added from 5 μM to 10 μM, meaning that EVs are becoming more fluorescent in opposition to more EVs being stained (**Figure 3.6.b**). The titration of Bodipy allowed determination of the optimal concentration for a maximum EV labelling coverage. Here, around 80 % of vesicles were labelled when using 5 μM of Bodipy.

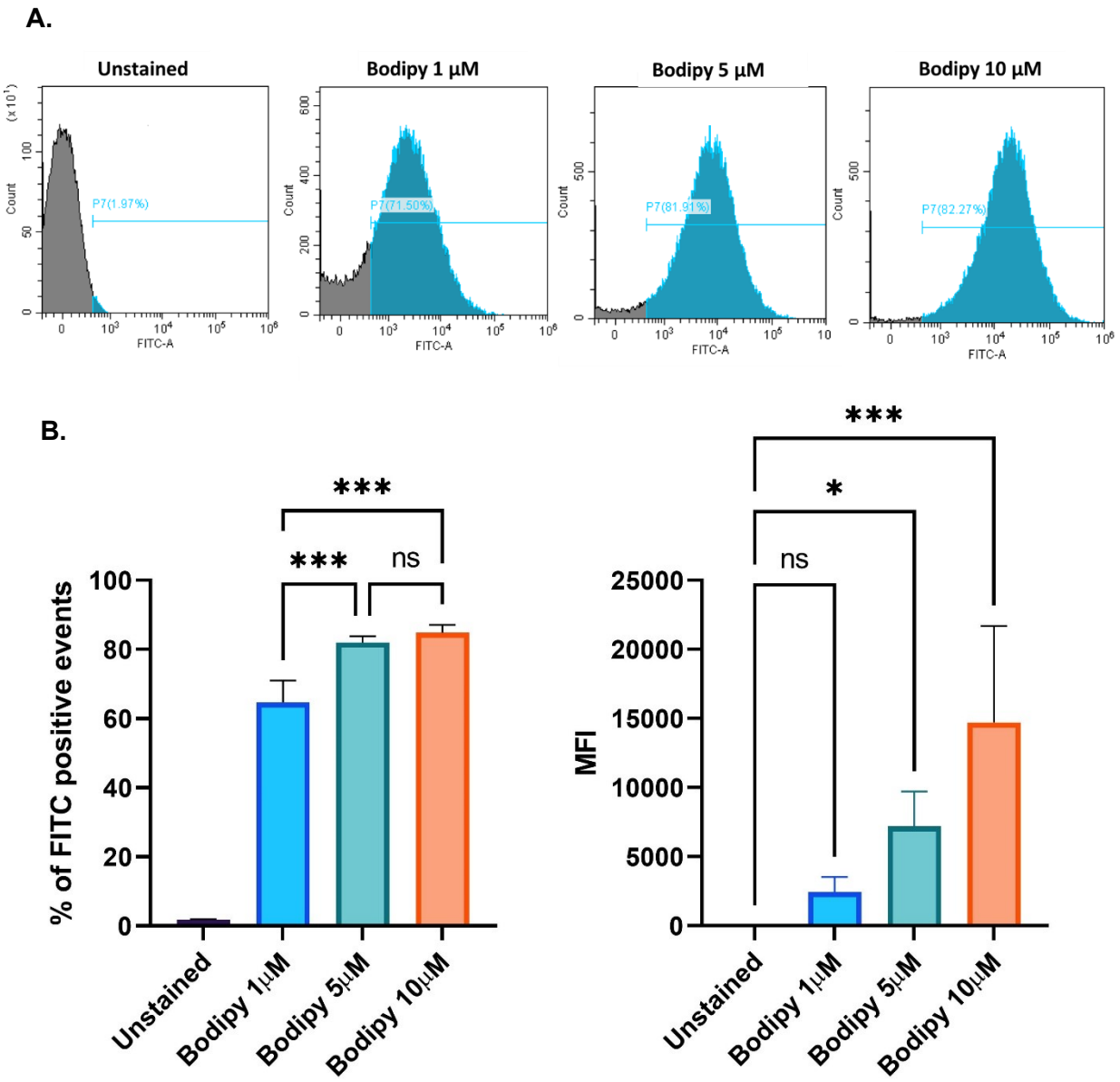

Figure 3.6: Titration of Bodipy FL for ACdEVs labelling. *18H ACdEVs from Jurkats were incubated with the Bodipy dye and detected by FCM.* ***(a)*** *Representative flow cytometry plots from 4 biological repeats showing Bodipy positive ACdEVs in the FIT-C channel, stained with 1-, 5-, and 10-µM of Bodipy.* ***(b)*** *The percentage of positive events is represented (left) as well as the FIT-C MFI (right). Samples were measured in four independent biological repeats (N=4). Error bars represent SD, statistical test used: one-way anova for multiple comparisons.*

As the use of flow cytometry to detect small particles can be challenging due to their size in comparison with the laser wavelength, violet side scatter was used as a trigger as this laser

has a shorter wavelength of 405 nm compared to the commonly used 488 nm laser. Additionally, Megamix-Plus SSC and FSC fluorescent beads were used to gate relative size regions of 100-, 160-, 200-, 240-, 300-, 500-, and 900 nm to allow further determination of the ACdEVs size (**Figure 3.7.a**). By amplifying the FITC signal in the FITC fluorescent channel, as represented by the gain increase from 200 to 1500, smaller stained particles were detected (**Figure 3.7.a**). Using the optimized flow cytometry settings, a gating strategy was drawn to detect all EVs present in the measured samples against the unstained population (**Figure 3.7.b**).

Lastly, the size of the labelled particles suggests the presence of EVs rather than contaminant, as the majority of the FITC positive events falls within the 100 nm diameter region (**Figure 3.7.c**). The size distribution of the Bodipy-labelled particles depicts a typical EV population, supporting the previous statement. Ultimately, Bodipy labelled ACdEVs were detected by flow cytometry using violet side scatter trigger and a 1500 FITC gain.

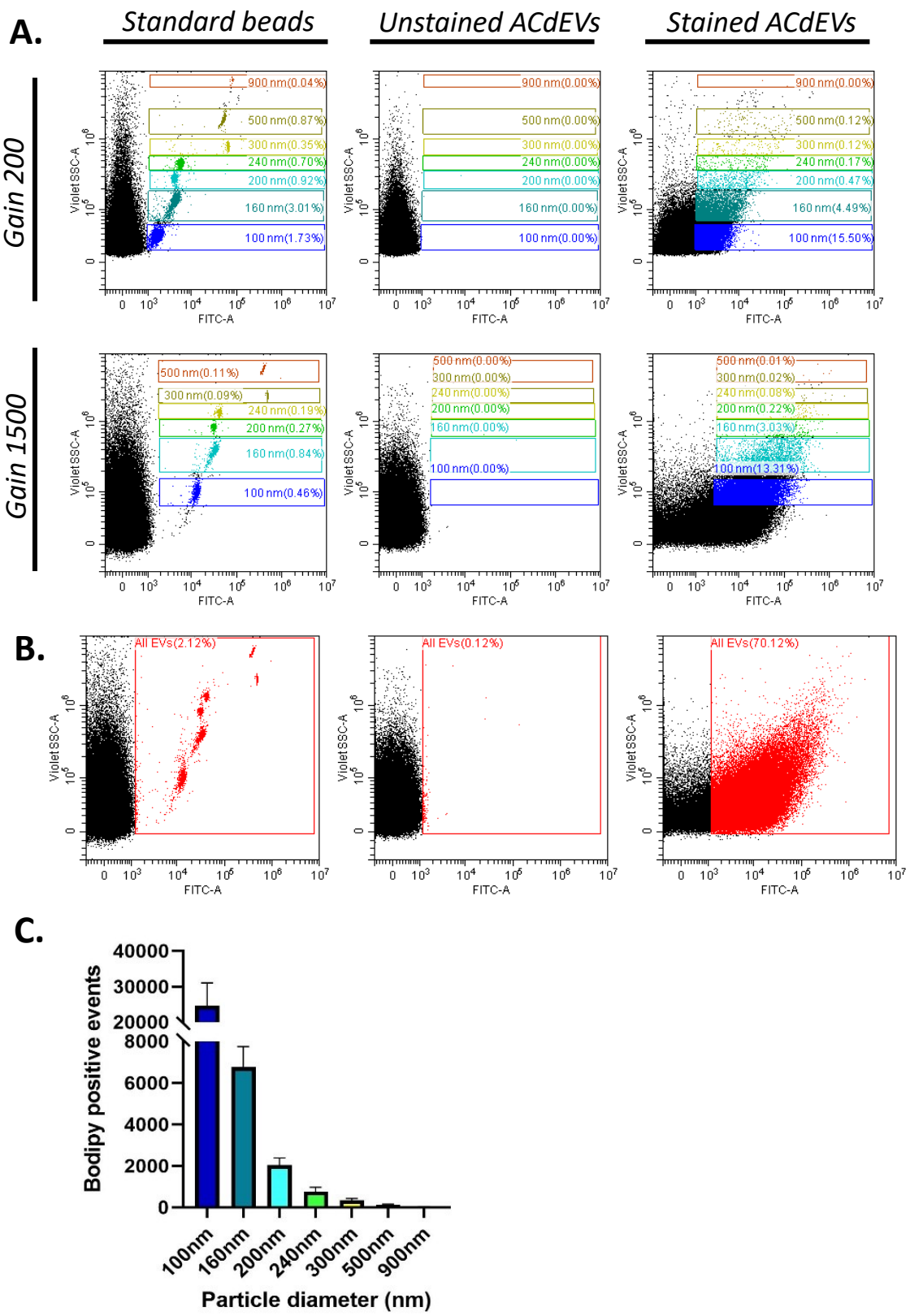
A.
Standard beads
Unstained ACdEVs
Stained ACdEVs
Gain 200
Gain 1500
900 nm(0.04%)
500 nm(0.87%)
300 nm(0.35%)
240 nm(0.70%)
200 nm(0.92%)
160 nm(3.01%)
100 nm(1.73%)
900 nm(0.00%)
500 nm(0.00%)
300 nm(0.00%)
240 nm(0.00%)
200 nm(0.00%)
160 nm(0.00%)
100 nm(0.00%)
900 nm(0.00%)
500 nm(0.12%)
300 nm(0.12%)
240 nm(0.17%)
200 nm(0.47%)
160 nm(4.49%)
100 nm(15.50%)
500 nm(0.11%)
300 nm(0.09%)
240 nm(0.19%)
200 nm(0.27%)
160 nm(0.84%)
100 nm(0.46%)
500 nm(0.00%)
300 nm(0.00%)
240 nm(0.00%)
200 nm(0.00%)
160 nm(0.00%)
100 nm(0.00%)
500 nm(0.01%)
300 nm(0.02%)
240 nm(0.08%)
200 nm(0.22%)
160 nm(3.03%)
100 nm(13.31%)
B.
All EVs(2.12%)
All EVs(0.12%)
All EVs(70.12%)
C.
Bodipy positive events
40000
30000
20000
8000
6000
4000
2000
0
100nm
160nm
200nm
240nm
300nm
500nm
900nm
Particle diameter (nm)

Figure 3.7: Optimisation of extracellular vesicles detection by flow cytometry. *The detection of EVs present in the 2000 x g SN of apoptotic Jurkat T cells incubated for 18h was optimized. MegaMix side scatter beads and Bodipy labelled EVs were detected by fluorescence in the FITC channel, and their size was differentiated by violet side scatter.* ***(a)*** *Optimization of flow cytometry settings using 200 and 1500 gain settings on MegaMix beads, unstained EVs, and stained EVs.* ***(b)*** *Representative scatter plots of the gating strategy for EV detection.* ***(d)*** *Histogram representing Bodipy positive events frequency gated by size according to the regions in which the bead standards fall. Samples were measured in three independent biological repeats (N=3). Error bars represent +SD.*

3.4 Conclusion

This chapter has validated an *in vitro* method to induce apoptosis using UV irradiation and defined its kinetics using anV/PI staining. Early and late apoptosis time points were set at 6H and 18H post UV treatment. The apoptotic cell secretome was analysed by nanoparticle tracking analysis and interferometric light microscopy where particles were detected. The presence of EV was then confirmed by cryo-TEM, showing a vast heterogeneity in structures, morphology, and size at both time points. Finally, EVs were successfully stained using a thiol reactive dye and detected by flow cytometry for further analysis. The size of the labelled particles as well as the presence of a lipidic bilayer suggest that most of the particles in the samples are EVs.

4. Chapter 2: Characterization of ACdEVs

4.1 Introduction

Chapter 1 demonstrated the isolation of particles consistent with ACdEVs, which now require further characterisation. The characterisation of EVs can be based on several parameters, but often it is particle size distribution (PSD) that prevails. However, the small size of EVs can be challenging as it can be below the resolution thresholds of detection methods. Additionally, there is yet to be a standard method for the detection of EV. Based on the MISEV guidelines (Théry *et al.*, 2018), the best approach is to combine a variety of techniques to get reliable and appropriate measurements. Conventional method includes nanoparticle tracking analysis (NTA), flow cytometry (FCM), dynamic light scattering (DLS), tunable pulse resistive sensing (TRPS), electron microscopy (EM), and atomic force microscopy (AFM).

DLS is a popular technique for particle sizing as it is inexpensive and relatively easy to use. The principle of this technique is based on the ability of particle to scatter light, the more a particle scatters light, the bigger the particle and vice and versa (Rozo *et al.*, 2020), assuming that all particles are spherical. However, as bigger particles will scatter more light, it can oversize a polydisperse sample. NTA is also based on light scattering, however, it is equipped with a camera that can track the trajectory of a particle (Filipe, Hawe and Jiskoot, 2010). Based on the Brownian motion of the particles present in the sample, their size can be measured. In TRPS, particles passing through a tunable nanopore are detected by a transient change in the ionic current. The amplitude and frequency of this event gives information on the particle size and sample concentration. A newly improved method called microfluidic RPS (MRPS), is based on the same principle with the advantages of using single use, pre-calibrated microfluidic cartridges for sterility and contamination purposes. Another improvement of a conventional technique has led to a better detection of small particles. Indeed, high resolution FCM (HR-FCM) measures the PSD of samples by using a highly sensitive side-scatter channel to trigger particle events enabling the detection of particles as small as 40 nm. Interferometric light microscopy (ILM) is another method that allows the detection of particles under the diffraction limit of standard FCM. The ILM technique utilizes an optic system coupled to a camera that generates a movie based on real time displacement of the particles. Their size and number are based on their trajectories' speed and distance. Whilst size is clearly an

important parameter for nanoparticles, it is likely that their biophysical properties and components also influence their function.

Membranes are a major physical barrier against the extracellular environment. Here we focus on membrane fluidity as it is important for cell communication and function such as lipid and protein diffusion, permeability, membrane fusion, molecule distribution, etc. Membrane fluidity refers to the viscosity of the lipid component of a membrane. In this study, the laurdan assay is used to quantify the membrane fluidity of cells and EVs, even though other techniques can be used (Szalontai *et al.*, 2000; Poojari *et al.*, 2019). In more detail, the laurdan assay is measured by observing the emission shift of the fluorescent hydrophobic probe 2-dimethylamino-6-laurylnaphalene (laurdan) incorporated in the membrane (Parasassi and Gratton, 1995). As laurdan is sensitive to the polarity in the lipidic bilayer, the shifts in its emission spectrum are caused by the variations in membrane contents allowing indirect measurement of membrane fluidity. It should be noted that laurdan does not measure fluidity directly, rather the accessibility of water around the lipid headgroups which is strongly influenced by the phase of the membrane. This can be analysed through the generalized polarisation (GP) value (**Equation 1**). I_{440} stands for the fluorescence intensity measured using a 440 nm filter, while I_{490} is the fluorescence intensity measured using a 490 nm filter. The closer the GP is to 1, the more rigid the lipidic bilayer is, and vice versa. The membrane lipid order of different EV subtypes has been previously characterised using flow cytometry where the following GP values were measured: −0.14, 0, and 0.36 for apoptotic bodies (APOs), microvesicles (MVs), and EXOs, respectively (Osteikoetxea, Balogh, *et al.*, 2015). This study shows that ACdEVs (here, apoptotic bodies) are the most fluid type of EVs compared to MVs and EXOs. Membrane fluidity can be affected by the membrane composition in lipids, proteins, and sterols, as well as thermodynamic parameters such as temperature and pressure (Los and Murata, 2004).

Lipids are extremely important when it comes to membranes as they are the fundamental building blocks. The main components of plasma membranes are phospholipids (PLs) which consist of a hydrophobic tail made of two fatty acids (FA) linked to a hydrophilic head made of a glycerol backbone and a polar head group linked by a phosphoric acid. The position of FA is numbered based on their stereospecificity relative to which glycerol carbon they are attached to (sn-1, sn-2, and sn-3).

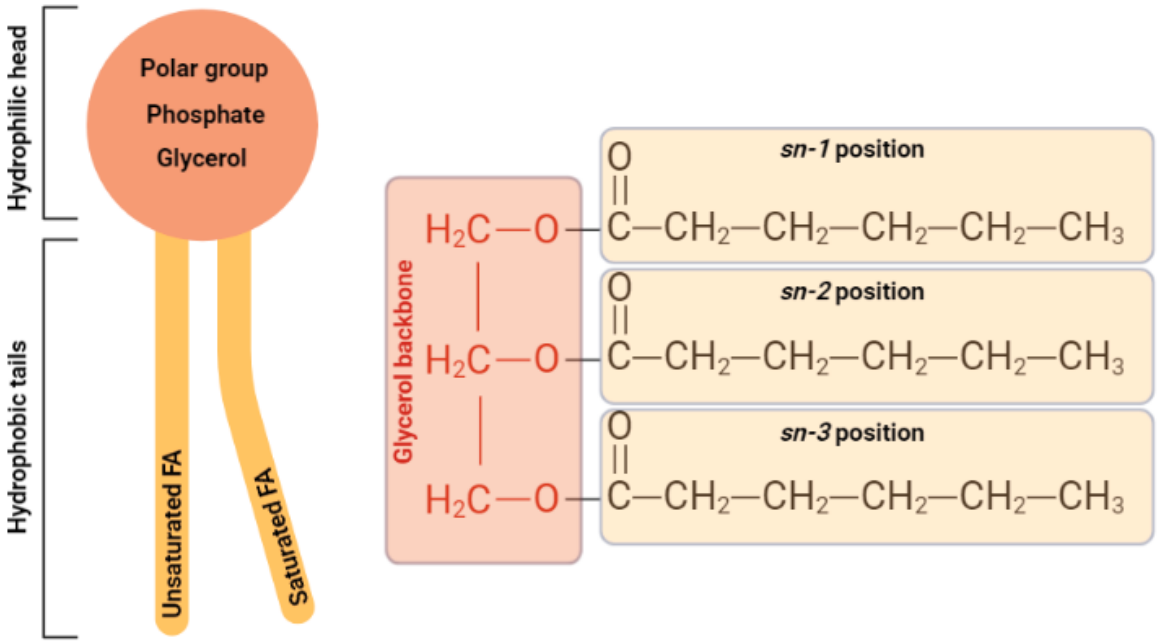

Figure 4.1: Generic structure of lipids*. Schematic representation of a phospholipid structure composed of a hydrophilic head (a polar group attached to a glycerol via a phosphate), and a hydrophobic tail (unsaturated and/or saturated fatty acids based on the absence or presence of double bonds). The FA chains are linked to the glycerol backbone at sn-1, sn-2 in phospholipids or sn-3 positions in a TAG.*

Other lipid classes can be found based on the structure of the lipids such as glycolipids, sphingolipids, sterols, and more. The degree of unsaturation of lipid corresponds to the number of double bounds found in lipid acyl chains. It is highly regulated and can influence the viscosity of a membrane (Ballweg *et al.*, 2020). Saturated lipid chains are more closely packed leading to a more rigid membrane whereas unsaturated lipid chains increases the fluidity (Koynova and Caffrey, 1998; Lee *et al.*, 2020). This is largely due to the formation of hydrogen bonds between the acyl chains, which are less able to form between "kinked" unsaturated chains. The length of the acyl chains will influence the fluidity of the membrane as well (Denich *et al.*, 2003). The longer the tails are, the more interactions between the phospholipids tails there will be thus adding rigidity to the membrane. Additionally, short acyl chains under twelve carbons cannot form hydrophobic interactions with surrounding proteins and lipid and display an increased tail motion (increased fluidity). Short acyl chains such as these are rare within natural phospholipid bilayers. The lipid shape, also known as packing parameter, can directly influence the curvature of the membrane, based on the polar head to acyl chain ratio (Yang, 2016). Small area ratio of polar head to acyl chain result in a cone shaped lipid (phosphatidylethanolamine), leading to a negative curvature. Additionally, equal

head to chain ratio forms cylinder shaped lipid (phosphatidylcholine, sphingomyelin), resulting in a neutral curvature. Finally, larger head than the acyl chain area leads to inverted cone shaped lipid (Lyso-phosphatidylcholine), leading to a positive curvature. Ultimately, curvature is linked to the complex lipid composition of membranes (Holthuis and Menon, 2014), as well as plasma membrane protein activities as it can modulate their conformation (McIntosh and Simon, 2006).

4.2 Aims and objectives

The aim of this chapter is to characterise both early and late ACdEVs' composition and properties to have a better understanding of their functions. The objectives are to select an appropriate analytical technique for particle sizing, as well as defining the membrane fluidity of EVs and their lipidic composition.

4.3 Results

4.3.1 Particle size distribution

Since there is an important number of sizing methods and instruments and that it is impossible to assess them all for the analysis of ACdEVs, a few common techniques were chosen (**Figure 4.1**).

Here the ACdEVs mean size diameter was compared by DLS, TRPS, MRPS, HR-FCM, FCM, ILM and NTA (**Figure 4.2.a**). It should be noted that the particles mean diameter is not representative of the ACdEVs polydispersity, but it gives information on the instrument resolution and reproducibility of the measurements. The lowest mean particle diameter (MPD) measured for ACdEVs samples was using MRPS with 75.9 nm followed closely by HR-FCM with 80.64 nm. Interestingly, the TRPS method that uses the same principle as MRPS with a similar measurement range showed a MPD of 257.3 nm. The other techniques showed a higher MPD with FCM (124.9 nm), NTA (174.3 nm), DLS (232.7 nm) and ILM (269 nm), in increasing order. It is worth noting that each instrument and techniques have their own limitations in regard to their resolution (**Figure 4.2.b**). Some are tunable with different sized nanopores/cartridges to focus on a specific measurement range (MRPS and TRPS). Some have a wider resolution allowing a wider representation of the entire population while maybe losing in precision (DLS, FCM, NTA, and ILM). Whereas other techniques are focused on the nanoscale allowing an accurate representation of smaller particles, often relevant when working with exosomes size like EVs (HR-FCM).

When possible, a representation of the particle size distribution was plotted for each technique (**Figure 4.1.c**). Even if all the techniques show a similar PSD with the majority of the ACdEVs being around 100 – 200 nm, the particle mean diameter is highly variable when looking at the same samples from different biological repeat on various instruments. As mentioned before, the mean diameter is not a good representation of heterogeneous samples and can vary based on the instruments and analysis range. NTA, TRPS and ILM shows a higher heterogeneity in size with the presence of bigger EV, whereas MRPS, FCM, and HR-FCM fail to do so. Additionally, MRPS upper size cut off for this measurement is at 300 nm which explain the lack of larger EVs. Interestingly the TRPS 500 nm size cut off still allowed larger vesicles to pass through the nanopore possibly due to the applied pressure and stretch.

A.

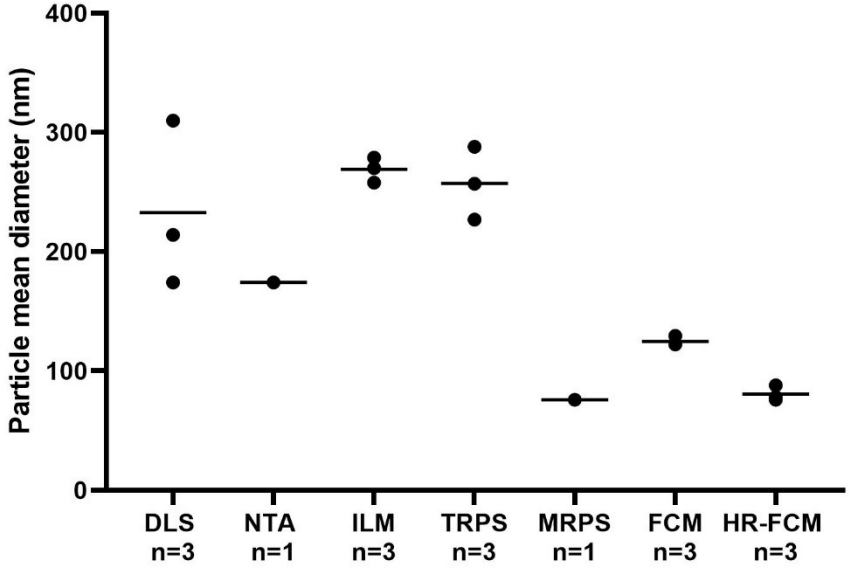

B.

Technique	Manufacturer	Analysis range (nm)	Mean diameter (nm)	Standard deviation	Number of repeat (N)
DLS	Brookhaven - NanoBrook	0.3-10000	232.76	69.62	3
NTA	Particle Metrix - Zeta Viewer	20-1000	174.3	0	1
ILM	Myriade - Videodrop	60-1000	269	10.53	3
TRPS	Izon - qNano	85-500	257.33	30.50	3
MRPS	Spectradyne – nCS1	50-300	75.9	0	1
FCM	Beckam - CytoFLEX	80-100000	124.9	3.99	3
HR-FCM	NanoFCM ltd - NanoFCM	40-200	80.64	6.40	3

C.

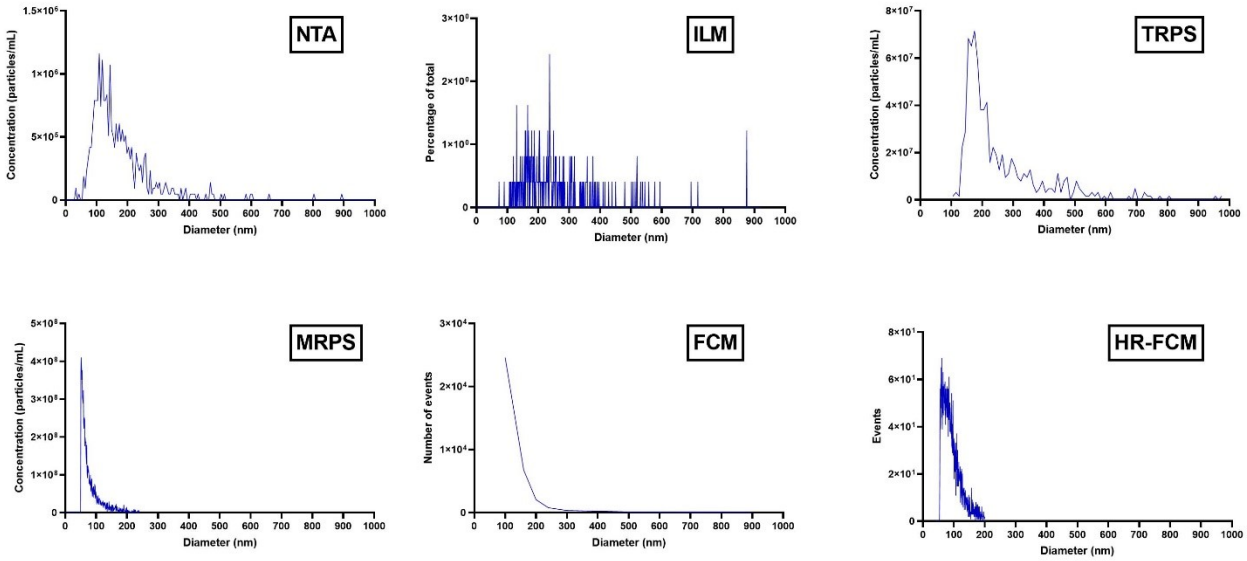

Figure 4.2: Comparison of various particle size distribution techniques for EV measurements. ***(a)*** *Particles mean diameter of late AC 2000 x g SN measured by various sizing techniques.* ***(b)*** *Information on the technique used and the measurements.* ***(c)*** *Representative particle size distribution of particles present in the 2000 x g supernatant measured by NTA, ILM, TRPS, MRPS, FCM and HR-FCM.*

This comparison enabled an informed decision based on methodological limitations and instruments availability. Going forwards, the PSD of ACdEVs will be measured by TRPS using the qNano instrument as it offers tunability of the detection size through the choice of nanopores. This tunable technique will give the best chance for a maximal optimization of heterogenous samples. A few parameters can be altered such as the voltage for the signal to noise ratio, the pressure for the particle rate, and the stretch of the pores for the blockade magnitude and sample resolution. In addition, TRPS is becoming a go to sizing technique in the EV field (Maas, Vrij and Broekman, 2014; Vogel *et al.*, 2016).

PSD techniques can also measure similar size contaminants present in the samples. Further purification methods can help limit this issue. For this reason, SEC was used to further purify ACdEVs released by early or late apoptotic cells prior to measurement by TRPS. By using NP 200 nanopores, ACdEVs between 80- and 500- nm in diameter can be detected. Both samples show a similar heterogeneous PSD with a modal diameter of 164.3 nm (+/- 30.43) for early ACdEVs, and 178.6 nm (+/- 30.92) for late ACdEVs (**Figure 4.3.a**). This suggests that apoptotic cells release exosome- and microvesicle- size like extracellular vesicles. Additionally, 18H samples are more concentrated than 6H samples suggesting that ACdEVs are released continuously by apoptotic cells, as seen by the proportional increase in total protein amount (**Figure 4.3.b**). Previously, the mean size of particles was used to compare various sizing techniques as some instrument did not give enough information to give a mode size. Here, the qNano instrument gives more detail of the measurements such as the mode size, best used with a polydisperse population like ACdEVs.

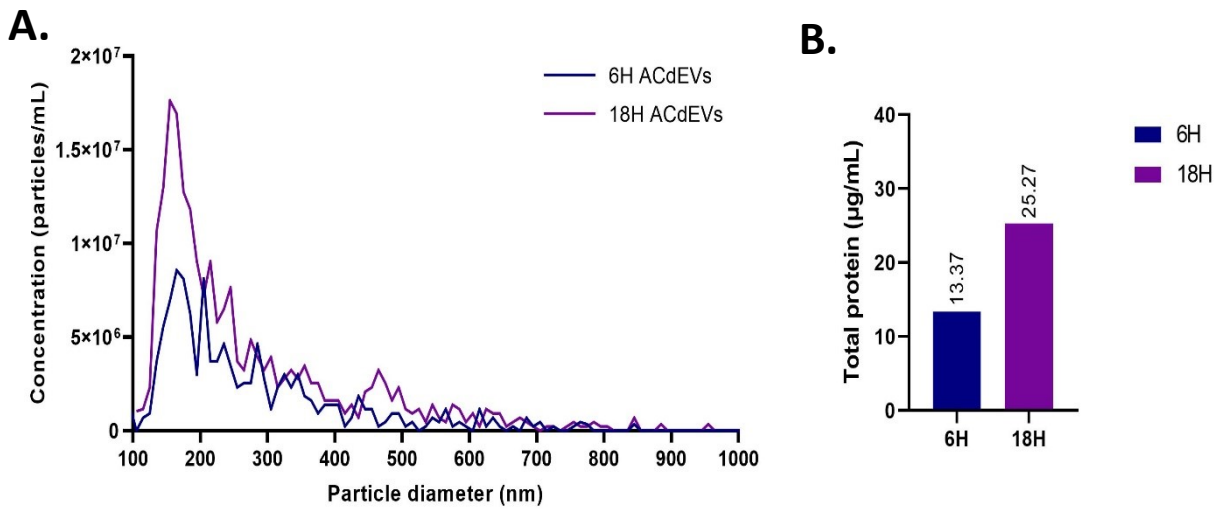

Figure 4.3: Basic characterization of early and late ACdEVs. *6H and 18H ACdEVs from Jurkat cells were purified by SEC and measured by TRPS using the qNano.* ***(a)*** *Mean particle size distribution of 6H and 18H ACdEVs, 500 particles were recorded using a NP200 nanopore calibrated with CPC100 beads. Samples were measured in three independent biological repeats (N=3).* ***(b)*** *Total protein concentration of 6H and 18H ACdEVs measured by Micro BCA assay (N=2 biological repeats), error bars represent + standard deviation.*

Like any particle sizing instrument, the qNano instrument has its limitations. The major drawback encountered is that it is highly time consuming (Maas *et al.*, 2015), as each measurement needs to be calibrated. In comparison to ILM for example, which only takes a few minutes, TRPS can sometime take up to an hour to measure one sample. In addition, nanopore clogging events are also frequent, even more so when measuring heterogeneous samples as particle build ups or larger particles present in the sample can cause partial blocking of the nanopore. Furthermore, the nanopore efficiency and characteristics can differ between individual nanopore, set up, storage condition, and time, which can account for a higher variability (Willmott *et al.*, 2014). This method is best suited for monodisperse particle population of known size rather than polydisperse particles population of unknown sizes, such as ACdEVs.

A recently optimized technique based on TRPS principle is the microfluidic pulse resistive sensing (MRPS) technique. Theoretically, this improved technique should overcome most of the problems encountered with the TRPS method. Indeed, there is no need for calibration as it utilizes pre-calibrated single use microfluidic cartridges. Moreover, the cartridges are composed of a pre-filter to reduce the clogging events.

Similarly to the qNano, the nCS1 instrument is tunable and offers various cartridges with multiple size cut-offs to measure a wide range of particles diameter (Rozo *et al.*, 2020b). Using both TS-400 and TS-2K cartridges allowed the analysis of the whole ACdEV population by combining both measurements range of 65- to 400- nm and 250- to 2000- nm, respectively. The addition of a pre-filter to the cartridges means that the surface tension in smaller cartridges, such as TS-400, is harder to overcome and prevent the flow from flowing into microfluidic channels. For this, the manufacturer recommends the addition of a detergent (Tween-20) as a surfactant to lower the surface tensions. Thus, a range of Tween-20 concentrations from 0.02 % to 1 % were evaluated to determine the lowest concentration that will allow for a full flow rate (**Figure 4.4.a**). In each condition, particles were counted per 10 seconds run until 1000 particles were recorded. As seen below, the lower the tween concentration is, the higher the number of runs and the lower the number of particles per run. The concentration of 1 % Tween-20 gave the highest particles per run with a total number of 12 runs required, which is the best option as full flow rate could not be achieved in low tween concentration such as 0.02 % with up to 103 runs. These results demonstrate the importance of the use of a surfactant or wetting agent to allow the flow into the microfluidic channels of smaller cartridges.

However, the use of detergent is undesirable when it comes to lipid particles due to its possibility to integrate into the EV membrane and potentially affect their functionality, integrity, and characteristic (Lichtenberg, Ahyayauch and Goñi, 2013; Osteikoetxea, Sódar, *et al.*, 2015). Indeed, when comparing the PSD of ACdEVs with increasing Tween-20 concentration, the analysis revealed that the more Tween-20 was added, more smaller particles were measured (**Figure 4.4.b**). This result suggests that Tween-20 potentially lyse ACdEVs, especially larger EVs.

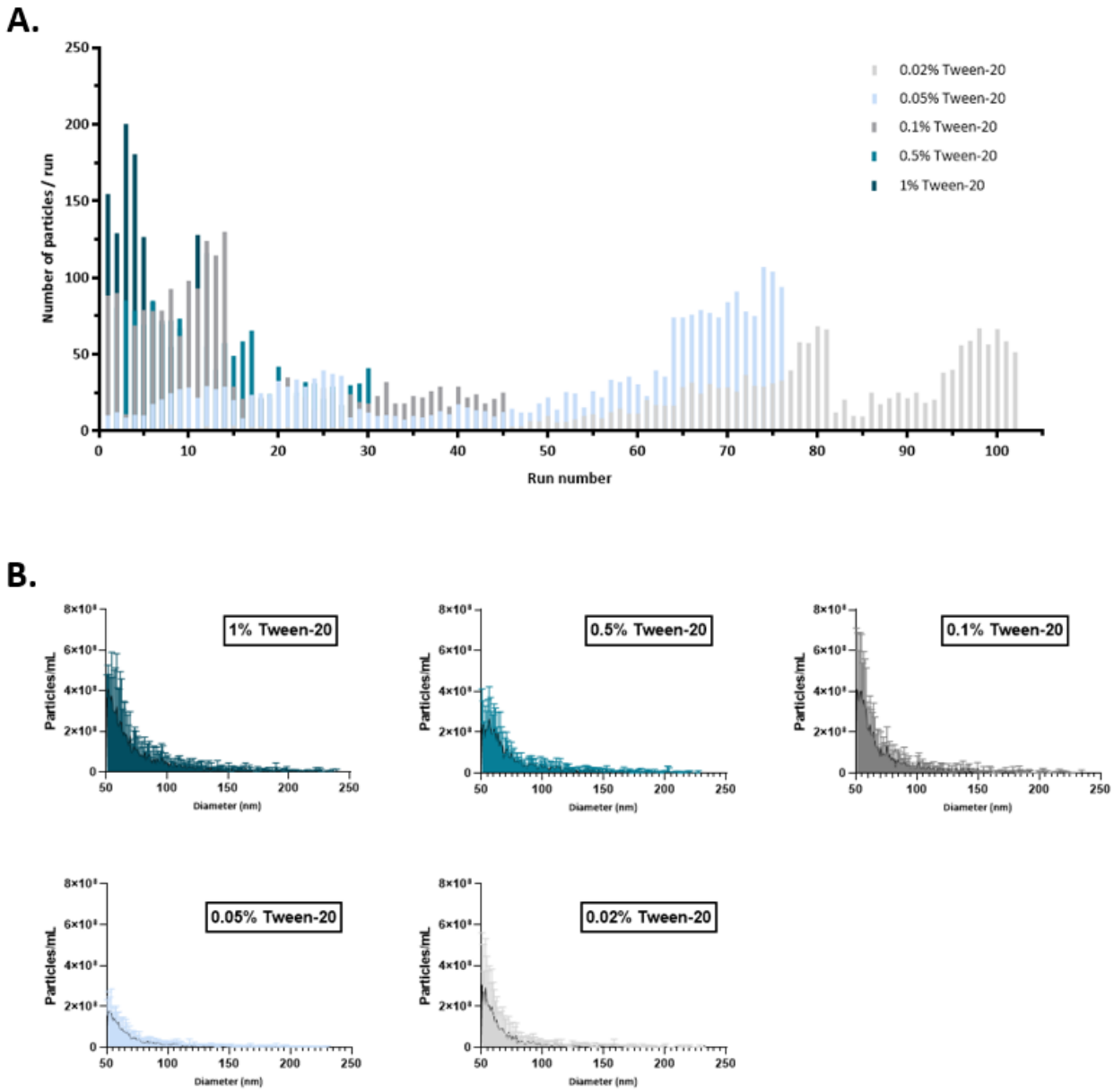

Figure 4.4: Effect of Tween-20 on particle size and run measurements. *Late AC 2000 x g SN sizing and quantification was measured by MRPS using Tween-20 as a wetting agent at a concentration ranging from 0.02 % to 1 % using a TS-300 cartridge.* ***(a)*** *Number of particles per run represented by the mean only of three biological repeats (N=3).* ***(b)*** *Comparison of the mean size distribution of late ACdEVs. Samples were measured as three independent biological repeats (N=3). Error bars represents SD.*

It should be noted that the various Tween-20 concentration tested above are all above the critical micelle concentration (CMC) of Tween-20 of 0.0074 (% W/V) (OpenWetWare contributors, 2022). The CMC is defined as the concentration of detergent above which spontaneous micelles are formed. The Tween-20 micelles being around 8.5 nm in diameter, they would not be detected by the instrument when looking at the PSD of ACdEVs. However, above the CMC, membranes are being solubilized more effectively which could explained the observed increase in smaller size ACdEVs when using higher Tween-20 concentration such as 1% (Lichtenberg, Ahyayauch and Goñi, 2013).

Although Tween is widely used within the EV field (Bachurski *et al.*, 2019), it would be preferable not to use detergents to make accurate size measurements of lipid particles. Therefore, bovine serum albumin (BSA) was investigated as an alternative wetting agent for ACdEVs PSD measurements, as it was previously showed to decrease the surface tension of water and other liquids (Windvoel *et al.*, 2010). 100 nm polystyrene size standard beads suspended in 0.1 % BSA in PBS were measured using a TS-400 cartridge (**Figure 4.5**). The PSD shows an accurate sizing of the beads with a mean diameter of 105 nm (**Figure 4.5.a**). Additionally, when looking at the transit time against particle diameter, the included events are particles with a transit time below 50 µs which is under the 60 µs calibration of the TS-400 cartridges (proprietary data). Particles with elongated transit time were automatically excluded from the analysis (**Figure 4.5.b**). The elongated transit time means that particles take longer to cross the aperture. This is often due to a coincident particle passage, or when two or more particles are crossing the aperture at the same time. Those events need to be excluded as it can result in a lower particle counts and larger counted particles thus affecting the PSD. Finally, all the included events were above the noise threshold of 50 µm, excluding all the events falling below this threshold.

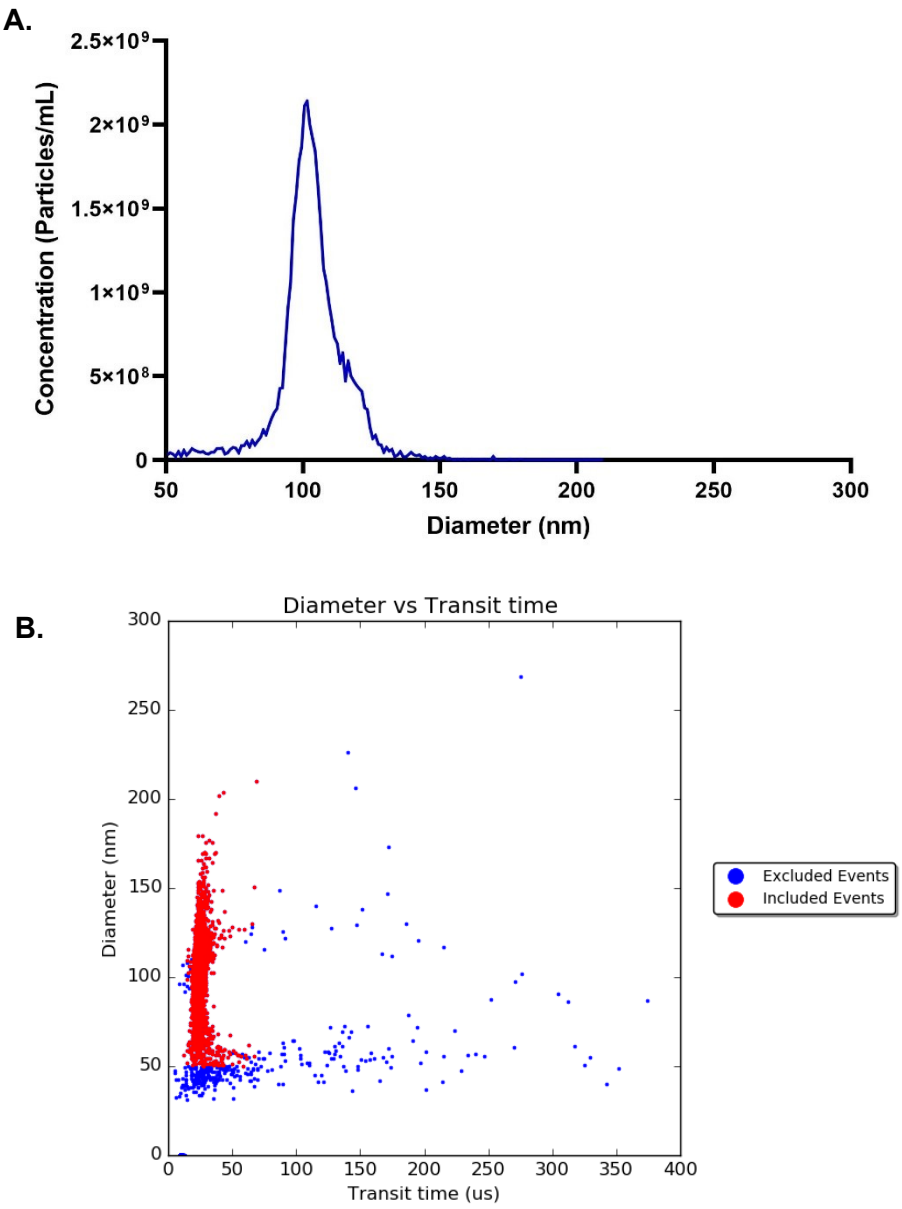

Figure 4.5: Use of BSA as a wetting agent for MRPS measurements. *100 nm polystyrene size standard beads were measured in 0.1 % BSA using a TS-400 cartridge.* ***(a)*** *Particle size distribution.* ***(b)*** *Dot plot of measured diameter (nm) versus transit time (µs).*

Altogether these results show that the use of BSA as a surfactant for measurements of particles using smaller cartridge is promising for accurate particle sizing. Following this, 2000 x g 18H ACdEVs were measured in 0.1 % BSA using both TS-400 and TS-2K cartridges to cover the wide PSD of our sample (**Figure 4.6**). Prior to the measurements, samples were diluted in PBS in order to fall in both cartridges specific concentration range being $1x10^{7}$ to $1x10^{11}$ particles/mL, and $5x10^{5}$ to $5x10^{9}$ particles/mL for TS-400 and TS-2K, respectively. By combining both PSDs, EVs of diameters ranging from 65- to 2000- nm were detected, with a

majority being around 200 nm in size. The observed difference in particles concentration is due to the fact that the TS-2k cartridge has a lower size cut off of 250 nm thus excluding most of the small particles present in the samples, detected with the TS-400 cartridge.

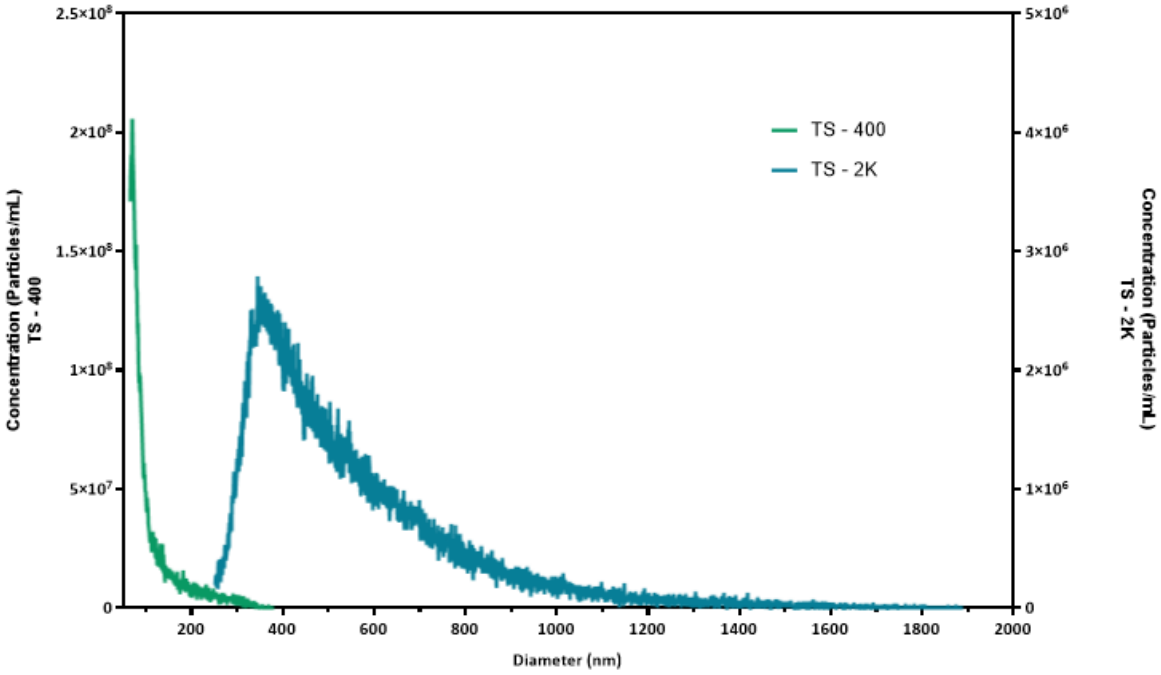

Figure 4.6: Particle size distribution of late ACdEVs measured by MRPS. *Late ACdEVs diluted 1:10 in PBS were measured in 0.1 % BSA using both TS-400 (green) and TS-2K (cyan) cartridges for a full coverage, with analysis range from 65 to 400 nm and from 250 to 2000 nm, respectively. Data represents N=1.*

The MRPS was found to be more challenging in practice than expected due to the difficulty of getting the samples to flow through the channels in small cartridges. To lower the surface tension, Tween-20 was assessed as a surfactant. However, we demonstrated that the use of detergent affected the particle size distribution of the samples. As an alternative, BSA proved to successfully measure lipid particles PSD with accuracy.

In conclusion, it is necessary to be cautious when choosing a particle sizing technique. The chosen technique should be best fitted to the characteristic of the sample such as its size, concentration, and buffer. All techniques have limitations, and it is thus recommended to combine several techniques to have an accurate representation of EVs PSD. Now that the

PSD of early and late ACdEVs was defined, other parameters such a membrane fluidity were investigated.

4.3.2 Membrane fluidity

For membrane fluidity measurements, the incubation temperature of laurdan has to be above the phase transition temperature of the lipids so the membrane can become fluid and allow the probe to integrate into the lipid bilayer. Here, the incubation temperature of 37°C was used as it is the temperature used to culture Jurkat cells as well as being above the transition temperature of 1-palmitoyl-2-oleoyl-sn-glycero-3-phosphocholine (POPC) used to form liposomes. Firstly, membrane fluidity measurement was optimized in different systems (liposomes, EVs, and cells) by testing the recommended or excess concentration of laurdan as well as different buffers (liposome buffer, PBS, and SF-RPMI) (**Figure 4.7**).

Results show that the three systems tested were within the same GP range (**Figure 4.7**). However, ACdEVs are more rigid than live cells as seen by a higher GP value, although not significantly so. POPC liposomes were found to be the most fluid compared to cells and EVs. This could be explained by the fact that liposomes do not contain proteins and sterols which is likely to affect their membrane fluidity. POPC, like most lipids, has a phase transition of -2 °C, thus, by choosing an experimental temperature of 37 °C, it allowed the membrane to become fluid and incorporate the laurdan probe. The water exposure increases with fluidity, so if there is an excess of laurdan the increased exposure due to it being in an aqueous environment rather than the lipid bilayer will make it falsely appear more fluid. This is why it is important to calculate the lowest amount of laurdan that can effectively be used. Laurdan was added at the recommended concentration of 0.1–0.3 mol% of the total lipid concentration which correspond to 2.5 and 5 μM for EVs and cells, respectively (Learmonth and Gratton, 2002). When laurdan was added in excess with EVs at 2.5 mM, the GP decreased slightly, however not significantly. Thus, the excess of laurdan tested was not sufficient to have an effect on membrane fluidity, and 2.5 μM laurdan will be used to assess EV membranes fluidity. Finally, no significant difference was observed when using SF-RPMI and PBS as buffer for the membrane fluidity of live cells (**Figure 4.7**).

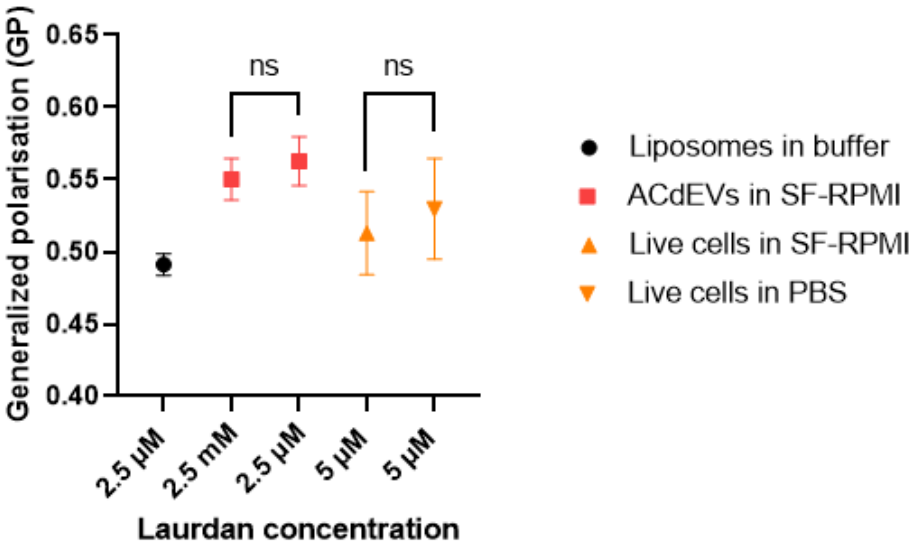

Figure 4.7: Optimization of laurdan assays to measure lipid particle membrane fluidity. *Membrane fluidity assay optimisation on 200 nm POPC liposomes, 18H Jurkat ACdEVs, and live Jurkat cells. Samples were measured in triplicates in three independent biological repeats (N=3). Error bars represent +/- SEM, statistical test used: unpaired t test.*

For further membrane fluidity assay, the samples were measured in ACdEVs buffer, SF-RPMI, and further incubated with either 2.5- or 5- µM of laurdan for EVs and cells, respectively. Afterwards, the membrane fluidity of cells and EVs was measured throughout apoptosis, comparing live cells, early AC and ACdEVs, and late AC and ACdEVs in both Jurkat and THP-1 cell lines (**Figure 4.8**). Across the studied cell lines, the GP value of viable cells was the highest compared to the other conditions suggesting that viable cells are more rigid than apoptotic cells and ACdEVs. Indeed, during apoptosis structural changes occur to prepare the cells for clearance by phagocytes, these changes include PS exposure on the outer layer of the plasma membrane and other trans bilayer migration of glycerophospholipids which results in an increased spacing in lipids affecting biophysical parameters such as membrane fluidity (Appelt *et al.*, 2005; Gibbons *et al.*, 2013). Interestingly, the similarity in membrane fluidity of EVs and their parent cells could be explained by a similar membrane composition which gives insights on EVs biogenesis, as they could be deriving from the AC plasma membrane rather than exocytosis. Furthermore, early AC and ACdEVs have a lower GP value compared to late AC and ACEVs which indicates a difference in membrane properties during early and late apoptotic phases, although statistical analysis showed no significant differences. Finally, the increase of variability observed for both late AC and ACdEVs could be explained by the fact that during late apoptosis/necrosis, the membrane integrity of some apoptotic cells is

compromised, making it difficult to accurately measure the membrane fluidity. Additionally, the passage number of Jurkat cells at the time of the assay was 2 times higher than the one of THP-1 cells which could also affect the difference in variability. However, Gibbons et al. (2013) suggest that during late apoptosis the membrane becomes more rigid due to the formation of blebs and release of larger vesicles, supporting the observed increased in GP values.

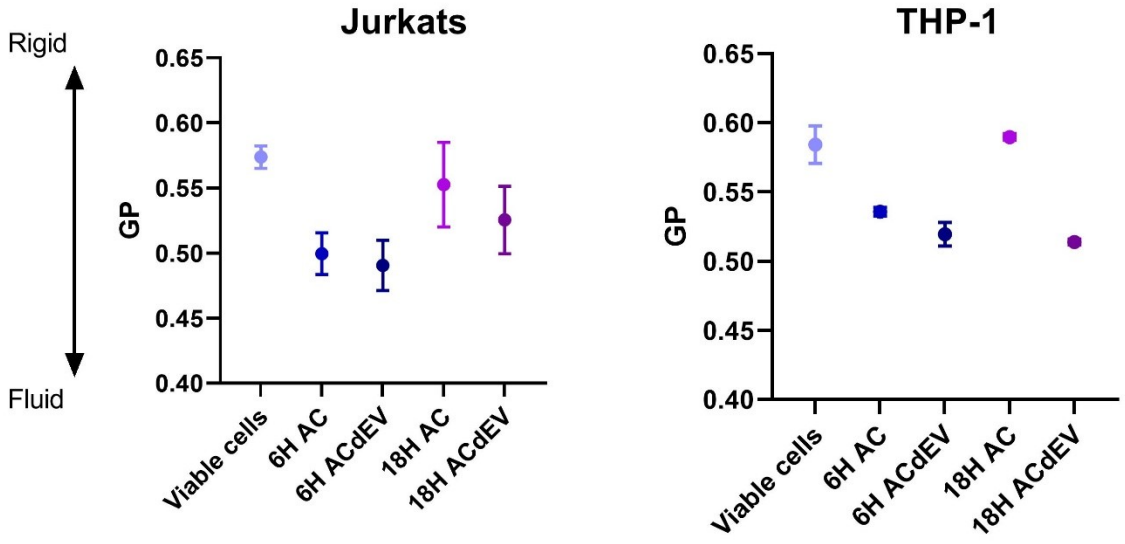

Figure 4.8: Generalized polarisation distribution in cells and EVs throughout apoptosis. *Generalized polarisation was measured using the laurdan probe in both Jurkat and THP-1 cell lines. Conditions are the following: viable cells, early and late apoptotic cells, and early and late ACdEVs. Samples were measured in triplicates in three and two independent biological repeats (N=3 and N=2) in Jurkat cell and THP-1 cell line, respectively. Error bars represent +/- SEM.*

In conclusion, membrane fluidity is affected by apoptosis in both AC and ACdEVs, with a general increase in fluidity during early apoptosis and an increase in rigidity during late apoptosis. As observed in other studies, a high protein to lipid ratio in early apoptotic conditions could explain the fluidisation of the membranes (Osteikoetxea, Balogh, *et al.*, 2015). For this reason, further investigations focusing on the lipid, protein, and sterol composition of early and late conditions were conducted to better understand the observed fluctuation in membrane fluidity.

4.3.3 ACdEVs composition

It should be noted that the following quantifications of cholesterol, protein and lipid are total quantification and not only reflect the ACdEVs membrane composition but also the ACdEVs cargo and internal membranes of multilamellar vesicles as well. The initial observations made in this chapter would have to be verified with ACdEVs membrane extracts.

4.3.3.a Cholesterol and protein quantification

Sterol molecules in phospholipid bilayers can alter packing density and membrane fluidity by packing against acyl chains in the hydrophobic tail groups (Li et al., 2003). Ordered packing of lipid tails around the four-ring structure of cholesterol reduces the entropy of lipid bilayers, leading to decreased mobility of the bilayer as well as increased membrane thickness and reduced membrane permeability (Bui, Suga and Umakoshi, 2016). In other situations, sterols can increase fluidity by intercalating between lipids. Cholesterol functions as a buffer to control the fluidity of the membrane when facing temperature variations: preventing lower temperatures from inhibiting fluidity and preventing higher temperatures from increasing it (Subczynski et al., 2017). Additionally, the ratio of lipid to protein can influence membrane fluidity. Generally, an increase in density of membrane protein results in a more rigid membrane (Osteikoetxea, Balogh, *et al.*, 2015).

To have a better understanding of ACdEVs membrane properties, the amount of cholesterol and protein per ACdEVs was quantified in both early and late ACdEVs. Firstly, colorimetric assays were used to measure the total level of cholesterol and proteins. Secondly, the samples were measured by ILM using the Videodrop to get an accurate concentration in order to calculate the amount of cholesterol and protein per ACdEV. The results showed no significant difference in both conditions (**Figure 4.9.a**). The protein per ACdEVs quantification observed here is quite similar to what is found in the literature on various EV subtypes often ranging from 0.1 to 10 $x10^{-15}$ g of protein per EV (Koliha *et al.*, 2016). However, it can be hypothesised that the protein loading in the ACdEVs seems to be less controlled than the one of cholesterol as seen by the higher variability in protein quantification. To compare the amounts of both measured components, the estimated molar ratios were calculated based on the average molecular weight of a human protein (38200 g/mol) from UniProt database, and the molecular weight of cholesterol (386.65 g/mol) (**Figure 4.9.b**). The observed difference of ratios in early and late ACdEVs (6.63 and 12.9, respectively) indicate that there is a greater number of cholesterol molecules in late ACdEVs, or a lesser number of proteins compared to early ACdEVs.

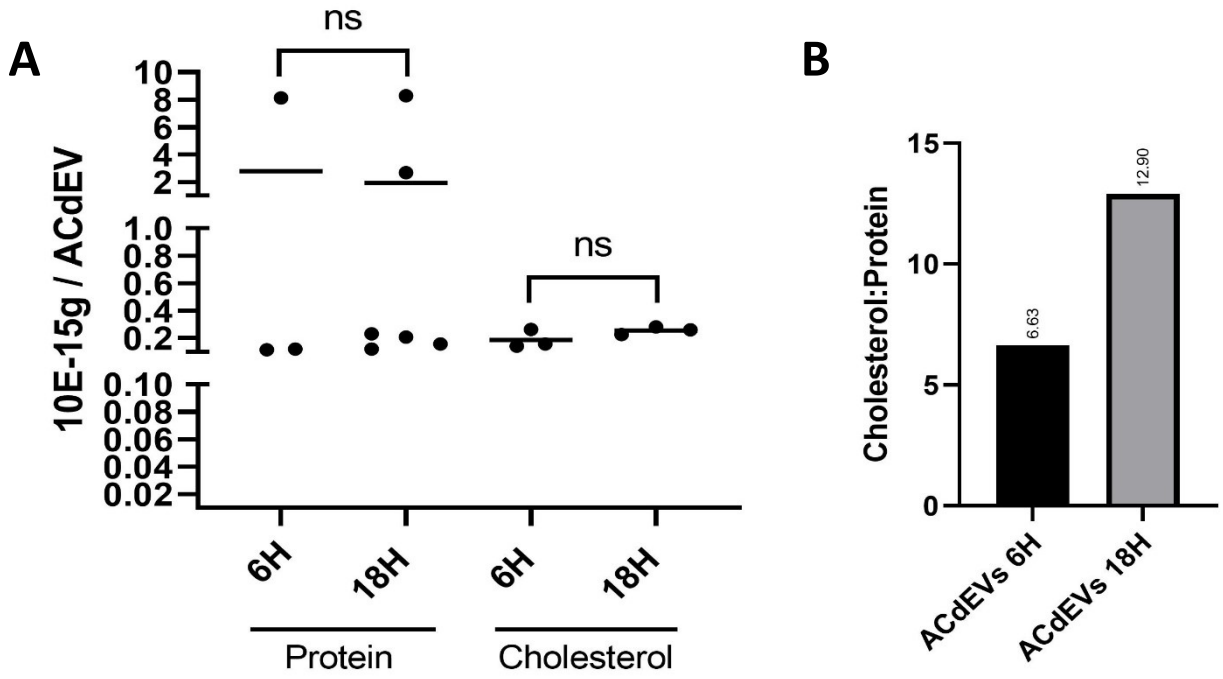

Figure 4.9: Protein and cholesterol quantification of early and late ACdEVs. *Particle concentration was determined using ILM; protein concentration was measured by micro–BCA Assay, and cholesterol concentration by a cholesterol assay kit. EVs were isolated from either early or late apoptotic Jurkats and purified by SEC.* ***(a)*** *Total proteins and cholesterol quantifications in early and late ACdEVs.* ***(b)*** *Estimated cholesterol:protein molar ratios. Samples were measured in triplicates in three or six independent biological repeats (N=3 and N=6) for all conditions but protein level in 18H ACdEV.*

As previously mentioned, the protein and cholesterol quantification observed here represents the total amount of cholesterol and protein including the ACdEVs cargo as well. As seen by the electron low and high ACdEVs imaged by cryo-TEM (**Figure 3.4**), the cargo of these EVs is highly variable which could account for the variability in protein and cholesterol quantification.

Cholesterol effects on fluidity can be difficult to predict, however, if the late ACdEVs contain more proteins, it could potentially increase their rigidity, as seen in the previous section. Additionally, membrane fluidity is not necessarily homogenous within a membrane and local variation of fluidity can be caused by membrane microdomains such as lipid rafts. These are highly ordered dynamic domains composed of cholesterols, saturated lipids and sphingomyelin (SM), decreasing the overall and local membrane fluidity (Simons and Sampaio, 2011). The microfluidity of lipid raft domains regulates the activation of receptors

present in these domains (Morenilla-Palao *et al.*, 2009; Szoke *et al.*, 2010). As several studies report that EVs are significantly enriched in cholesterol compared to their parent cells (De Gassart *et al.*, 2003), this could indicate that lipid rafts are incorporated more in ACdEVs.

4.3.3.b Lipidomic analysis

In an EV field where studies are predominantly focusing on membrane proteins for surface markers identifications and disease diagnosis, it is crucial to shed some lights on the important role of lipids. A comprehensive analysis of the lipid composition of cells and ACdEVs during early and late apoptosis will undoubtably help understand the biophysical properties of EVs membranes.

For this, an untargeted high-resolution MS was used to extensively analyse the molecular lipidomic profile of the T cell line Jurkat cells and the ACdEVs released during early and late apoptosis. As the initial dataset generated by lipid mass spectrometry was extremely large with 1780 lipid species identified belonging to 23 lipid class, a pre-analysis was required (**Figure 4.10**).

Mammalian lipid biogenesis only produces even numbers of carbons in FA chains, this is why the odd chain fatty acids (OCFA) lipids were removed as they most likely come from the diet, or in this case from the serum which is supplemented to the culture media. Serum is important to promote cell growth by providing the cells with basic nutrients and growth factors. Even though the sample preparation before mass spectrometry analysis included washing steps to remove any lipids deriving from the serum, lipids and factors already taken up by cells prior to serum depletion remained. By removing the OCFA from the lipid data set, 537 lipid species were removed corresponding to 6.97 % of the total lipids.

The stability of lipids can be influenced by hydrolysis and oxidation during sample collection, storage, and preparation (Ulmer *et al.*, 2021). Hydrolysis of lipids leads to free FA and lysolipids production. Lysolipids are lipids in which one or both acyl derivatives have been removed and they have been identified as extracellular mediators activating specific GPCRs (Heringdorf, 2008). Even though the samples have been spiked with internal standards, lipid degradation such as hydrolysis prior to the spiking was not accounted for. For this reason, the lysolipids identified here may not be representative of the true lysolipids levels. Additionally, the removed lysolipids represent less than 0.5 mol% of the total lipids and thus might not be significant structural components of ACdEVs although they might still have important role in signalling. Consequently, 46 lysolipids species and 8 lipid class were removed.

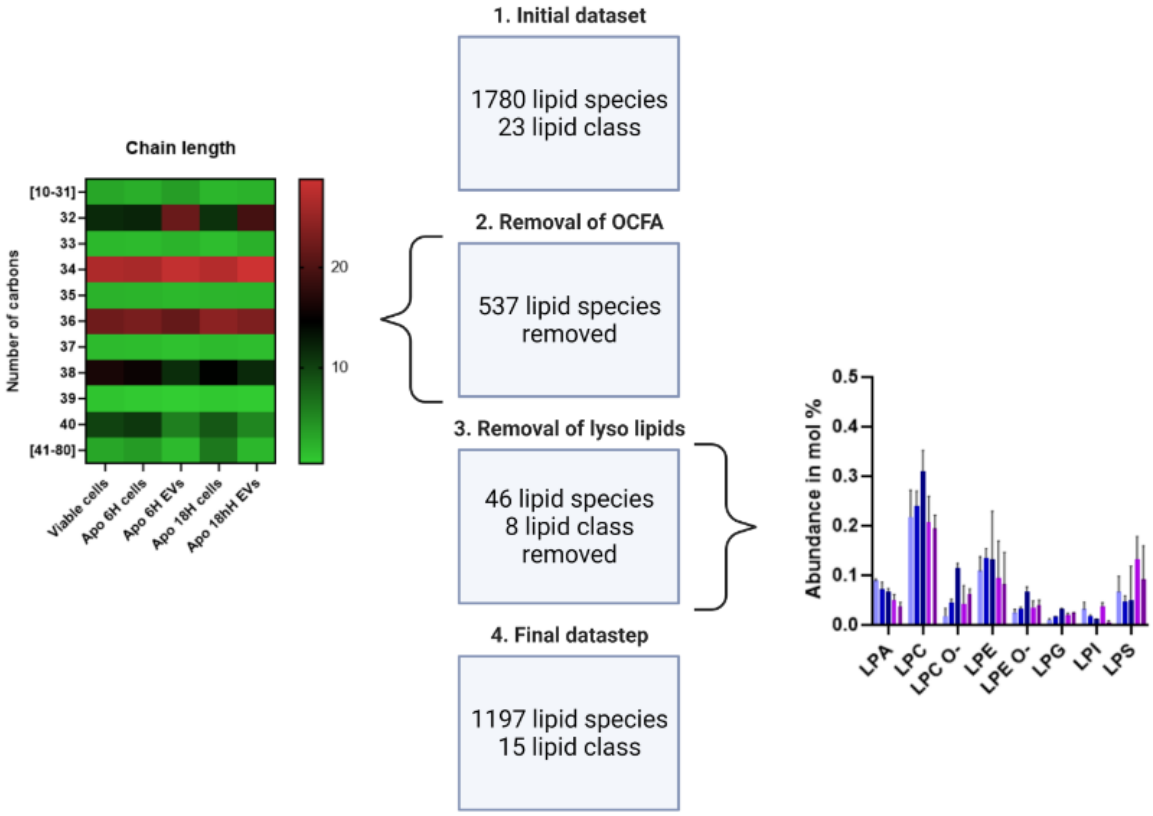

Figure 4.10: Steps followed for lipidomics analysis. *The initial dataset was provided by Lipotype, from which odd chain fatty acids (OCFA) were removed, followed by lysolipids, leading to a final dataset used for further analysis. The heat map represents the mol% lipids with each number of carbons in FA chains in each condition. Heat map range: smallest value = 0.46; baseline value = 14.62; largest value = 28.78. The bar graph represents the abundance of lysolipids in mol %. LPA Lyso Phosphatidate, LPC Lyso Phosphatidylcholine, LPC O- Lyso Phosphatidylcholine (-ether), LPE Lyso Phosphatidylethanolamine, LPE O- Lyso Phosphatidylethanolamine (-ether), LPG Lyso Phosphatidylglycerol, LPI Lyso Phosphatidylinositol, LPS Lyso Phosphatidylserine.*

Following this first lipidomic analysis, a total of 1644 and 1338 lipid species were identified in Jurkat cells and ACdEVs, respectively, sharing 1248 species in common. The quantified lipid species belong to 4 main lipid classes including sterol esters (STE), sphingolipids (SL), glycerolipids (GL), and glycerophospholipids (GPL), encompassing 15 sub lipid classes (**Figure 4.11**). As expected, phosphatidylcholine (PC) was the most abundant lipid across all the conditions with a minimum abundance of 24 mol %. Indeed, phospholipids are the most abundant class of lipid in mammalian cells, with PC representing 45-55% of the total phospholipids (Cockcroft, 2021). On the other hand, cholesteryl esters (CE) were the less abundant lipids with a maximum abundance of 0.35 mol %.

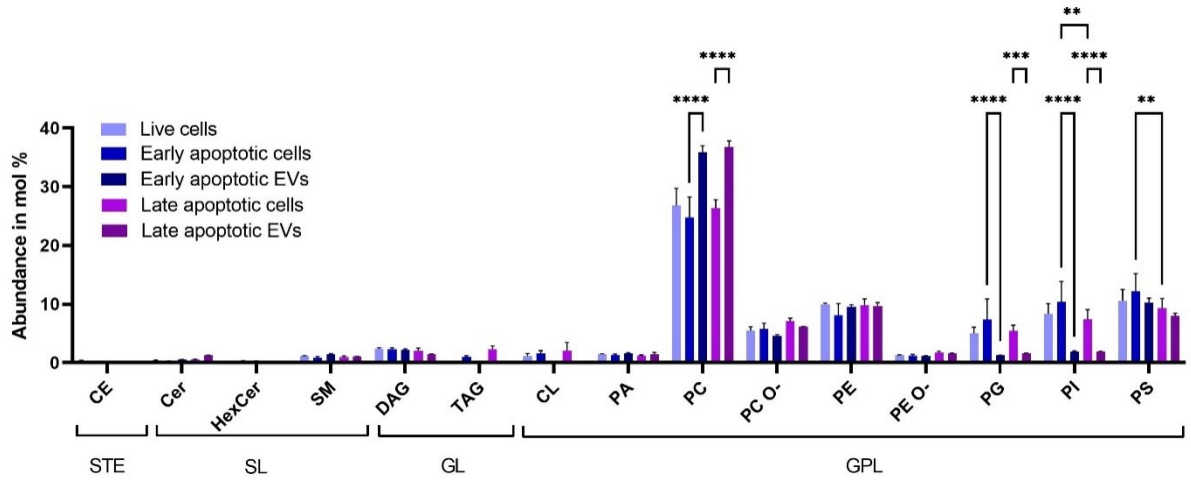

Figure 4.11: Abundance of specific lipid class from the final dataset. *Abundance is represented as mol % of total lipids. Statistical test used: 2way ANOVA, Tukey's multiple comparisons. Samples were measured in triplicates in three independent biological repeats (N=3). Error bars represent + SD. CE, cholesterol esters, Cer Ceramide, HexCer Hexosylceramide, SM sphingomyelin, DAG Diacylglycerol, TAG Triacylglycerol, CL Cardiolipin, PA Phosphatidate, PC Phosphatidylcholine, PC O- Phosphatidylcholine (-ether), PE Phosphatidylethanolamine, PE O- Phosphatidylethanolamine (-ether), PG Phosphatidylglycerol, PI Phosphatidylinositol, PS Phosphatidylserine, STE Sterol, SL Sphingolipid, GL Glycerolipid, GPL Glycerophospholipid.*

The abundance of lipid classes showed significant differences between EVs and their parent cells as well as between early and late apoptotic cells in PC, PG, PI and PS (**Table 4.1**). To confirm such differences, a principal component analysis (PCA) was then realised to observe possible correlations between the different conditions and the abundance of sub lipid classes (**Figure 4.12**). The PCA was plotted based on the first and second principal component (PC1 and PC2) which represents the maximum variance direction in the data. The PCA analysis shows similarities between cells as seen by a low PC1 score whereas ACdEVs are characterised by a higher PC1 score. Comparably, early apoptosis is illustrated by a positive PC2 score, whereas late apoptosis is characterised by a negative PC2 score. Additionally, the results show a distinct clustering between the biological replicates which indicates a low intra variability between conditions. This result indicates that the composition in lipid classes in cells differs from ACdEVs and is also different during early and late apoptosis.

	Mean Diff.	95.00% CI of diff.	Below threshold	Summary	P Value
PC					
Early apoptotic cells vs. Early apoptotic EVs	-11.04	-13.42 to -8.658	Yes	****	<0.0001
Late apoptotic cells vs. Late apoptotic EVs	-10.43	-12.81 to -8.047	Yes	****	<0.0001
PG					
Early apoptotic cells vs. Early apoptotic EVs	6.124	3.741 to 8.506	Yes	****	<0.0001
Late apoptotic cells vs. Late apoptotic EVs	3.785	1.403 to 6.168	Yes	***	0.0002
PI					
Early apoptotic cells vs. Early apoptotic EVs	8.506	6.124 to 10.89	Yes	****	<0.0001
Early apoptotic cells vs. Late apoptotic cells	3.01	0.6275 to 5.392	Yes	**	0.0057
Late apoptotic cells vs. Late apoptotic EVs	5.515	3.133 to 7.898	Yes	****	<0.0001
PS					
Early apoptotic cells vs. Late apoptotic cells	2.94	0.5578 to 5.323	Yes	**	0.0074

Table 4.1: Summary statistics table. *Significant statistics comparing lipid class abundance within each condition, (CI) confidence interval. Statistical test used: 2way ANOVA, Tukey's multiple comparisons. ** P < 0.01 *** P < 0.001; **** P < 0.0001.*

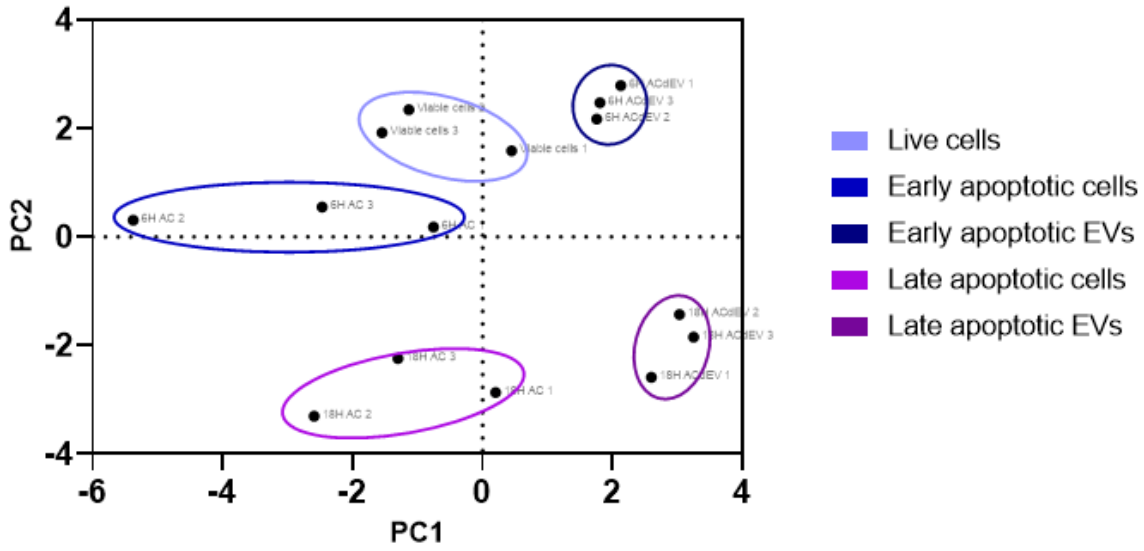

Figure 4.12: PCA analysis based on lipid classes. *PC scores of each replicate based on lipid classes (mol%) was plotted. Samples were measured in triplicates in three independent biological repeats (N=3). Ovals were manually drawn as a visual representation of the clusters.*

As the differences observed by the PCA analysis gives us a glimpse on the importance of the lipidic compositions, the enrichment in lipid classes in each condition was then quantified. For this, significant fold increases in mol% were plotted to compare ACdEVs with cells, ACdEVs and their parent cells, and early and late apoptosis (**Figure 4.13**).

Analysis of lipid composition in cells compared to ACdEVs showed a significant 9.2-fold increase in the abundance of triacylglycerol (TAG) in cells. Additionally, when comparing ACdEVs and parent cells, during both early and late apoptosis, TAG was found to be enriched in ACs by an 8.6- and 16.5-fold increase, respectively. This suggests that TAG is most likely found in live cells prior to the serum depletion and apoptosis induction. Through apoptosis TAG seems to remain in cells rather than loaded in vesicles. As TAG is mainly found in lipid droplets and lipoprotein it is most likely that TAG may also derive from the serum or particulates contaminations. Similar observations apply to cholesteryl ester (CE) which is also associated with such contaminating particulates and is found to be enriched in ACdEVs and especially 6H ACdEVs. Both TAG and CE will most likely be vesicular cargo rather than membrane component especially based on the highly hydrophobic nature of CE. Depleting the samples in lipoproteins could help discriminating between TAG and CE as contaminants or as part of the membrane lipids. However, other studies revealed a similar enrichment in both TAG and CE in exosomes (Skotland *et al.*, 2020). Interestingly, diacylglycerol, which derives from TAG, was found to be enriched in 6H ACdEVs.

Cardiolipin (CL), a phospholipid located in the inner mitochondrial membrane, was enriched in 6H AC compared to 6H ACdEVs. This indicates that during the early stages of apoptosis mitochondrial lipids and associated materials are not actively loaded in ACdEVs. Indeed, cardiolipin is a crucial lipid involved in the process of apoptosis, as upon apoptotic signalling, CL is translocated from the inner- to the outer- mitochondrial membrane to form a cytochrome *c*/CL complex (Paradies et al., 2019). This complex formation allows the peroxidation and further release of the cytochrome *c* which then assemble with APAF-1 to form the apoptosome. Additionally, CL was found to be directly involved in mitochondrial outer membrane permeabilization (Gonzalvez and Gottlieb, 2007). Nevertheless, cardiolipin synthesis was shown to decrease during apoptosis (Ostrander *et al.*, 2001; Manganelli *et al.*, 2015).

Interestingly, ACdEVs were always enriched in ceramide (Cer) when compared to cells. Ceramide is generated by hydrolysis of sphingomyelin (SM) and can be further transformed into S1-P which is a well know find me signal sensed by efferocytes. Additionally, all of those sphingolipids were found to be involved in cargo sorting and secretion of exosomes (Yuyama *et al.*, 2012; Kajimoto *et al.*, 2013) which could indicate a similar role of Cer in ACdEVs loading and secretion. Cer was also enriched in 18H EV compared to 6H EVs. SM is also one of the main constituents of lipid rafts together with cholesterol. Like most studies, enrichment from cells to EVs of SM was observed in 6H ACdEVs with a 1.6-fold increase (Skotland *et al.*, 2020). These ordered raft membrane microdomains tend to decrease the overall and local membrane fluidity and regulate membrane protein localization and activity. 6H ACdEVs are thus more likely to contain such domains. Lipid raft domains were shown to give membranes a higher resistance to detergent and physiochemical changes (Biró *et al.*, 2005; Simons and Sampaio, 2011). Lipid raft enriched particles such as early ACdEVs could thus have a longer lifetime and possibly diffuse longer and have better chances of interacting with recipient cells in distant area. Alternatively, as SM was enriched in 6H ACdEVs compared to 18H ACdEVs, it can be hypothesized that the SM present in vesicles during early apoptosis is further hydrolysed into Cer during late apoptosis. Another type of sphingolipid, hexosylceramide (HexCer), was only enriched in 6H ACdEVs compared to 18H ACdEVs. It is found in the literature that HexCer are predominantly enriched in smaller EVs as opposed to larger EVs (Brouwers and Al., 2013), which could potentially indicate that 6H AC tend to release smaller ACdEVs in greater numbers.

Regarding phospholipids, the lipid class analysis revealed that phosphatidylinositol (PI) and phosphatidylglycerol (PG) were depleted in ACdEVs compared to cells whereas phosphatidylcholine (PC) was enriched. Phosphatidylcholine (-ether) (PC O-) was found to be enriched in 18H AC and ACdEVs which could be specific to late apoptosis, whereas phosphatidylethanolamine (-ether) (PE O-) was only enriched in 6H ACdEVs.

When the lipid classes of live and apoptotic cells were compared, no significant differences were observed (data not shown). Additionally, when comparing early vs late apoptosis only Cer was significantly enriched during late apoptosis compared to early apoptosis with a 0.44-fold increase.

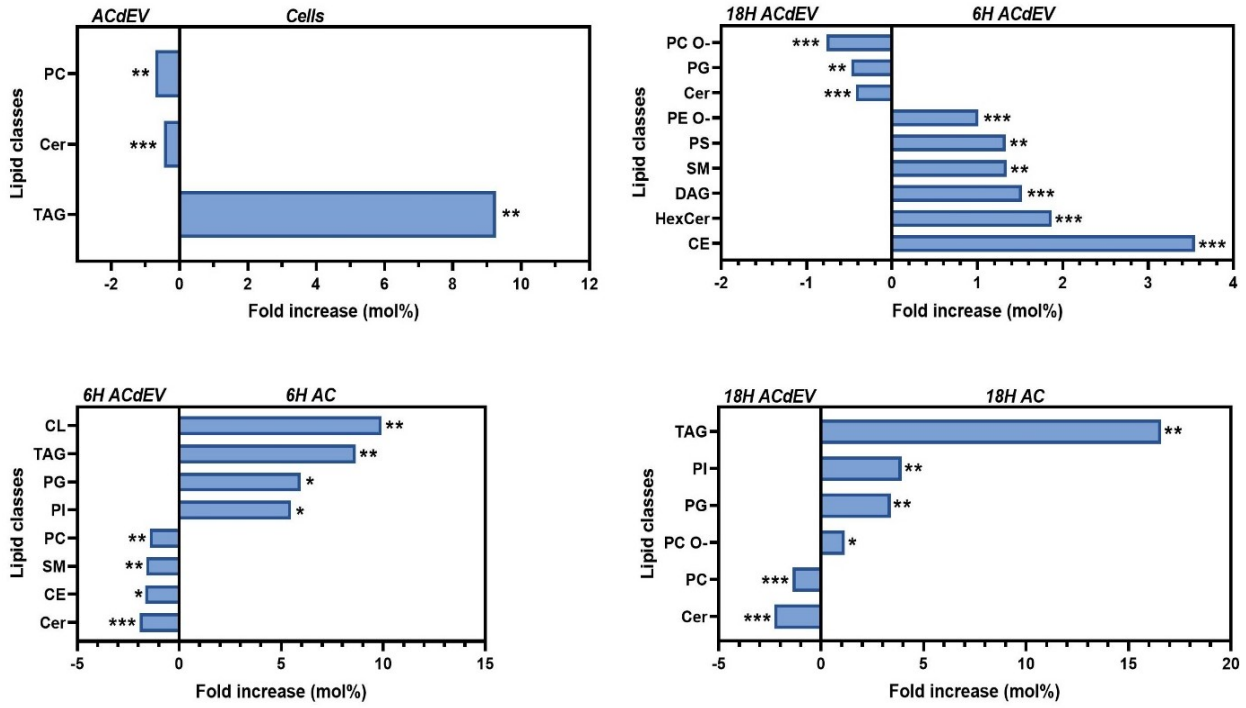

Figure 4.13: Lipid class enrichment in cells and early and Late ACdEVs in Jurkats. *Enrichment of lipid classes in live-, apoptotic-cells, and ACdEVs calculated as mol% of lipids in the compared samples. Statistically significant data only was plotted. Statistical test used: multiple unpaired t test.*

Other characteristics in lipidomics can be investigated when looking at membrane fluidity such as the degree of unsaturation of the acyl chains. The abundance of saturated FA (SFA), monounsaturated FA (MUFA), diunsaturated FA (DUFA) and polyunsaturated FA (PUFA) lipids was quantified (**Figure 4.14**). Results show that most lipids contain MUFA (**Figure 4.14.a**). ACdEVs contain more SFA and less MUFA than cells, in agreement with previous studies on exosomes (Llorente *et al.*, 2013). Late apoptotic cells and EVs contain more DUFA and less PUFA than early apoptotic cells and EVs. Additionally, the UFA:SFA lipid ratios was calculated (**Figure 4.14.b**). The significant decrease in UFA:SFA ratio in 6H ACdEVs compared to 6H AC is also observed in 18H conditions. The lesser the number of unsaturation the more rigid the membrane becomes. These results suggest that EVs are more rigid than cells, however the laurdan assay results showed that EVs share the same membrane fluidity as their parent cells. As mentioned previously, various parameters can affect the membrane fluidity and it is most likely that the degree of unsaturation alone does not reflect the membrane properties.

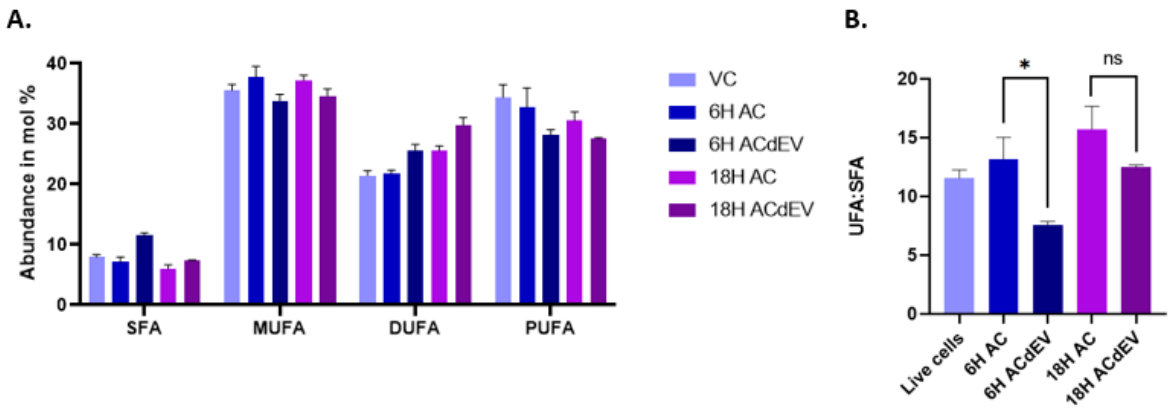

***Figure 4.14: Degree of saturation of lipids in Jurkat cells and ACdEVs**. **(a)** Abundance of lipids and degree of unsaturation. **(b)** Proportion of unsaturated/saturated lipid ratios across all conditions. Samples were measured in triplicates in three independent biological repeats (N=3). Error bars represent + SD, statistical test used: unpaired t test. SFA: saturated fatty acids; MUFA: monounsaturated fatty acids; DUFA: diunsaturated fatty acids; PUFA: polyunsaturated fatty acids.*

The degree of hydroxylation, or numbers of hydroxyl groups (-OH), was then quantified (**Figure 4.15**). When the abundance of lipids was under 1 mol %, the data was excluded, number of hydroxylation not shown: 3. The majority of lipids were not hydroxylated with only a maximum abundance of 7.2 mol% of lipids containing 2 hydroxyl groups (**Figure 4.15.a**). The ratio of non-hydroxylated:hydroxylated lipids across the different conditions showed no significant difference (**Figure 4.15.b**).

Interestingly, the lipids that contained hydroxyl group were sphingolipids (SM, HexCer and Cer) only. SM was found to be the most abundant hydroxylated lipid across all conditions compared to the other types of SL (**Figure 4.15.c**). This can be explained by the fact that the total amount of SM is 10 times higher than Cer in cells (Adada, Luberto and Canals, 2016). Several studies have highlighted the importance of SL hydroxylation in interactions with the surrounding membrane and enzymes. Indeed, sphingomyelin synthases which produce SM, have a better affinity for hydroxylated SM rather than non-hydroxylated SM (Sessa *et al.*, 2021). ACdEVs were found to have the highest total abundance of hydroxylated lipids with 7.2 and 6.1 mol% for 6H- and 18H-ACdEVs, respectively. This could indicate that SL are actively hydroxylated within ACdEVs. Additionally, 18H ACdEVs had a higher percentage of Cer-OH and a lower percentage of SM-OH than the other conditions. This leads to the suggestion that during late apoptosis, SM is further hydrolysed into Cer.

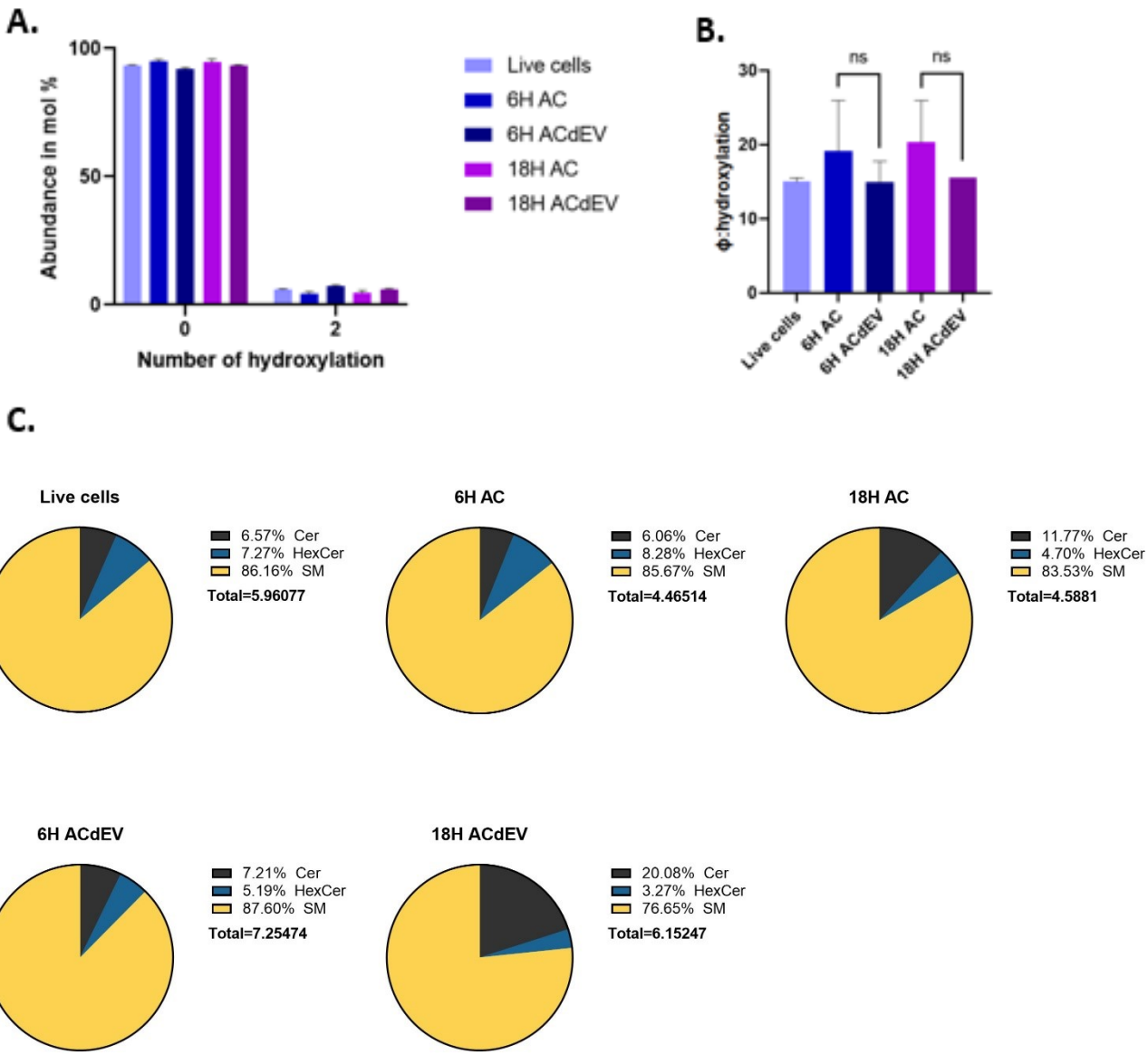

***Figure 4.15: Degree of hydroxylation of lipids in Jurkat cells and ACdEVs**. **(a)** Abundance of lipids and amount of hydroxylation. **(b)** Proportion of non-hydroxylated/hydroxylated lipid ratios across all conditions. **(c)** Representations of hydroxylated SL proportions across all conditions. Samples were measured in triplicates in three independent biological repeats (N=3). Error bars represent + SD, statistical test used: unpaired t test.*

Sterols also seems to have a better affinity for SM-OH to form highly ordered membrane domains (Jaikishan and Slotte, 2013), the decrease in SM towards late apoptosis could induce a decrease in lipid raft like domains, affecting the membrane lipid packing.

When looking at the molecular level, a total of 1197 unique species were identified across all conditions after removal of OCFA and lysolipids (**Figure 4.10**). As expected from the Lipid class enrichment data (**Figure 4.13**), most of the lipid species enriched in ACdEVs belong to the PC and Cer lipid class, and most of the species highly enriched in cells are TAG. Similarly, most of the lipid species enriched during early apoptosis belong to CE, HexCer, DAG, SM, PS and PE O- lipid classes, and most of the species highly enriched during late apoptosis belong to the PC O-, PG and Cer lipid classes.

Many mediators of inflammation are derived from phospholipids and polyunsaturated FA. Here we focus on a key lipid mediator precursor: arachidonic acid (AA). AA is a 20-carbon fatty acid with 4 double bonds (20:4) and a crucial precursor of inflammatory lipid mediators such as prostaglandin, leukotriene, prostacyclin, and thromboxane (**Figure 1.4**). Potential AA lipid precursor were identified in both 6H and 18H ACdEVs by looking at unique lipid species containing 20:4 FA chains (**Figure 4.16**). The analysis resulted in the identification of 5.8 and 5.4 mol% of total lipids, respectively. In both ACdEV populations, the species identified belong to the PC, PE O- and PE lipid classes. Interestingly, the same unique lipid species were identified in both 6H and 18H ACdEVs in similar proportions with PC 14:0_20:4; PE O-16:1/20:4; and PC 16:0_20:4. The slash separating the FA chains of the PE O- signifies that the sn-position on the glycerol was resolved (sn-1/sn-2), whereas the underscore separating the other FA chains of PC and PE could not be discriminated. Like in PE O-, a 20:4 FA chain in sn-2 position can be further hydrolysed by PLA2. Therefore, it is possible that those specific lipids are further hydrolysed into AA and further inflammatory lipid mediators, as EVs can carry active enzymes. Thus, ACdEVs can potentially deliver inflammatory lipid mediators to recipient cells and modulate immune cells response.

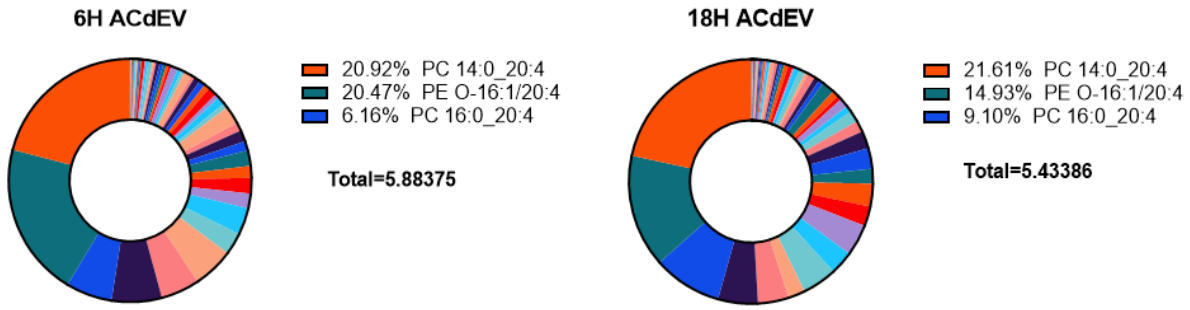

Figure 4.16: Possible arachidonic acid precursors in ACdEVs*. Quantification of unique lipid species present in 6H and 18H ACdEVs containing a 20:4 FA chain.*

Taken together, these lipidomic results demonstrate that a selective incorporation of lipids is occurring when AC release ACdEVs, and that it is different in EVs from early and late phases of apoptosis. Those distinct lipidic profiles are likely to dictate ACdEVs membranes biophysical properties and could affect their uptake and functions.

4.4. Conclusion

This chapter has reviewed the extensive characterization of early and late ACdEVs by looking at their PSD, membrane fluidity, cholesterol and protein level, as well as their lipidic composition. The PSD was similar in both 6H and 18H ACdEVs showing a highly heterogeneous population of EV predominantly of exosome-like size (up to 120 nm). The TRPS particle sizing technique was time consuming due to the needed calibration and pore clogging. The optimized MRPS revealed to be a successful alternative technique for the measurement of lipid particles. The high surface tension of small cartridges was overcome by using BSA as a wetting agent rather than detergent. The membrane fluidity was successfully measured using the laurdan probe on both cells and EVs. The membrane fluidity was found to fluctuate through apoptosis by first increasing and then decreasing towards late apoptosis. Those observations were then investigated by looking at the EVs cholesterol and protein amount, which showed no significant difference between early and late apoptosis. Finally, the MS lipidomics data were analysed by looking at the lipid classes, species, degree of saturation and lipid hydroxylation. The lipid classes results indicated a selective incorporation of lipids in EVs during early and late apoptosis. EVs were found to have less SFA and more hydroxylated SL than cells, showing how complex and multifactorial membrane fluidity is.

5. Chapter 3: ACdEV's role in modulating immune response

5.1 Introduction

As mentioned previously, the macrophage lineage derives from hematopoietic stem cells in the bone marrow and are mainly composed of vascular monocytes and tissue resident macrophages. Upon inflammatory stimuli, activated monocytes (M0) can differentiate into two main polarisation states of macrophages (MØ): either classically activated M1 MØ, or the alternatively activated M2 MØ, depending on the environmental stimulus (cytokines, microbial products, etc.). CD14 and CD11b surface markers expression is known to increase upon activation in monocytes (Kohro *et al.*, 2004). CD14 is a co-receptor for Toll like receptor that binds LPS and other PAMPs, whereas CD11b integrin family member that pairs up with CD18 to form CR3 cell surface receptor. The macrophage lineage is composed of a highly heterogeneous population of myeloid cells (Gordon and Taylor, 2005).

The role of EVs released from dying cells has been less characterised than those released by healthy cells. However, increasing evidence have highlighted the role of ACdEVs in regulating immune responses (Caruso and Poon, 2018). As mentioned in the introduction, ACdEVs harbour find me and eat me signals to attract and promote uptake of AC by efferocytes. Additionally, ACdEVs can be involved in direct antigen presentation by having MHC II molecules on their surface, or in indirect antigen presentation by delivering antigens to antigen presenting cells (Braciale, 1987; Joffre *et al.*, 2012). Finally, ACdEVs can transport proinflammatory cytokines like IL-1α and promote inflammation (Berda-Haddad *et al.*, 2011). ACdEVs were also found to inhibit dendritic cell function and aid the infection of neighbouring cells in HIV infection (Frleta *et al.*, 2012). As ACdEVs can deliver cargo to recipient cells, it likely that ACdEVs influence the polarisation of MØ towards M1 or M2 and modulate the immune response. The delivery of cargo to recipient cells in ACdEVs is poorly understood and is often cell specific. Many uptake pathways can be used by efferocytes to engulf ACdEVs such as endocytosis and cell surface membrane fusion.

5.2 Aims and objectives

In this chapter, the aim is to characterize the functions of ACdEVs in recruiting and modulating the immune function of efferocytes. For this, both early and late ACdEVs' ability to attract macrophages will be assessed by a transwell migration assay. Furthermore, the uptake of ACdEVs will be investigated by monitoring the kinetics of labelled EV's engulfment by macrophages via FCM and the possible role of membrane fluidity in modulating this process.

5.3 Results

5.3.1 Monocytes differentiation into macrophages

To study the mechanisms of ACdEV mediated apoptotic cell clearance, macrophage recruitment was investigated as it is the predominantly recruited efferocyte compared to other phagocytic cell type such as neutrophils (Eguchi *et al.*, 2015). As a model to study macrophages, the THP-1 monocytic cell line was used. Myeloid leukaemia cells can be differentiated in macrophages upon vitamin D3 (VD3) treatment in both human and mice (Abe *et al.*, 1981; Tanaka *et al.*, 1982) by binding to its nuclear receptor and promoting the transcription of macrophages genes. Prior to any functional assay, THP-1 cells were first activated by (VD3) treatment for 48 hours. The VD3 treated monocytes were then checked for the activated monocyte markers CD14 and CD11b levels by flow cytometry gated on side and forward scatter (**Figure 5.1.a**). The isotype controls for both CD14 and CD11b were incubated with activated THP-1 cells and measured by flow cytometry. Both isotypes had a similar signal in the PE channel than the unstained cells, ensuring the specificity of the antibodies staining and a low non-specific background (**Figure 5.1.b**). Upon VD3 treatment a significant increase of THP-1 cells expressing the CD11b monocyte marker compared to untreated cells was observed. However, this increase was not significant for CD14 (**Figure 5.1.c**) as the majority of the cells were already positive for CD14 prior to VD3 treatment. The significant MFI increase in CD14 expressing cells suggests that upon VD3 treatment, macrophages express more CD14 on their surface (**Figure 5.1.d**).

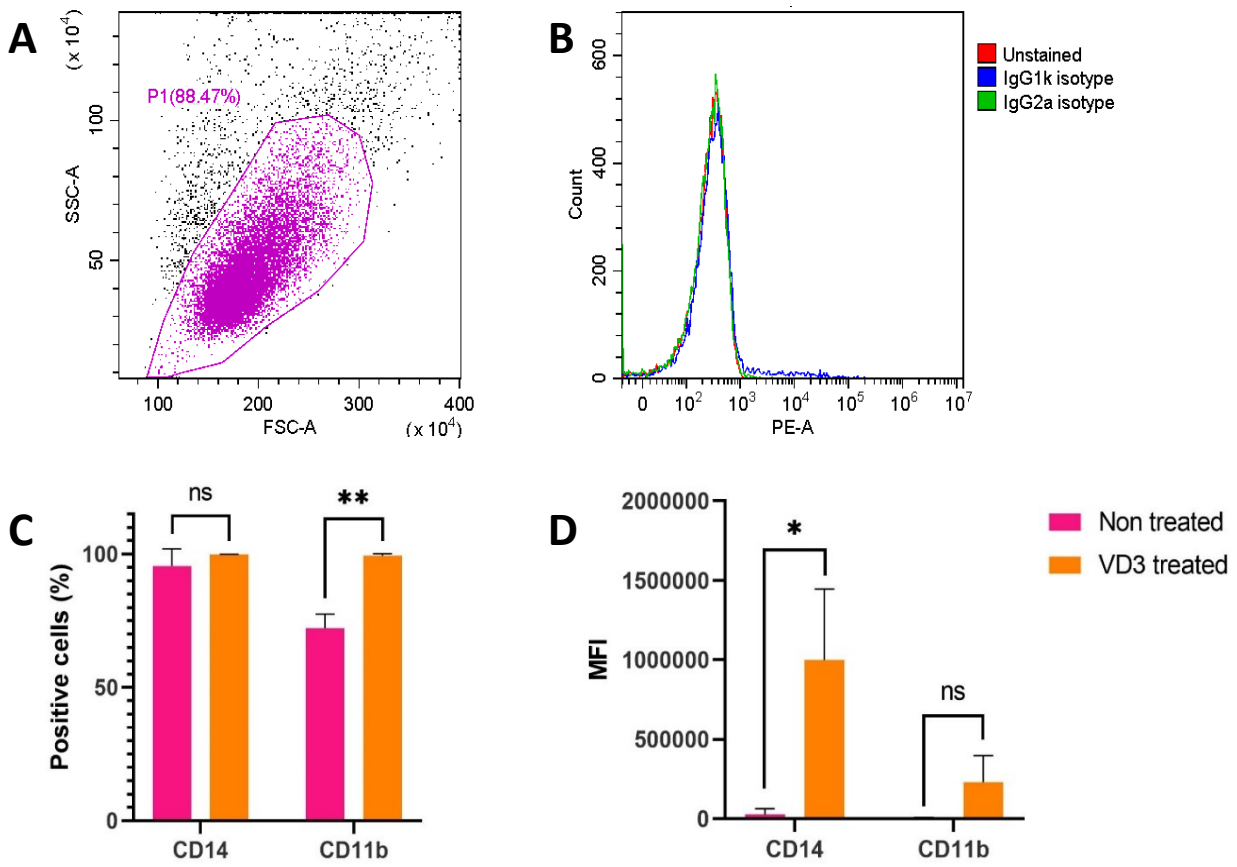

Figure 5.1: Differentiation of monocytes in macrophages. *THP-1 monocytes were treated with 100 nM VD3 for 48 hours to induce macrophage differentiation. Non-treated and treated cells were analysed by flow cytometry, gated on side and forward scatter, P1 represents live cells* ***(a)***. ***(b)*** *Isotype controls for Cd11b (IgG1k) and CD14 (IgG2a)* ***(c)*** *Percentage of THP-1 cells expressing CD14 and CD11b surface markers.* ***(d)*** *Mean fluorescence intensity (MFI). Samples were measured in three independent biological repeats (N=3). Error bars represent + SEM, statistical test used: unpaired t-test.*

Both the percentage of positive THP-1 cells and the MFI data indicate that THP-1 leukaemia cells successfully differentiate along the monocytic lineage following exposure to VD3. This method will further be used to investigate the role of ACdEVs in modulating macrophages immune response.

5.3.2 ACdEVs function as chemoattractants for macrophages

To quantify the migratory response of macrophages to ACdEVs, a transwell migration assay was used. For this, ACdEVs were seeded at the bottom of a well separated by a porous insert, while THP-1 activated monocytes were seeded in the top chamber (**Figure 5.2.a**). The plate was then inserted in the automated Cytation 5 high resolution microscopy where images were taken at 4 positions per well, every 30 minutes over 12 hours. Afterwards, the images were processed to count the migrated macrophages. To further analyse the kinetics of the migration assay, further optimisation was required using the Gen5™ software (**Figure 5.2.b**). Firstly, the 4 images per well were stitched to create one image per well at each time point. Secondly, a plug was drawn and applied to all the images in order to get rid of dark edges created by the insert than can bias the final cell count. This step also ensured that the same surface area was analysed through all the dataset making it comparable between the different conditions. Finally, the migrated cells were counted by dividing all the objects (sum area) by the average area of a single cell, where each yellow dot represents a counted cell. Initially, data showed a small cell count number that did not increase over time. This was caused by the focus of the camera that was automatically set on the insert membrane. This issue was overcome by setting a fixed focal height for the focus of the camera at the bottom of a well, where only macrophages were seeded, and no inserts were added. With the accurate image analysis and instrument settings, the migrated cells were counted over time (**Figure 5.2.b**).

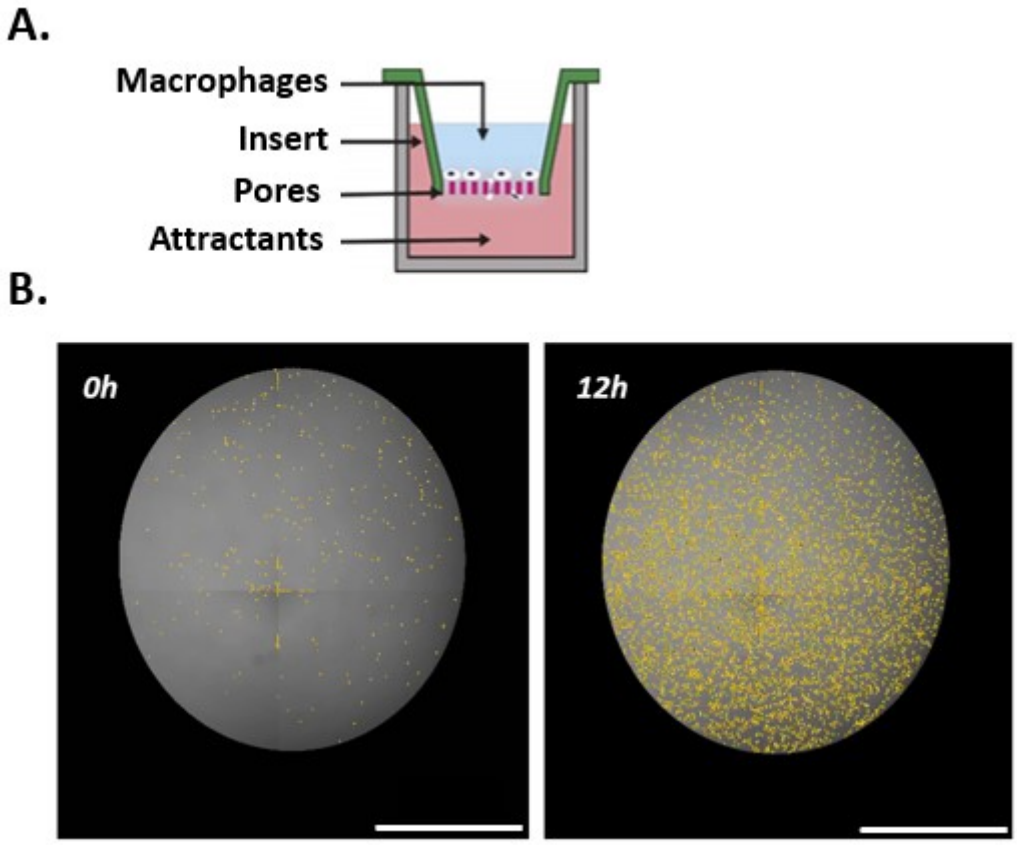

Figure 5.2: Transwell assay set up and analysis for the quantification of migrated macrophages. *Transwell migration assay of VD3 treated THP-1 cells towards 18H 2000 x g ACdEVs over time.* ***(a)*** *Schematic representation of the transwell assay.* ***(b)*** *Stitched and plugged images generated with the Gen5™ software after analysis at 0h and 12h, each yellow dot represents a counted cell. Scale bar = 2000 µm. Link to the video: https://aston.box.com/s/d4sp917n75p1l3aaz64yer51wzvejd7f.*

The 2000 x g supernatant was used as a positive control as it contains intact EVs and the apoptotic cell secretome containing all the find-me signals. The EVs collected after SEC purification have a lower concentration than the ones present in the 2000 x g supernatant as measured by ILM. The concentration of ACdEVs decreases after SEC purification from $1.67x10^9$ to $3.9x10^8$ particles/mL for early ACdEVs, and from $1.59x10^9$ to $2.1x10^8$ particles/mL for late ACdEVs (**Figure 5.3**). Indeed, 500 µL of EVs are loaded on the SEC column and 3,5 mL of purified EV fraction is collected. To ensure that the migration assay results are not due to a dose response effect, 10 mL of 2000 x g supernatant was concentrated down to 1 mL by centrifugation at 3200 x g in 10 kDa centrifugal filter tubes, prior to SEC purification to make up for the diluted SEC purified fraction.

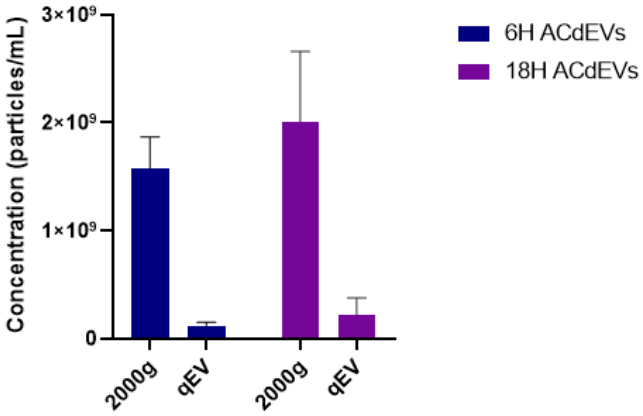

Figure 5.3: EV concentration decreases with SEC purification. *Concentration of 2000 x g supernatant or qEV purified EVs samples were measured by interferometric light microscopy using the Videodrop (Myriade). Concentration is represented in (particles/mL). Samples were measured in three independent biological repeats (N=3). Error bars represent + SEM.*

To compare the chemoattractivity of early and late apoptotic vesicles, purified 6H ACdEVs and 18H ACdEVs were seeded for the transwell assay (**Figure 5.4**). As mentioned above, the cell count corresponds to the cells counted after the plug is drawn (**Figure 5.4.a**). As the plug is different between each biological repeat it is desirable to normalise the data based on the number of seeded macrophages after the analysis (**Figure 5.4.b**). The positive control (PC) for both early and late conditions attracted macrophages increasingly until 5 hours where the number and percentage of migrated cells reached a plateau, compared to the negative control (NC) where SF-RPMI alone did not recruit macrophages over time. This indicates that within 5 hours all the macrophages have migrated, and they did so more efficiently towards the early apoptotic cell secretome (PC 6H). Similarly, to the NC, both purified ACdEV conditions showed no macrophage recruitment. The SEC purification step seems to affect the bioactivity of ACdEVs by either resulting in the loss of some important surface molecules, or by depleting the samples of crucial soluble factors.

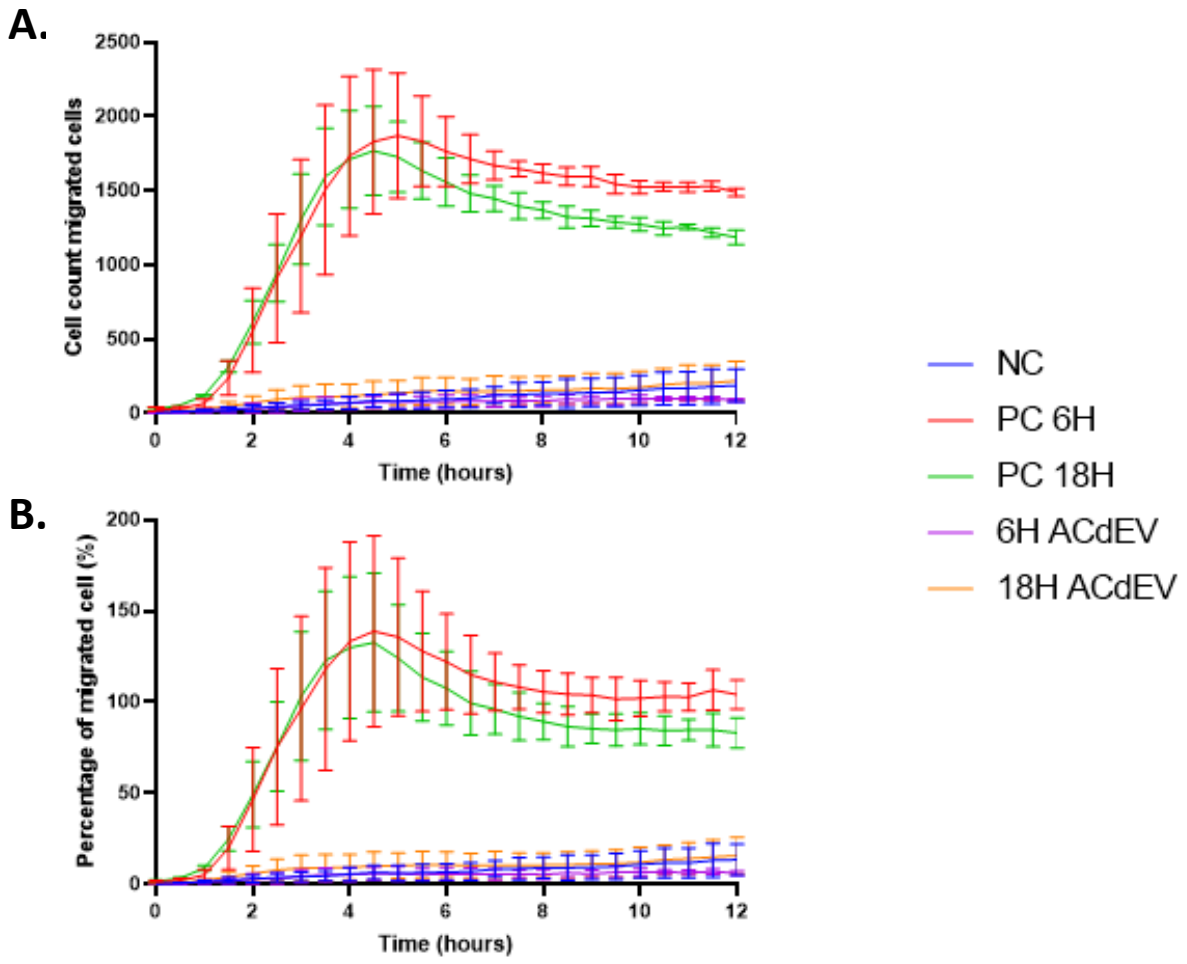

Figure 5.4: ACdEVs function as attractants for activated THP-1 monocytes. *Graphs representing THP-1 monocyte migration assay over 12 hours using different types of attractants: SF-RPMI alone for the negative control (NC), AC 2000 x g SN as the positive control (PC) and SEC purified ACdEVs derived from both early and late apoptotic Jurkat cells. Migration was quantified using the Cytation 5 equipment by* ***(a)*** *the cell count of migrated cells and* ***(b)*** *the percentage of migrated macrophage. Samples were measured in triplicates in two independent biological repeats (N=2). Error bars represent +/- SEM.*

The rapid recruitment towards early apoptotic cell secretome could be due to the fact that it contains more chemoattractants. Indeed, it was shown that lysophosphatidylcholine (LPC) was released by UV induced early apoptotic cells and acted as a chemoattractant for phagocytes (Lauber *et al.*, 2003). Even though the lysolipids were removed from the lipidomics dataset for further analysis, the abundance of LPC showed a significant 0.63-fold increase in early ACdEVs compared to late ACdEVs (data not shown), which could also participate in the rapid recruitment of macrophages.

During the early stage of apoptosis, apoptotic cells release find-me signal in the extracellular environment such as nucleotides, that aid macrophages recruitment. In an attempt to understand why macrophages are not recruited towards purified ACdEVs, a luminescent luciferin/luciferase ATP assay was conducted to detect the extracellular level of ATP present in the EV sample before and after SEC (**Figure 5.5**). Detergent was also added to quantify the intravesicular level of ATP. Results show a significant decrease in ATP concentration between 2000 x g and SEC samples suggesting that the qEV columns deplete the EV samples in soluble factors. This is very likely to happen as the qEV columns used have a recovery range of 70 to 1000 nm, meaning that small molecules like ATP will elute later. Additionally, the ATP concentration increased when adding detergent with 2000 x g EVs indicating that EVs may contain ATP.

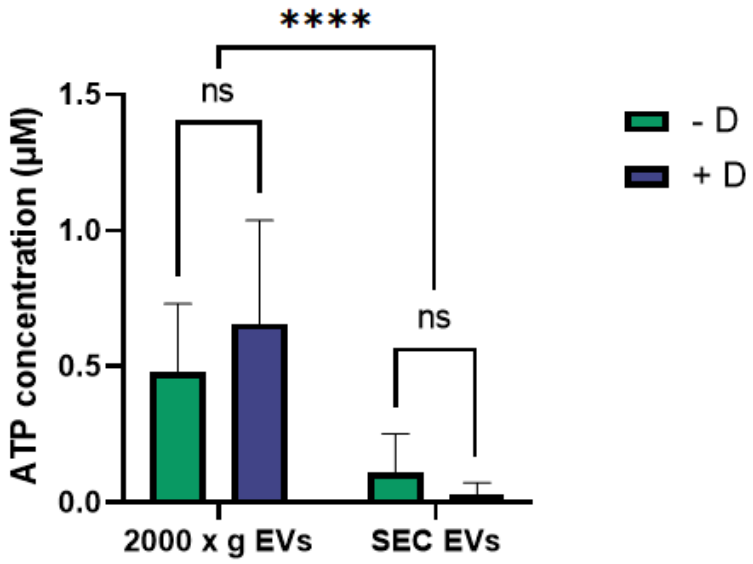

Figure 5.5. ATP quantification before and after SEC purification. *Luminescent ATP assay was used to measure the extravesicular, - Detergent (-D), or intravesicular , + Detergent (+D), level of ATP in both 2000 x g SN and SEC purified EVs. ATP concentration was quantified based on the Relative luminescence unit (RLU) of ATP standards. Statistical test used: Ordinary 2-way Anova, error bars represent SD. Samples were measured in triplicates in three independent biological repeats (N=3).*

Here, it was shown that purified ACdEVs lose their ability to recruit macrophages due to a likely depletion in soluble factor during the SEC purification step. It can be hypothesized that the same thing happens for other soluble find me signals such as UTP, CX3CL-1, LPC and S1-P. Additionally, this shows that ACdEVs alone are not sufficient to recruit macrophages (**Figure 5.4**). Finally, other evidence shows that the protein surface corona of ACdEVs is

damaged during SEC and could potentially affect their chemo attractive functions (Gomes *et al.*, 2022).

The ability of ACdEVs to release find me signals in the environment was also investigated. For this the 2000 x g SN was further centrifuged at 100,000 x g to pellet the ACdEVs in order to get rid of the ATP released by AC. Results show that the extravesicular level of ATP did not increase over time (data not shown) suggesting that ACdEVs do not release ATP in the environment.

However, it is unclear if ACdEVs are aiding the migration of macrophages by simply interacting through surface markers or by being internalized. For this an experiment was designed where labelled vesicles are incubated with activated THP-1 monocytes.

5.3.3 ACdEVs are engulfed by macrophages

As phagocytosis is mainly aimed at cells and larger entities, it is most likely that ACdEVs are engulfed via another mechanism. To investigate this hypothesis, an uptake assay was first optimized using flow cytometry. Secondly, lipid raft mediated uptake was investigated for both early and late ACdEVs, by depleting the EVs in cholesterol ultimately changing their membrane fluidity.

ACdEVs were labelled with the thiol reactive Bodipy TMR dye. Bodipy TMR gave the same results when measuring labelled EVs in the PE channel than when using Bodipy FL in the FIT-C channel, data not shown. By labelling ACdEVs with Bodipy TMR and incubating them with activated monocytes the uptake of EVs was quantified by measuring Bodipy cells in the PE channel, gated on live cells using SSC and FSC (**Figure 5.6.a**). Excess free dye can be incorporated in the macrophages membranes as well as the ACdEVs and could bias the quantification of macrophage positive cells. However, this was minimized by the wash of excess dye using SEC columns. Additionally, macrophages were washed with PBS before FCM measurements to remove bound ACdEVs. Firstly, different density of labelled ACdEVs were added to macrophages to investigate the optimal kinetics for this assay. The more ACdEVs were added, the more Bodipy positive cells were measured. However, for all the different density tested, the uptake reached a plateau indicating that all the ACdEVs have been engulfed or that macrophages phagocytotic activity was at its maximum. The 25 µL volume of ACdEVs seemed the best option as it gave a plateau at ~ 60% of Bodipy positive macrophages after 1h, which allows to compare early and late ACdEVs engulfment (**Figure**

5.6.b). Indeed 50 µL of ACdEVs was engulfed to quickly study the uptake, while 10 µL showed a very low number of Bodipy positive macrophages.

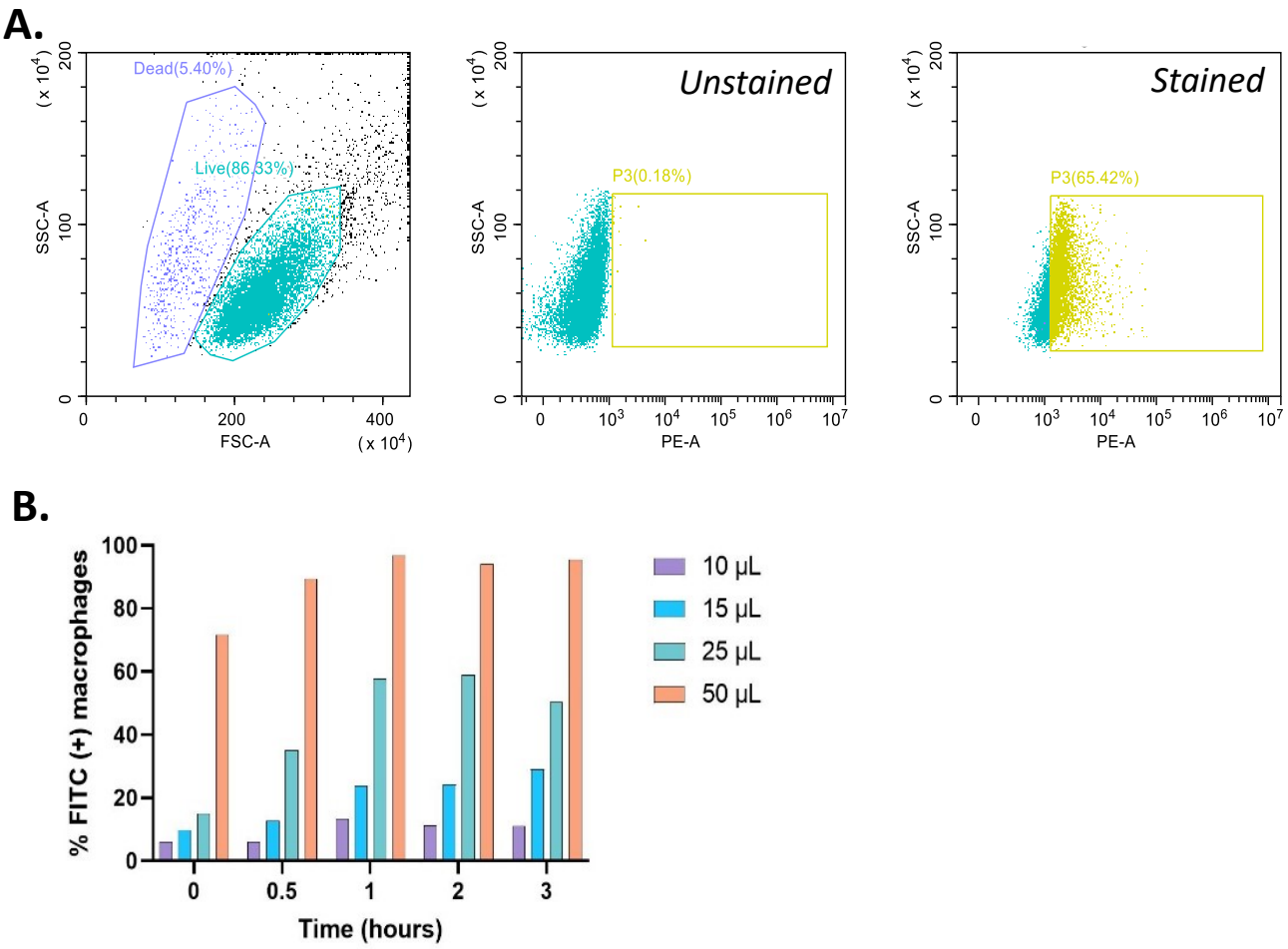

Figure 5.6: Optimisation of the EV uptake assay. *10 mL of late AC 2000 x g was concentrated down to 1 mL and stained with 5 µM of Bodipy TMR, prior to SEC purification. Bodipy labelled purified ACdEVs were then added to VD3 treated THP-1 at a density of 1x106 cells/mL. The Bodipy positive THP-1 cells were measured by flow cytometry gated on side and forward scatter, in the PE channel where 10 000 events were recorded.* ***(a)*** *Representative plots of Bodipy positive macrophages measured in the PE channel, gated on live cells using SSC and FSC.* ***(b)*** *Quantification of EV uptake over time with increasing late ACdEVs volume. N=1.*

After successfully measuring the uptake of ACdEVs by macrophages using flow cytometry, early and late ACdEVs were compared and membrane fluidity's role in this process was investigated. As the previous lipidomics data revealed, the ACdEVs are enriched in raft lipids. Lipid raft microdomains can affect the membrane fluidity and were also shown to play a role

in EV uptake. To investigate whether lipid rafts domains and membrane fluidity are involved in ACdEVs uptake, cholesterol was depleted prior to the uptake assay.

Here, methyl-β-cyclodextrin (MBCD) was used as a cholesterol depleting agent. MBCD is a heptasaccharide composed of seven glucopyranose units which forms a hydrophobic pocket (**Figure 5.7.a**). Due to the high affinity of cholesterol for MBCD's hydrophobic core, cholesterol is spontaneously extracted from the membrane, ultimately changing its composition and properties (**Figure 5.7.b**). MBCD was first incubated with 18H ACdEVs at different concentration to see whether a change in fluidity was observed as a result of cholesterol depletion. The laurdan assay data show a clear increase in GP values upon MBCD treatment proportional to its concentration compared to the negative control where no MBCD was added, although statistical analysis showed no significant differences (**Figure 5.7.c**). Thus, it can be said that depleting the ACdEVs in cholesterol leads to an increased rigidity of the membrane. This change in lipid order packing could be due to the micro fluidity of lipid raft domains affected by the depletion of cholesterol, as EVs are enriched in lipid raft like domains. For further experiments, 20 mM of MBCD will be used to deplete the membrane in cholesterol as it shows the most difference in membrane fluidity compared to the control.

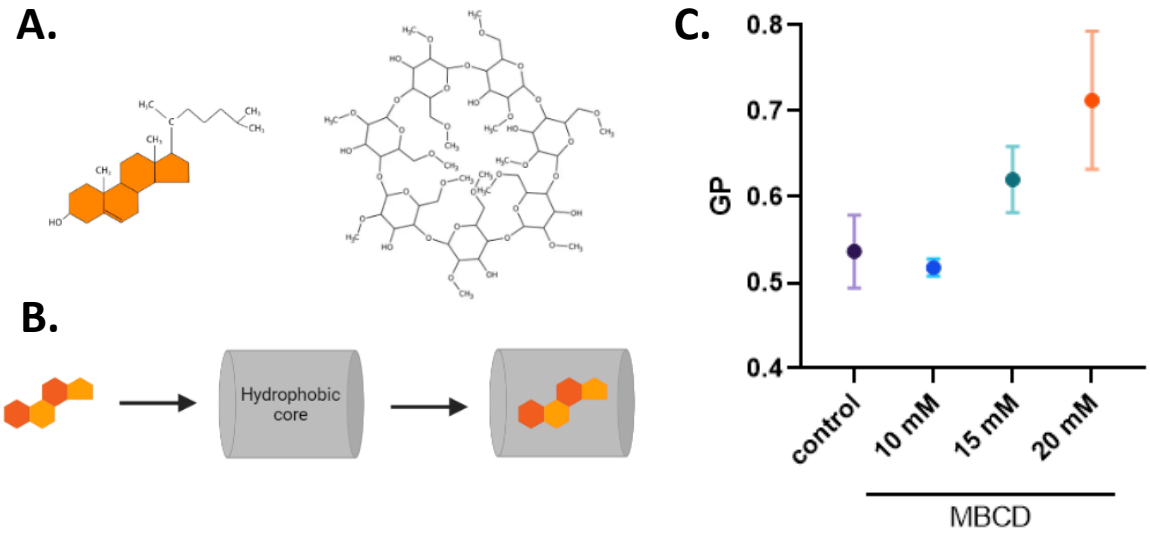

Figure 5.7: Membrane fluidity decreases upon cholesterol depletion. *18h ACdEVs were incubated with MBCD at 10 mM, 15 mM, or 20 mM for 1h at 37 °C. Generalized polarisation was measured using the laurdan assay.* ***(a)*** *Structure of a cholesterol molecule and MBCD. (**b**) Representative schematic of cholesterol depletion by MBCD.* ***(c)*** *GP values of 18H ACdEVs with titration of MBCD concentration. Samples were measured in triplicates in three independent biological repeats (N=3). Error bars represent +/- SD.*

Although MBCD depletes the outer membrane in cholesterol, it is not specific to lipid raft microdomains. As lipid raft contains more cholesterol than the rest of the membranes, they will significantly be more targeted. By incubating cholesterol depleted labelled ACdEVs with macrophages, the role of membrane fluidity and lipid raft domains in EV uptake can be assessed. Bodipy labelled early ACdEVs were added at a concentration of $1.8x10^9$ whereas late ACdEVs were added at $1.4x10^9$ particles/mL. Results show that macrophages are more efficient at taking up 18H ACdEVs rather than 6H ACdEVs (**Figure 5.8**). Indeed, within 1h only 4.16 % macrophages were Bodipy positive when incubated with 6H ACdEVs against 19.25 % when incubated with 18H ACdEVs. In both conditions, MBCD treatment increased the percentage of Bodipy positive cells suggesting that more ACdEVs are being engulfed as seen by the proportional increase in MFI. Another study has shown that liposomes with a higher fluidity exhibited a lower cellular uptake (Mitoxantrone *et al.*, 2009), supporting our findings.

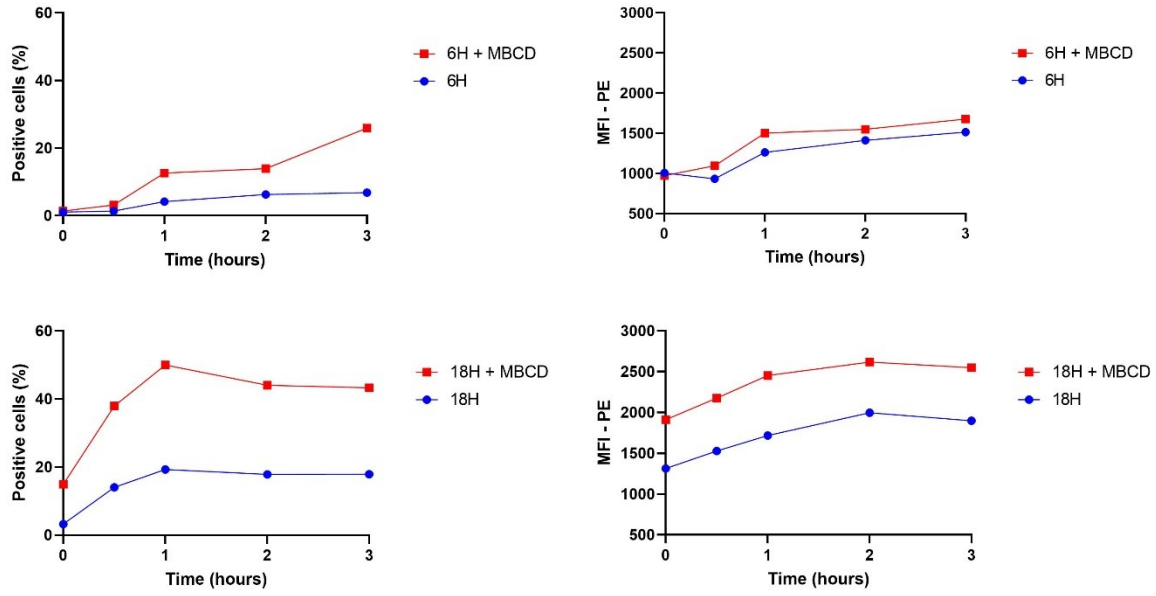

Figure 5.8: Role of membrane fluidify in early and late ACdEV's uptake. *Early and late ACdEVs were stained with 5 µM of Bodipy TMR and purified by SEC and incubated with MBCD at 20 mM. Bodipy labelled and MBCD treated ACdEVs were incubated with VD3 treated monocytes over 3 hours. Bodipy positive macrophages were measured by flow cytometry in the PE channel, gated on live cells using FSC and SSC. Data represent one measurement (N=1).*

Oxidized lipids are known to activate scavenger receptor of macrophages and promote engulfment (Vogel *et al.*, 2022). The most common form of oxidation reaction is hydroxylation. Here, the observed accumulation of oxidized lipids in late apoptotic cells and EVs (**Figure 4.15**) could contribute to the preferential uptake of 18H ACdEVs compared to 6H ACdEVs (**Figure 5.8**).

As the treated EVs were not washed a second time before incubation with macrophages, it is possible that excess MBCD depletes the macrophages membrane of cholesterol as well. Indeed, by lowering cholesterol levels in macrophages using lovastatin, an increase in apoptotic cell clearance was observed (Morimoto *et al.*, 2006). This suggests that the increased uptake of ACdEVs upon MBCD treatment could be due to a cholesterol depletion in macrophage's membrane rather than in ACdEV's membrane.

As ACdEVs carry eat me signals on their surface similarly to AC, it could explain why 18H ACdEVs were engulfed more efficiently than 6H ACdEVs. Indeed 18H ACdEVs might harbour more PS on their outside than 6H ACdEVs. To confirm this hypothesis the PS level on both ACdEVs surface was measured using fluorescent Annexin V (AnV) conjugates which binds to PS in the presence of calcium. The AnV positive ACdEVs were detected by flow cytometry in the FIT-C channel, gated against the unstained ACdEVs (**Figure 5.9.a**). The results showed a significant increase from 46 % to 68 % of AnV positive events in 18H ACdEVs compared to 6H ACdEVs, supported by the proportional MFI results (**Figure 5.9.b**). This data suggests that 18H ACdEVs have more engulfment signal and thus are preferably taken up by macrophages compared to 6H ACdEVs.

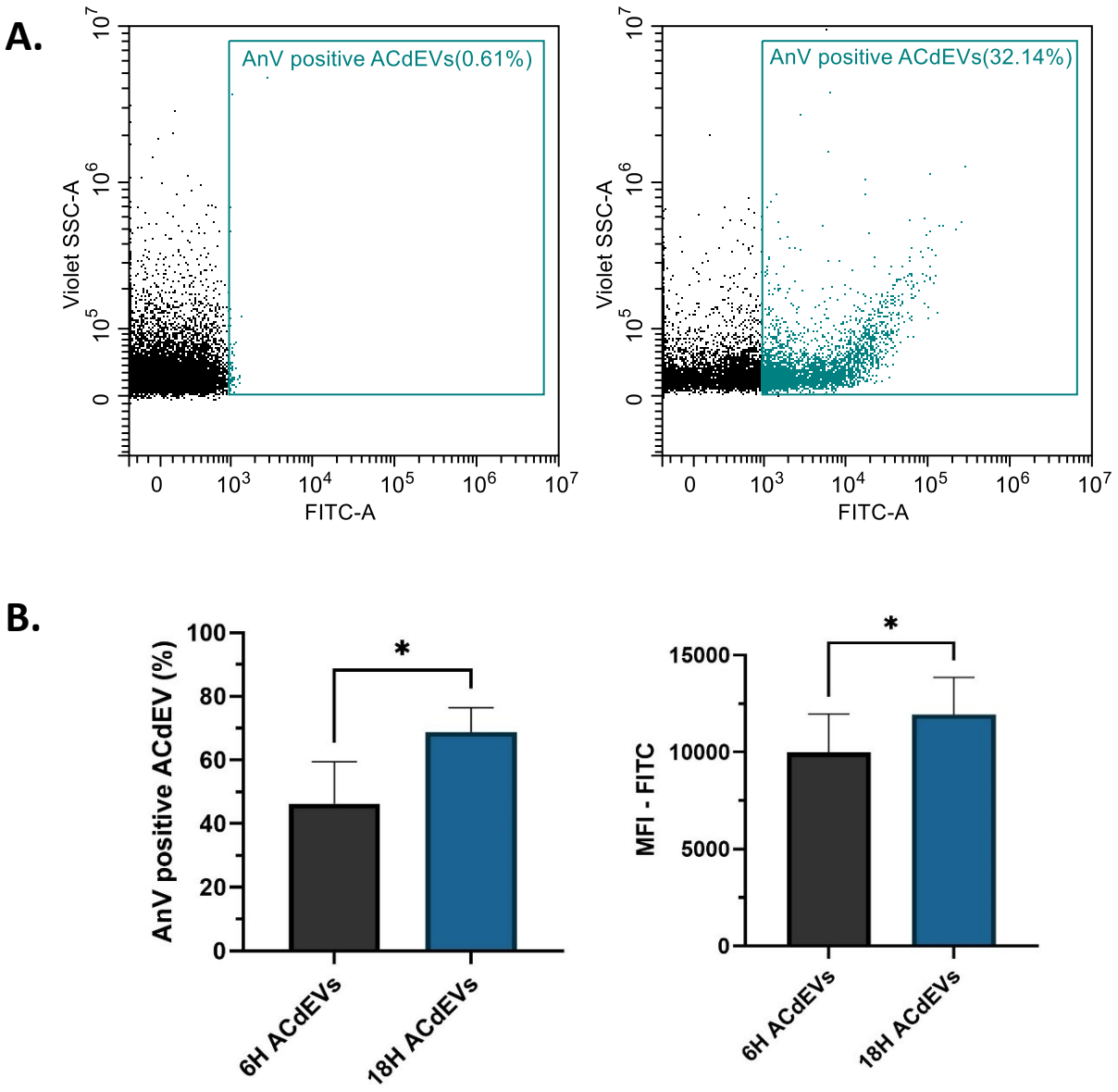

Figure 5.9: EVs released by late AC have greater PS levels than those released by early AC. *6H and 18H EVs from apoptotic Jurkat cells were isolated and purified by SEC before staining with annexin V-FITC for surface PS.* ***(a)*** *EVs were gated on size and fluorescence using violet side scatter and the FITC channel. Unstained samples were used for the initial setting of the gate.* ***(b)*** *Percentage of positive cells and mean fluorescence intensity is represented. Statistical test used: paired t test. Samples were measured as three biological repeats (N=3).*

These previous results are in contradiction with the MS data. Indeed, the lipidomic analysis revealed that PS was significantly enriched in 6H ACdEVs compared to 18H ACdEVs (**Figure 4.13**). Although AnV only binds to the PS present on the external leaflet of the EV membrane, the MS quantifies the total level of PS. It can be proposed that overall late ACdEVs have less PS than early ACdEVs, however, more of it is found on the surface of the EV and therefore more accessible to AnV suggesting that PS continues to be flipped from the inner leaflet towards the outer leaflet of the membrane throughout apoptosis.

The increased uptake of MBCD treated ACdEVs by macrophages could be the results of various changes within the membrane. As previously shown, cholesterol depletion can increase the membrane rigidity of ACdEVs. Cholesterol depletion can also affect the membrane surface charges. Indeed, decreasing the cholesterol level in a phospholipid membrane was found to increase its surface charges (Magarkar *et al.*, 2014), becoming more positive. As cholesterol is depleted, the membrane becomes more negatively charged, interacting more with positive extracellular ions such as Na^+. As ACdEVs are depleted in cholesterol, their surface charges might increase which could effectively affect their uptake by macrophages. The zeta potential, or electrokinetic potential, is a popular indicator of surface charges and is used here to look at ACdEV surface charges. For this, MBCD treated- and non-treated 18H ACdEVs were measured by TRPS. As observed in other EVs, ACdEVs were found to have an overall negative zeta potential (Midekessa *et al.*, 2020). As EV's most abundant lipids are phospholipids, it is thus expected that they carry a negative charge due to the phosphate group presence in PL head group. Results show that MBCD treated ACdEVs have a more positive zeta potential than non-treated ACdEVs with a mean zeta potential of -19.25 mV compared to -38.89 mV, respectively (**Figure 5.10**). It can also be observed that non-treated ACdEVs comprise small vesicles of various zeta potential ranging from -100 to 100 mV, whereas MBCD treated ACdEVs tend to have a similar zeta potential.

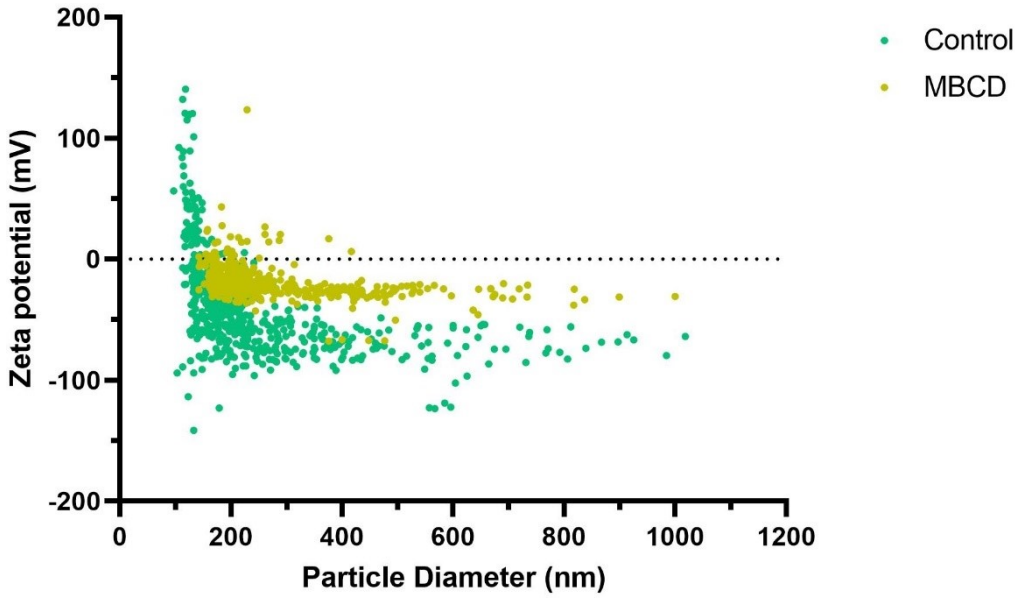

Figure 5.10: Cholesterol depletion increases the surface charges of ACdEVs. *Non-treated and MBCD-treated 18H ACdEV's membrane zeta potential was measured by TRPS with the Exoid. A NP-200 nanopore was used, with a 49.99 mm stretch and a 300 mV baseline voltage.*

The surface charges can influence different biological processes associated with EVs such as their uptake. Indeed, phagocytic cells preferentially take up anionic nanoparticles (Fröhlich, 2012). Upon MBCD treatment, the ACdEVs become less anionic but their uptake is still more efficient than the non-treated more anionic ACdEVs. This shows how complex ACdEVs membranes are, and that by changing their composition and properties we can affect their uptake, possibly by influencing membrane protein activities involved in EV uptake.

5.4 Conclusion

This chapter has successfully reviewed some of ACdEVs role in modulating immune response by characterizing the mechanisms behind their ability to recruit and being engulfed by macrophages. For this, THP-1 monocytes were successfully differentiated in macrophages upon VD3 exposure, and both migration and uptake assays were optimised. SEC purified ACdEVs did not recruit macrophages due to a soluble factor depletion containing find me signals such as ATP. ACdEVs uptake was increased when released during late apoptosis and upon cholesterol depletion. This is due to an increase level of eat me signals such as PS, and an increased membrane rigidity and surface charges, respectively.

6. Chapter 4: microfluidic passive filtration using hydrodynamic separation for EV separation

6.1 Introduction

It is important to isolate EV from non-vesicular components but also to fractionate the different EV subtypes for functional studies. Indeed, ApoBDs and ApoMVs found to be physiologically different due to dissimilarity in membrane integrity (Wickman *et al.*, 2013b). Additionally, small EVs and large EVs from apoptotic Jurkats were also found to carry different protein cargo (Tucher *et al.*, 2018). It can only be hypothesized that due to their difference in size, membrane properties, and composition, that small and large ACdEVs have different functions. To investigate this hypothesis, it is important to separate EVs based on their size. Current conventional method for size-based isolation of EVs can be damaging, time consuming and high-cost. Microfluidic isolation is a promising field, which offers miniaturisation of conventional techniques, quicker purification times and improved resolution while enabling a continuous separation of EVs. One alternative method for EV separation utilizes microfluidic chips to separate EV samples based on their size only to obtain small and large EVs based on the recovery range of the chip. This passive separation using hydrodynamic separation has the advantage of being less damaging for the EVs as it is a low energy isolation technique utilizing the flow field and channel's structure. Most microfluidic sized based particle separation are still in the microscale rather than nanoscale, as the miniaturization of techniques can be challenging.

In inflammation, soluble factors are key players of intracellular communication as they can stimulate and reprogram recipient cells in favour of the resolution of the inflammatory process (Abdulkhaleq *et al.*, 2018). Such soluble factors include cytokines, chemokines, pro resolving mediators, etc. Dying vascular smooth muscle cells can induce both apoptosis-induced apoptosis and proliferation in nearby cells, depending on their cytokine secretome (Aravani *et al.*, 2020), highlighting the importance of soluble factors in dictating the outcome. Similarly, apoptotic cells signal their presence and recruit immune cells to the site of cell death by secreting soluble factors, constituting ACdEVs microenvironment. Subsequently, it is crucial

to keep this microenvironment when investigating the mechanisms behind ACdEVs mediated apoptotic cell clearance, to mimic in vivo conditions and outcomes.

6.2 Aims and objectives

Given the limitations of current isolation methods, a low-force regime that can retain the soluble factors and any other loose associated components for size-based EV isolation is highly desirable. Here, a microfluidic, label free, high throughput, sized based separation technique was investigated for ACdEVs isolation. For this, the size of the recovery range was characterised as well as the fate of soluble factors.

6.3 Results

5.3.1 Characterization of the microfluidic chip

The microfluidic chips used in this study are manufactured by the company µFraction8. They are made of polymethyl-methacrylate (PMMA) and SU-8 clear polymer using photolithographic techniques. PMMA being a photoresistant and SU-8 a thermoplastic material, the combination of both makes a highly biocompatible microfluidic device. The chip can be manufactured with different channel size, here the chip with 15 µm channel size was investigated. The samples are continuously perfused through the chip via the input hole at a specific flow rate, generated by an algorithm (part of proprietary information from µFraction8). The branched side channels inside the microfluidic devices then separate the particles to different outlets based on their size (**Figure 6.1.a**). The smaller particles are expected to come out of both outlets, whereas the larger particles are expected to come out at the large outlet (LO) (**Figure 6.1.b**).

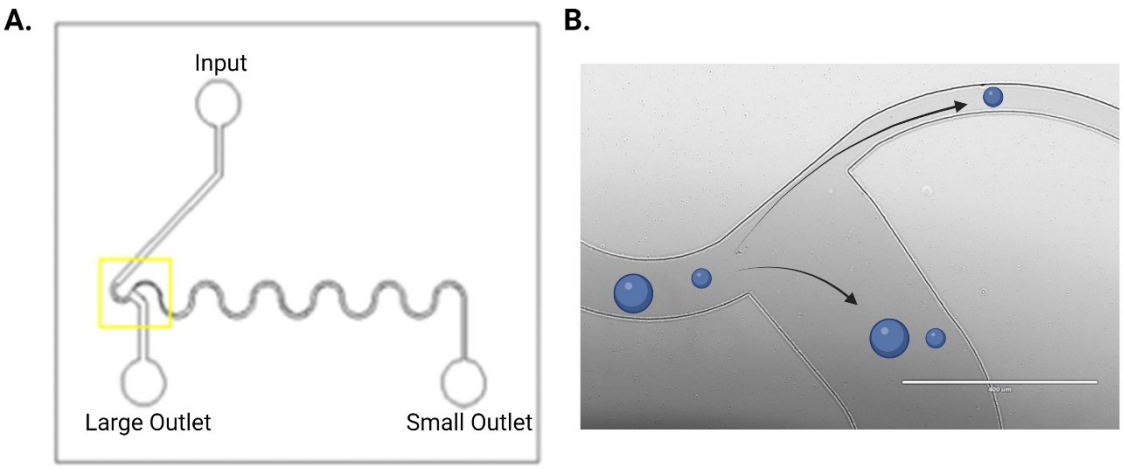

Figure 6.1: Microfluidic chip for particle separation by hydrodynamic separation. (a) *Microfluidic chip design showing input, the large outlet (LO) and the small outlet (SO).* ***(b)*** *Close up view of the LO intersection using EVOS inverted microscope, scale bar = 400 µm, 10x magnification. Schematic representation of particle flow shows large particles isolated at the LO while small particles are isolated at both outlets.*

Firstly, the chip was perfused with bromophenol blue to calculate its void volume of ~3.5 mL. To determine the recovery range at each outlet, a mix of standard size nano beads of 60-, 100-, 150-, 200-, 300-, and 1000 nm was perfused through the microfluidic chip and measured by MRPS using the nCS1 instrument. By combining the TS-400 and TS-2K measurements, the data showed that all the sized beads were able to be detected prior to perfusion (**Figure 6.2.a**).

All the beads were recovered at the LO (**Figure 6.2.b**), whereas the 1000 nm beads were absent from the small outlet (SO) fraction (**Figure 6.2.c**). These results showed that small particles remain diffuse through both outlets whereas the larger ones are being isolated at the LO, as expected. To overcome this issue, recirculation of the large outlet fraction would concentrate small particles at the SO while isolating large particles at the LO. The size of the larger vesicles that can be isolated will depend on the size cut-off of the microfluidic chip, which is somewhere between 300 nm and 1000 nm. The size cut-off of the chip will depend on the size and structure of the microfluidic channel as well as the flow field. Additionally, the concentration of the beads remains relatively unchanged following microfluidic isolation which constitute a significant advantage over SEC isolation.

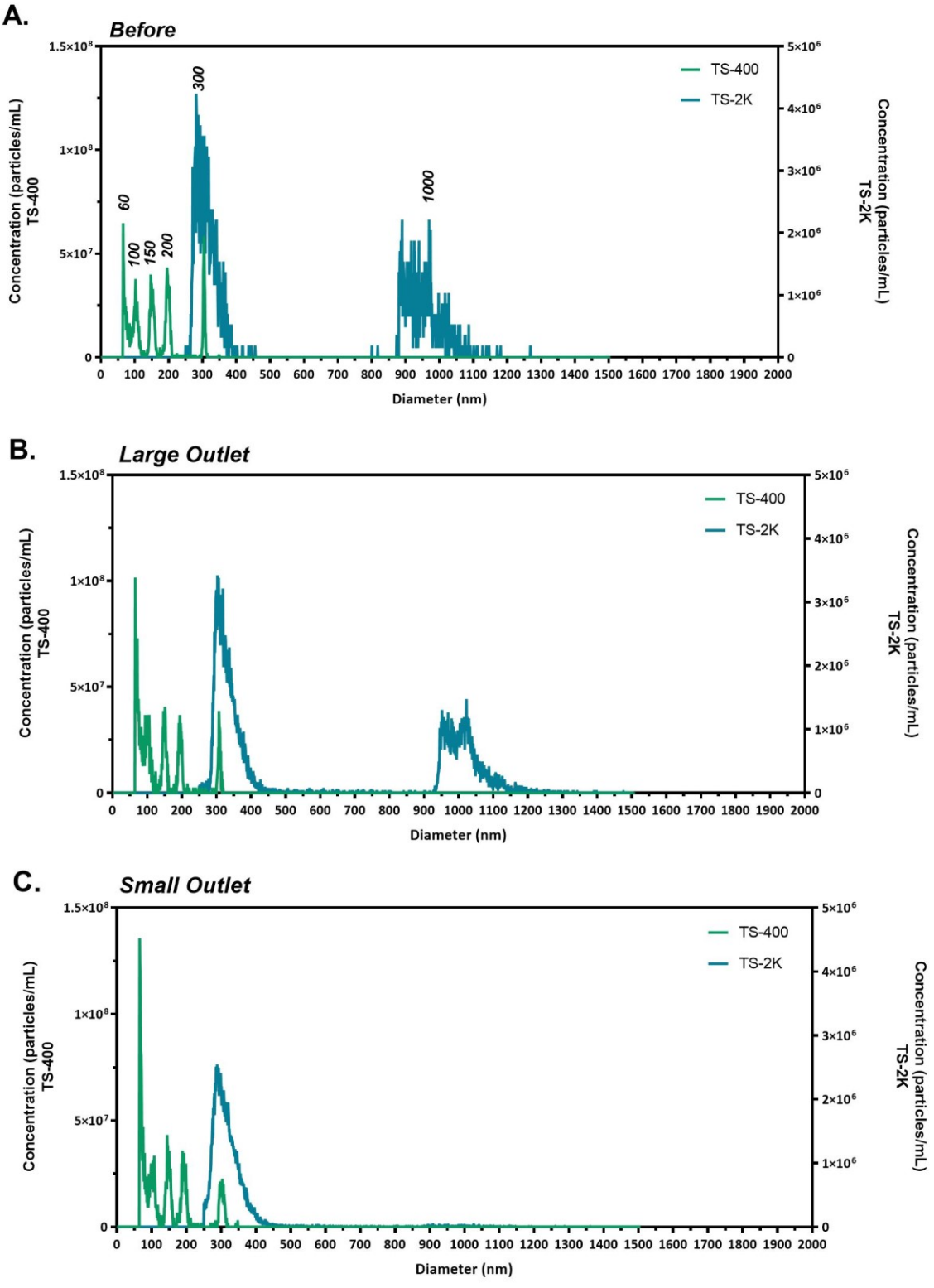

Figure 6.2: Size cut off determination of the microfluidic chip – Standard beads*. Sizing and quantification of a nanosphere mix measured before, at the large outlet and small outlet fractions by MRPS using TS-400 (65-400 nm) and TS-2k (250-2000 nm) cartridges.*

To get a more accurate sizing of the recovery range of the microfluidic chip, 18H ACdEVs were perfused as their heterogeneity will help to define the size cut off previously set between 300 nm and 1000 nm. Using the TS-400 cartridge no difference was observed between the SO and the LO meaning that the size cut-off of the microfluidic chip is above 400 nm (data not shown).

By focusing on the TS-2K measurements, data showed a similar size distribution trend for the measurements of EVs from the input and LO fractions. However, very few particles with a diameter above 550 nm were present in the SO fraction (**Fig 6.3.a**). This was confirmed by the analysis of the normalized area under the curve of different size ranges (**Fig 6.3.b**). Indeed, the percentage of area under the curve (AUC) for the 500-2000 nm section is of 32 % for the SO against 62 % and 65 % for the LO and Before measurements, respectively. Additionally, the percentage of AUC for the 550-2000 nm section was of 17 % for the SO against 49 % and 53 % for the LO and Before measurements, respectively (**Fig 6.3.b**). All together, these data showed that the microfluidic chip can isolate large particles above ~550 nm, collected at the LO.

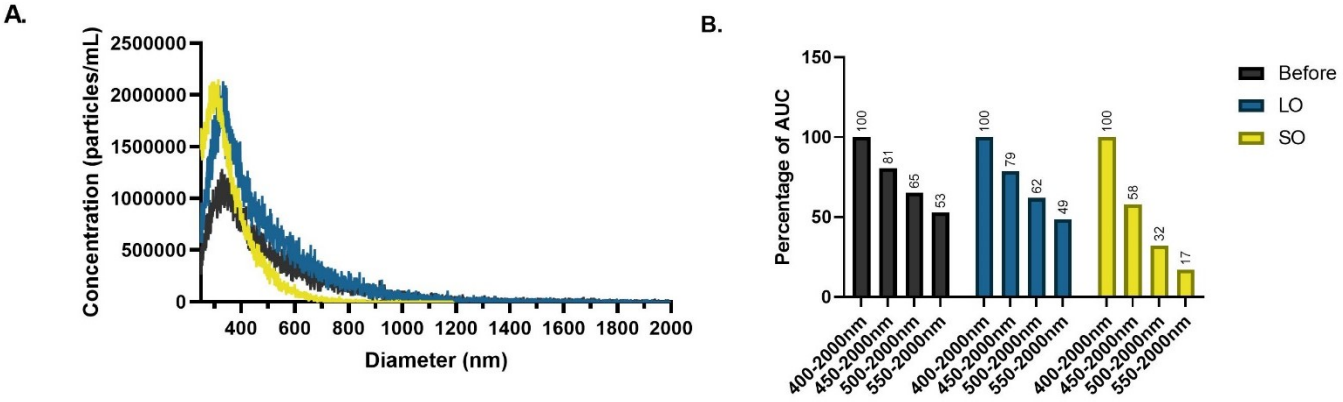

Figure 6.3: Size cut off determination of the microfluidic chip – ACdEVs. ***(a)*** *Sizing and quantification of 18H ACdEVs from the Before, LO and SO fractions, measured in 0.1% BSA using TS-2k cartridges on the nCS1.* ***(b)*** *Percentage of area under the curve (AUC) of different size ranges normalized by the total AUC from 400 to 2000 nm. N=1.*

Following up on the last experiments, the relevance of this microfluidic chip for the isolation of small and large ACdEVs was investigated. MegaMix forward and side scatter standard size beads were used to determine the relative sizes of small and large EVs after gating using FIT-C fluorescence (**Figure 6.4.a,b**). Small and large Bodipy labelled EVs were detected against

unstained ACdEVs in the manually drawn gates of 200 nm and under, and 200 nm and above (**Figure 6.4.c**). As shown on the representative FCM plot, 66.97 % of the stained ACdEVs are in the small EV region against 0.11% stained ACdEVs in the large EV region (**Figure 6.4.d**). The use of flow cytometry gating confirmed that this device is not suited for the separation of ACdEVs into two different sized subpopulations as the majority of the vesicles are of small diameter under 200 nm which is below the size cut-off of the previously characterised microfluidic chip.

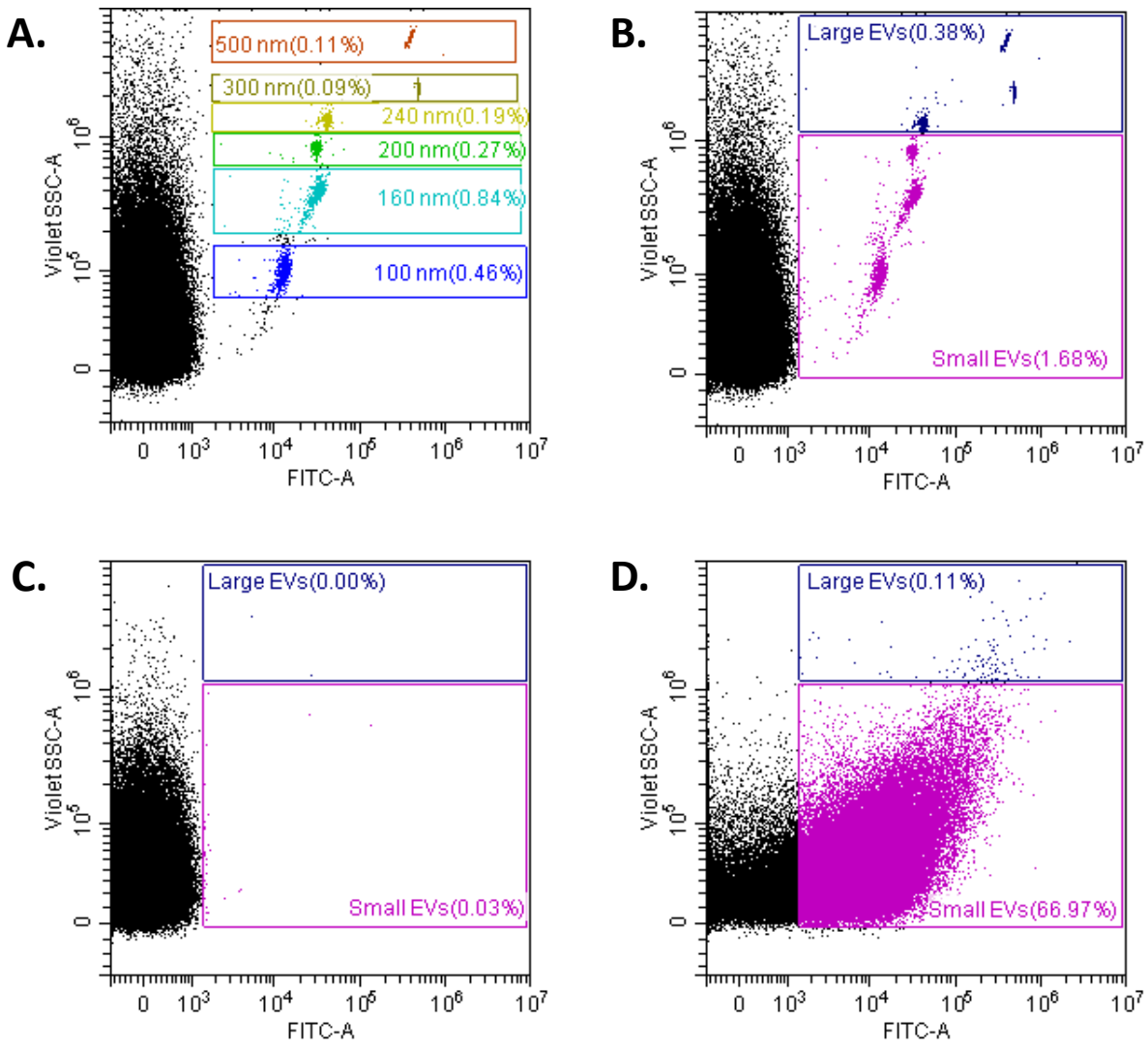

Figure 6.4: Application to ACdEVs samples. *MegaMix side scatter beads were detected by fluorescence in the FITC channel, and their size was differentiated by violet side scatter. Small and large regions were manually drawn.*

However, by downscaling the microfluidic chips production with the appropriate channel sizes, this isolation method could be used to isolate small and large ACdEVs. Indeed, our ACdEV samples are enriched in small EVs due to the depletion of larger vesicles during the differential centrifugation isolation step at 2000 x g. However, if the whole AC secretome (300 x g SN) was investigated, which contains larger vesicles and apoptotic bodies, this sized based separation method could be more suitable. Compared to other microfluidic devices, this microfluidic chip was able to separate particles in the nanoscale (Shen *et al.*, 2017; Palumbo *et al.*, 2020).

As shown in the previous chapter (section 5.3.2), soluble factors isolated alongside EVs form an important part of their biological activity and can be lost in some approaches such as SEC. The soluble factors fate upon microfluidic isolation was investigated by looking at their proportion at both outlets. To mimic the fate of soluble factors within the chip, BSA was used as it is composed of a highly soluble protein. For this, a 0.2 % BSA solution was perfused through the chip, and its absorbance at 280 nm was measured. Statistical analysis showed no significant difference in BSA concentration between the Before, SO and LO fractions (**Figure 6.5**). This demonstrates that unlike other isolation method, microfluidic isolation allows to retain the soluble factors as they diffuse equally to both outlets. This is promising for the isolation of ACdEVs as soluble factors present in the AC secretome plays an important role in directing the migration of immune cells and aid to the rapid clearance of apoptotic cells to avoid secondary necrosis.

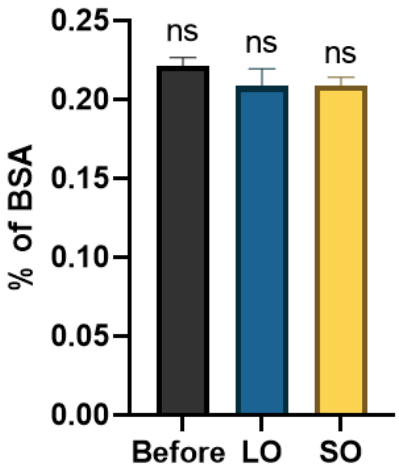

Figure 6.5: Soluble factor diffusion. *Percentage of BSA measured by Nanodrop before and after going through the chip (LO and SO) as an indicator of soluble factor diffusion. Samples were measured as three biological repeats (N=3). Statistical test used: Tukey's multiple comparison one-way ANOVA, error bars represent + SD.*

6.4 Conclusion

This chapter has attempted to provide an insight on a novel EV separation method using microfluidics. The potential of microfluidic passive separation technique using hydrodynamic separation as a novel sized-based EV isolation method was investigated. The microfluidic device used was shown to isolate large particles above ~550 nm at the LO while small particles and soluble factors remained diffused at both outlets. Whilst the data presented here suggests the channel size of the chips is too large for the envisaged application, if it is technically possible to produce chips with a smaller channel size, it should be possible to separate particles in a range relevant for EV studies. This would have the advantage of retaining soluble factors whilst allowing fractionation based on size, possibly using a number of microfluidic chips in series.

7. Chapter 5: General discussion and future work

7.1 General conclusion and discussion

While most ACdEVs studies have focused on the structure-function relationship of larger EVs such as apoptotic bodies (Xu, Lai and Hua, 2019), limited information is available on smaller ACdEVs. This is mainly due to the fact that apoptotic bodies were the first type of ACdEVs discovered and that their larger size allows for an easier isolation. Additionally, the proteome is often the first extensive characterization when studying such entities functions as ACdEVs associated proteins were found to be involved in various biological process (Caruso and Poon, 2018b). Although the proteome of EVs has been listed in several studies, the EV lipidome is less covered. This study gives a new perspective on ACdEV's role in apoptotic cell clearance by focusing on smaller ACdEVs and looking at different properties such as membrane fluidity, lipidomics and surface charges.

This project has extensively characterised ACdEVs in line with the minimal international society of extracellular vesicles (MISEV) guidelines for EV characterization published by ISEV (Théry *et al.*, 2018). The quantitative measure of the source was stated (apoptotic Jurkat cells at $4x10^6$ cells/mL), the abundance of EVs was quantified (particles/mL and protein quantification), the presence of component associated with EV was tested (externalized PS), and the presence of non-vesicular component was investigated (soluble factors quantification). Results showed that in addition form apoptotic bodies, apoptotic Jurkat cells continuously released a smaller EV population as well. The heterogeneity of this population was demonstrated through their various sizes, shapes, structures, compositions, and membrane properties.

ACdEVs released during early and late apoptosis exhibited significant differences in membrane fluidity, lipidic composition and functions. This suggests that early and late apoptotic cells are releasing two distinct ACdEVs populations, or that early ACdEVs formation and loading is a controlled process whereas late ACdEVs formation and loading occurs more randomly as the cell membrane loses its integrity. The immunological consequences of early and late apoptotic cell clearance being different, a similar outcome for ACdEVs could be observed. Indeed, early apoptotic cell uptake is anti-inflammatory whereas late apoptotic cell

or necrotic cell uptake is inflammatory (Poon, Hulett and Parish, 2010). However, this outcome can be influenced by many different factors such as the experimental model, the microenvironment, the cell type, the type of cell death, etc.

The recruitment of phagocytes was more efficient towards early apoptotic cell secretome. This rapid recruitment is probably required to prevent dying cells from undergoing further necrosis and releasing their content into the environment. When ACdEVs were isolated by SEC, they lost the ability to recruit phagocytes by depleting them of crucial soluble factors. It can be proposed that ACdEVs alone are not sufficient to actively recruit efferocytes. When looking at the functionality of EVs, it may be more appropriate to choose a different isolation method that retains the EVs microenvironment to mimic physiological conditions even though the complexity of in vivo conditions might not be reached. Novel isolation techniques such as microfluidic passive separation are very promising for the EV field, as it was shown to retain soluble factors while isolating the EV based on their size.

The uptake of ACdEVs by macrophages was more efficient towards late apoptotic EVs as they were found to carry more eat me signals on their surface, which triggers intracellular signalling required for uptake. It is well known that EVs can deliver their cargo to recipient cells. Here it could be hypothesized that ACdEVs deliver precursor of mediators of inflammation to efferocytes, modulating their phenotype and aiding the resolution of inflammation. Such process could be mediated by the delivery of arachidonic acid precursor upon ACdEVs engulfment by macrophages, which could be further processed by macrophages COX and LOX into inflammatory lipid mediators. Such enzymes have been identified in exosomes and could potentially be present in ACdEVs as well (Esser *et al.*, 2010). Additionally, the engulfment of EVs was inhibited or enhanced by modulating their membrane fluidity and surface charges.

Overall, ACdEVs are complex communicasomes able to modulate the immune response by recruiting and interacting with macrophages. Early ACdEVs, are more fluid and chemoattractive, whereas late ACdEVs are more rigid, and uptaken more efficiently. These results support the hypothesis that early ACdEVs are aiding the rapid recruitment of immune cells to the site of cell death, by forming a gradient. Additionally, the properties of late ACdEVs suggest the possible release of pro inflammatory bioactive lipid mediators and could thus prime macrophages towards a M1 phenotype to prepare them for an effective efferocytosis. Due to their ability to interact with immune cells such as phagocytes, ACdEVs-based therapies are especially relevant in transplantation tolerance, immunotherapy, vaccine development,

etc. Based on this study, ACdEVs could be potential therapeutical targets for inflammatory diseases with abnormal macrophages influx and efflux. Additionally, this study provides groundwork for ACdEVs, and more widely, EVs engineering as it shows that not only the EV cargo is of importance but other factors too (lipid composition, membrane fluidity, surface charges). Modulation of such factors can directly affect the uptake and efficiency of these engineered EVs. It is vital to have a comprehensive understanding of EV surface composition (and content) to fully understand their function. However, as highlighted in this study, there are challenges in the characterization and isolation of EVs, making it difficult to accurately define their functions. To advance the field, it is crucial to identify which criteria are the best to distinguish different subtypes of EVs and develop standardised techniques and protocols to study EVs. Lipidomics should support a new and fundamental way of discriminating between different EV subtypes and, indeed, the lipid composition of the membrane is likely vital in tuning the activity of these subtypes. Not only do the biophysical properties of the membrane affect functions such as membrane fusion, they also modulate the activity of membrane proteins within EVs, further affecting their activity.

7.2 Future work and recommendations

As noted above, whilst early and late ACdEVs had distinct differences in vitro, this work has raised a number of important questions and routes of investigations:

Future work could focus on the characterisation and functions of ACdEVs generated during other types of cell death such as necrosis and autophagy. Additionally, it would be interesting to compare whether the composition, properties and functions observed in early and late ACdEVs were affected by other types of apoptotic inducers (biological and chemical). Similarly, it would be beneficial to confirm these findings across different cell types and primary cell lines.

As the technique used here failed to isolate ACdEV to homogeneity, some other EV released by non-apoptotic cells remained. As EVs derived from non-apoptotic cells should have less exposed PS, it would be interesting to look at PS-high and PS-low proportions of EVs. As mentioned previously, AnV binds to PS in the presence of calcium. By using biotin-conjugated AnV, PS expressing vesicles can be magnetically captured with streptavidin coated beads in the presence of calcium. By progressively decreasing the concentration of calcium, low- to high-PS EVs could be eluted in different fractions, thus determining the proportions of ACdEVs vs non-apoptotic cells derived EVs.

There is a current limited knowledge on the biogenesis of ACdEVs that do not classify as apoptotic bodies. Here, the selective incorporation of lipids in early and late ACdEVs could indicate a different formation mechanism. To investigate this hypothesis, endosomal and plasma membrane lipids could be labelled prior to induction of apoptosis, and the proportions of both lipids could be looked at in the produced ACdEVs during early and late apoptosis. Furthermore, the ACdEVs lipid fate in recipient cells could be followed up. Finally, the fate of ACdEVs after engulfment by macrophages could also be looked into, by checking their presence in the phagolysosome by using the PH sensitive pHrodo dye.

My Publications

A. Rozo, M. Cox, A. Devitt, A. Rothnie, and A. Goddard. “Biophysical analysis of lipidic nanoparticles”. Methods, vol. 180, 2020, doi: 10.1016/j.ymeth.2020.05.001.

A. Goddard, J. Linney, **A. Rozo**, J. Oates, and A. Watts. “Membrane Proteins: Structure and Organization”. Encyclopaedia of Biophysics. Springer, pp. 1-4, 2020, doi:10.1007/978-3-642-35943-9_748-1.

References

Abdulkhaleq, L. A. *et al.* (2018) ‘The crucial roles of inflammatory mediators in inflammation: A review’, *Veterinary World*, 11(5), pp. 627–635. doi: 10.14202/vetworld.2018.627-635.

Abe, E. *et al.* (1981) ‘Differentiation of mouse myeloid leukemia cells induced by 1α,25-dihydroxyvitamin D3’, *Proceedings of the National Academy of Sciences of the United States of America*, 78(8 I), pp. 4990–4994. doi: 10.1073/pnas.78.8.4990.

Adada, M., Luberto, C. and Canals, D. (2016) ‘Inhibitors of the sphingomyelin cycle: Sphingomyelin synthases and sphingomyelinases’, *Chemistry and Physics of Lipids*. Elsevier Ireland Ltd, 197, pp. 45–59. doi: 10.1016/j.chemphyslip.2015.07.008.

Akers, J. C. *et al.* (2013) ‘Biogenesis of extracellular vesicles (EV): Exosomes, microvesicles, retrovirus-like vesicles, and apoptotic bodies’, *Journal of Neuro-Oncology*. doi: 10.1007/s11060-013-1084-8.

Aluvila, S. *et al.* (2014) ‘Organization of the mitochondrial apoptotic BAK pore: Oligomerization of the BAK homodimers’, *Journal of Biological Chemistry*. Â© 2014 ASBMB. Currently published by Elsevier Inc; originally published by American Society for Biochemistry and Molecular Biology., 289(5), pp. 2537–2551. doi: 10.1074/jbc.M113.526806.

Alvarez-Erviti, L. *et al.* (2011) ‘Delivery of siRNA to the mouse brain by systemic

injection of targeted exosomes', *Nature Biotechnology*. doi: 10.1038/nbt.1807.

Amato, L. *et al.* (2012) 'Integrated three-dimensional filter separates nanoscale from microscale elements in a microfluidic chip', *Lab on a Chip*, 12(6), pp. 1135–1142. doi: 10.1039/c2lc21116e.

Anchisi, L. *et al.* (2013) 'Cholesterol homeostasis: A key to prevent or slow down neurodegeneration', *Frontiers in Physiology*. doi: 10.3389/fphys.2012.00486.

Anderson, R. G. W. (1998) 'THE CAVEOLAE MEMBRANE SYSTEM', *Annual Review of Biochemistry*. doi: 10.1146/annurev.biochem.67.1.199.

Appelt, U. *et al.* (2005) 'Viable, apoptotic and necrotic monocytes expose phosphatidylserine: Cooperative binding of the ligand Annexin V to dying but not viable cells and implications for PS-dependent clearance [2]', *Cell Death and Differentiation*. doi: 10.1038/sj.cdd.4401527.

Aravani, D. *et al.* (2020) 'Cytokine regulation of apoptosis-induced apoptosis and apoptosis-induced cell proliferation in vascular smooth muscle cells', *Apoptosis*. Springer US, 25(9–10), pp. 648–662. doi: 10.1007/s10495-020-01622-4.

Arosio, P. *et al.* (2014) 'Density-gradient-free microfluidic centrifugation for analytical and preparative separation of nanoparticles', *Nano Letters*, 14(5), pp. 2365–2371. doi: 10.1021/nl404771g.

Asadi, M. *et al.* (2022) 'Caspase-3: Structure, function, and biotechnological aspects', *Biotechnology and Applied Biochemistry*, 69(4), pp. 1633–1645. doi: 10.1002/bab.2233.

Atkin-Smith, G. K. *et al.* (2015) 'A novel mechanism of generating extracellular vesicles during apoptosis via a beads-on-a-string membrane structure', *Nat Commun*, 6, p. 7439. doi: 10.1038/ncomms8439.

Bachurski, D. *et al.* (2019) 'Extracellular vesicle measurements with nanoparticle tracking analysis–An accuracy and repeatability comparison between NanoSight NS300 and ZetaView', *Journal of Extracellular Vesicles*. Taylor & Francis, 8(1). doi:

10.1080/20013078.2019.1596016.

Ballweg, S. *et al.* (2020) ‘Regulation of lipid saturation without sensing membrane fluidity’, *Nature Communications*. doi: 10.1038/s41467-020-14528-1.

Ban, E., Yoo, Y. S. and Song, E. J. (2015) ‘Analysis and applications of nanoparticles in capillary electrophoresis’, *Talanta*. Elsevier, 141, pp. 15–20. doi: 10.1016/j.talanta.2015.03.020.

Baxter, A. A. *et al.* (2019) ‘Analysis of extracellular vesicles generated from monocytes under conditions of lytic cell death’, *Scientific Reports*. Springer US, 9(1), pp. 1–13. doi: 10.1038/s41598-019-44021-9.

Berda-Haddad, Y. *et al.* (2011) ‘Sterile inflammation of endothelial cell-derived apoptotic bodies is mediated by interleukin-1α’, *Proceedings of the National Academy of Sciences of the United States of America*, 108(51), pp. 20684–20689. doi: 10.1073/pnas.1116848108.

Bhagat, A. A. S., Kuntaegowdanahalli, S. S. and Papautsky, I. (2009) ‘Inertial microfluidics for continuous particle filtration and extraction’, *Microfluidics and Nanofluidics*, 7(2), pp. 217–226. doi: 10.1007/s10404-008-0377-2.

Biró, É. *et al.* (2005) ‘The phospholipid composition and cholesterol content of platelet-derived microparticles: A comparison with platelet membrane fractions’, *Journal of Thrombosis and Haemostasis*. doi: 10.1111/j.1538-7836.2005.01646.x.

Boettcher, M. *et al.* (2011) ‘Filtration at the microfluidic level: Enrichment of nanoparticles by tunable filters’, *Journal of Physics Condensed Matter*, 23(32). doi: 10.1088/0953-8984/23/32/324101.

Böing, A. N. *et al.* (2014) ‘Single-step isolation of extracellular vesicles by size-exclusion chromatography’, *Journal of Extracellular Vesicles*. doi: 10.3402/jev.v3.23430.

Bouillet, P. *et al.* (2002) ‘BH3-only Bcl-2 family member Bim is required for apoptosis of autoreactive thymocytes’, *Nature*, 415(6874), pp. 922–926. doi: 10.1038/415922a.

Braciale, T. (1987) ‘Antigen Presentation Pathways to Class I and Class II MHC-Restricted T Lymphocytes’, *Immunological Reviews*.

Brouwers, J. and Al., E. (2013) ‘Distinct lipid compositions of two types of human prostasomes’, *Proteomics*, 13(10–11), pp. 1660–1666.

Brown, S. *et al.* (2002) ‘Apoptosis disables CD31-mediated cell detachment from phagocytes promoting binding and engulfment’, *Nature*, 418(6894), pp. 200–203. doi: 10.1038/nature00811.

Brunner, J. D. *et al.* (2014) ‘X-ray structure of a calcium-activated TMEM16 lipid scramblase’, *Nature*. Nature Publishing Group, 516(7530), pp. 207–212. doi: 10.1038/nature13984.

Bui, T. T., Suga, K. and Umakoshi, H. (2016) ‘Roles of Sterol Derivatives in Regulating the Properties of Phospholipid Bilayer Systems’, *Langmuir*, 32(24), pp. 6176–6184. doi: 10.1021/acs.langmuir.5b04343.

Cai, B. *et al.* (2016) ‘MerTK cleavage limits proresolving mediator biosynthesis and exacerbates tissue inflammation’, *Proceedings of the National Academy of Sciences of the United States of America*, 113(23), pp. 6526–6531. doi: 10.1073/pnas.1524292113.

Cantin, R. *et al.* (2008) ‘Discrimination between exosomes and HIV-1: Purification of both vesicles from cell-free supernatants’, *Journal of Immunological Methods*. doi: 10.1016/j.jim.2008.07.007.

Caruso, S. and Poon, I. K. H. (2018a) ‘Apoptotic cell-derived extracellular vesicles: More than just debris’, *Frontiers in Immunology*, 9(JUN). doi: 10.3389/fimmu.2018.01486.

Caruso, S. and Poon, I. K. H. (2018b) ‘Apoptotic cell-derived extracellular vesicles: More than just debris’, *Frontiers in Immunology*. doi: 10.3389/fimmu.2018.01486.

Chang, D. K. and Cheng, S. F. (2006) ‘pH-dependence of intermediate steps of membrane fusion induced by the influenza fusion peptide’, *Biochemical Journal*. doi:

10.1042/BJ20051920.

Chekeni, F. B. *et al.* (2010) 'Pannexin 1 channels mediate "find-me" signal release and membrane permeability during apoptosis', *Nature*. Nature Publishing Group, 467(7317), pp. 863–867. doi: 10.1038/nature09413.

Chernyshev, V. S. *et al.* (2015) 'Size and shape characterization of hydrated and desiccated exosomes', *Analytical and Bioanalytical Chemistry*, 407(12), pp. 3285–3301. doi: 10.1007/s00216-015-8535-3.

Choi, H. and Mun, J. Y. (2017) 'Structural Analysis of Exosomes Using Different Types of Electron Microscopy', *Applied Microscopy*, 47(3), pp. 171–175. doi: 10.9729/am.2017.47.3.171.

Clark, M., Kroger, C. J. and Tisch, R. M. (2017) 'Type 1 diabetes: A chronic anti-self-inflammatory response', *Frontiers in Immunology*, 8(DEC). doi: 10.3389/fimmu.2017.01898.

CLAYTON, A. *et al.* (2004) 'Adhesion and signaling by B cell-derived exosomes: the role of integrins', *The FASEB Journal*. doi: 10.1096/fj.03-1094fje.

Cockcroft, S. (2021) 'Mammalian lipids: Structure, synthesis and function', *Essays in Biochemistry*, 65(5), pp. 813–845. doi: 10.1042/EBC20200067.

Cocucci, E., Racchetti, G. and Meldolesi, J. (2009) 'Shedding microvesicles: artefacts no more', *Trends in Cell Biology*, 19(2), pp. 43–51. doi: 10.1016/j.tcb.2008.11.003.

Conde-Vancells, J. *et al.* (2008) 'Characterization and comprehensive proteome profiling of exosomes secreted by hepatocytes', *Journal of Proteome Research*. doi: 10.1021/pr8004887.

Costa Verdera, H. *et al.* (2017) 'Cellular uptake of extracellular vesicles is mediated by clathrin-independent endocytosis and macropinocytosis', *Journal of Controlled Release*. doi: 10.1016/j.jconrel.2017.09.019.

Cvjetkovic, A., Lötvall, J. and Lässer, C. (2014) 'The influence of rotor type and centrifugation time on the yield and purity of extracellular vesicles', *Journal of*

Extracellular Vesicles. doi: 10.3402/jev.v3.23111.

Czabotar, P., Lessene, G. and Strasser, A. (2014) 'Control of apoptosis by the BCL-2 protein family: implications for physiology and therapy.', *Nat rev Mol cell Biol*, 15, pp. 49–63.

Dalli, J. and Serhan, C. N. (2012) 'Specific lipid mediator signatures of human phagocytes: Microparticles stimulate macrophage efferocytosis and pro-resolving mediators', *Blood*, 120(15), pp. 60–72. doi: 10.1182/blood-2012-04-423525.

Davies, R. T. *et al.* (2012) 'Microfluidic filtration system to isolate extracellular vesicles from blood', *Lab on a Chip*, 12(24), pp. 5202–5210. doi: 10.1039/c2lc41006k.

Dayanand, K. and Widomska Justyna (2018) *乳鼠心肌提取 HHS Public Access*, *Physiology & behavior*. doi: 10.1038/s41596-019-0126-x.Asymmetric.

Denich, T. J. *et al.* (2003) 'Effect of selected environmental and physico-chemical factors on bacterial cytoplasmic membranes', *Journal of Microbiological Methods*. doi: 10.1016/S0167-7012(02)00155-0.

Denzer, K. *et al.* (2000) 'Exosome: From internal vesicle of the multivesicular body to intercellular signaling device', *Journal of Cell Science*.

Devitt, A., Griffiths, H. R. and Milic, I. (2018) 'Communicating with the dead: lipids, lipid mediators and extracellular vesicles', *Biochemical Society Transactions*. doi: 10.1042/BST20160477.

Dinarello, C. (2013) 'Anti-inflammatory Agents : Present and Future', 140(6), pp. 935–950. doi: 10.1016/j.cell.2010.02.043.Dinarello.

Distler, J. H. W. *et al.* (2005) 'The release of microparticles by apoptotic cells and their effects on macrophages', *Apoptosis*, 10(4), pp. 731–741. doi: 10.1007/s10495-005-2941-5.

Drexel, R. *et al.* (2020) 'Asymmetrical flow field-flow fractionation for sizing of gold nanoparticles in suspension', *Journal of Visualized Experiments*, 2020(163), pp. 1–23. doi: 10.3791/61757.

Ebara, M. *et al.* (2013) 'A photoinduced nanoparticle separation in microchannels via pH-sensitive surface traps', *Langmuir*, 29(18), pp. 5388–5393. doi: 10.1021/la400347r.

Eguchi, A. *et al.* (2015) 'Microparticles release by adipocytes act as "find-me" signals to promote macrophage migration', *PLoS ONE*, 10(4), pp. 1–19. doi: 10.1371/journal.pone.0123110.

Escrevente, C. *et al.* (2011) 'Interaction and uptake of exosomes by ovarian cancer cells', *BMC Cancer*. doi: 10.1186/1471-2407-11-108.

Esser, J. *et al.* (2010) 'Exosomes from human macrophages and dendritic cells contain enzymes for leukotriene biosynthesis and promote granulocyte migration', *Journal of Allergy and Clinical Immunology*, 126(5). doi: 10.1016/j.jaci.2010.06.039.

Evans, I. R. *et al.* (2013) 'SCAR/WAVE-mediated processing of engulfed apoptotic corpses is essential for effective macrophage migration in Drosophila', *Cell Death and Differentiation*, 20(5), pp. 709–720. doi: 10.1038/cdd.2012.166.

Falati, S. *et al.* (2003) 'Accumulation of tissue factor into developing thrombi in vivo is dependent upon microparticle P-selectin glycoprotein ligand 1 and platelet P-selectin', *Journal of Experimental Medicine*. doi: 10.1084/jem.20021868.

Feng, D. *et al.* (2010) 'Cellular internalization of exosomes occurs through phagocytosis', *Traffic*. doi: 10.1111/j.1600-0854.2010.01041.x.

Filipe, V., Hawe, A. and Jiskoot, W. (2010) 'Critical evaluation of nanoparticle tracking analysis (NTA) by NanoSight for the measurement of nanoparticles and protein aggregates', *Pharmaceutical Research*, 27(5), pp. 796–810. doi: 10.1007/s11095-010-0073-2.

Fitzner, D. *et al.* (2011) 'Selective transfer of exosomes from oligodendrocytes to microglia by macropinocytosis', *Journal of Cell Science*. doi: 10.1242/jcs.074088.

Franzen, C. A. *et al.* (2014) 'Characterization of uptake and internalization of exosomes by bladder cancer cells', *BioMed Research International*. doi:

10.1155/2014/619829.

Frleta, D. *et al.* (2012) 'HIV-1 infection-induced apoptotic microparticles inhibit human DCs via CD44', *Journal of Clinical Investigation*, 122(12), pp. 4685–4697. doi: 10.1172/JCI64439.

Fröhlich, E. (2012) 'The role of surface charge in cellular uptake and cytotoxicity of medical nanoparticles', *International Journal of Nanomedicine*, 7, pp. 5577–5591. doi: 10.2147/IJN.S36111.

Furman, D. *et al.* (2019) 'Chronic inflammation in the etiology of disease across the life span', *Nature Medicine*. Springer US, 25(12), pp. 1822–1832. doi: 10.1038/s41591-019-0675-0.

Galluzzi, L. *et al.* (2018) 'Molecular mechanisms of cell death: Recommendations of the Nomenclature Committee on Cell Death 2018', *Cell Death and Differentiation*, 25(3), pp. 486–541. doi: 10.1038/s41418-017-0012-4.

Gardai, S. J. *et al.* (2005) 'Cell-surface calreticulin initiates clearance of viable or apoptotic cells through trans-activation of LRP on the phagocyte', *Cell*, 123(2), pp. 321–334. doi: 10.1016/j.cell.2005.08.032.

Gardiner, C. *et al.* (2016) 'Techniques used for the isolation and characterization of extracellular vesicles: Results of a worldwide survey', *Journal of Extracellular Vesicles*. doi: 10.3402/jev.v5.32945.

De Gassart, A. *et al.* (2003) 'Lipid raft-associated protein sorting in exosomes', *Blood*. doi: 10.1182/blood-2003-03-0871.

Gelibter, S. *et al.* (2022) 'The impact of storage on extracellular vesicles: A systematic study', *Journal of Extracellular Vesicles*, 11(2). doi: 10.1002/jev2.12162.

Gheibi Hayat, S. M. *et al.* (2019) 'Efferocytosis: molecular mechanisms and pathophysiological perspectives', *Immunology and Cell Biology*, 97(2), pp. 124–133. doi: 10.1111/imcb.12206.

Gholijani, N. *et al.* (2015) 'Modulation of cytokine production and transcription factors

activities in human jurkat t cells by thymol and carvacrol', *Advanced Pharmaceutical Bulletin*, 5(Suppl 1), pp. 653–660. doi: 10.15171/apb.2015.089.

Gibbons, E. *et al.* (2013) 'Molecular details of membrane fluidity changes during apoptosis and relationship to phospholipase A2 activity', *Biochimica et Biophysica Acta (BBA) - Biomembranes*, 1828(2), pp. 887–895. doi: 10.1016/j.bbamem.2012.08.024.

Giri, P. K. and Schorey, J. S. (2008) 'Exosomes derived from M. bovis BCG infected macrophages activate antigen-specific CD4+ and CD8+ T cells in vitro and in vivo', *PLoS ONE*. doi: 10.1371/journal.pone.0002461.

Gomes, F. G. *et al.* (2022) 'Synergy of Human Platelet-Derived Extracellular Vesicles with Secretome Proteins Promotes Regenerative Functions', *Biomedicines*, 10(2). doi: 10.3390/biomedicines10020238.

Gonzalvez, F. and Gottlieb, E. (2007) 'Cardiolipin: Setting the beat of apoptosis', *Apoptosis*, 12(5), pp. 877–885. doi: 10.1007/s10495-007-0718-8.

Gordon, S. and Taylor, P. R. (2005) 'Monocyte and macrophage heterogeneity', *Nature Reviews Immunology*. doi: 10.1038/nri1733.

Granger, D. and Senchenkova, E. (2010) 'Inflammation and the Microcirculation', in. San Rafael (CA): Morgan & Claypool Life Sciences.

Gude, D. R. *et al.* (2008) 'Apoptosis induces expression of sphingosine kinase 1 to release sphingosine-1-phosphate as a "come-and-get-me" signal', *The FASEB Journal*. doi: 10.1096/fj.08-107169.

Guescini, M. *et al.* (2010) 'Astrocytes and Glioblastoma cells release exosomes carrying mtDNA', *Journal of Neural Transmission*. doi: 10.1007/s00702-009-0288-8.

Haeberle, S. and Zengerle, R. (2007) 'Microfluidic platforms for lab-on-a-chip applications', *Lab on a Chip*. doi: 10.1039/b706364b.

Haney, M. J. *et al.* (2015) 'Exosomes as drug delivery vehicles for Parkinson's disease therapy', *Journal of Controlled Release*. doi: 10.1016/j.jconrel.2015.03.033.

Harrison, R. E. *et al.* (2003) 'Phagosomes Fuse with Late Endosomes and/or Lysosomes by Extension of Membrane Protrusions along Microtubules: Role of Rab7 and RILP', *Molecular and Cellular Biology*, 23(18), pp. 6494–6506. doi: 10.1128/mcb.23.18.6494-6506.2003.

Heckmann, B. L. and Green, D. R. (2019) 'Correction: LC3-associated phagocytosis at a glance (Journal of Cell Science (2019) 132 (jcs222984) DOI: 10.1242/jcs.222984)', *Journal of Cell Science*, 132(5). doi: 10.1242/jcs.231472.

Heringdorf, D. M. . (2008) 'Lysophospholipids', in *Encyclopedia of Molecular Pharmacology*. Springer, Berlin. doi: https://doi.org/10.1007/978-3-540-38918-7_90.

Holthuis, J. C. M. and Menon, A. K. (2014) 'Lipid landscapes and pipelines in membrane homeostasis', *Nature*. doi: 10.1038/nature13474.

Italiani, P. and Boraschi, D. (2014) 'From monocytes to M1/M2 macrophages: Phenotypical vs. functional differentiation', *Frontiers in Immunology*, 5(OCT), pp. 1–22. doi: 10.3389/fimmu.2014.00514.

Izquierdo-Useros, N. *et al.* (2009) 'Capture and transfer of HIV-1 particles by mature dendritic cells converges with the exosome-dissemination pathway', *Blood*. doi: 10.1182/blood-2008-05-158642.

de Jager, T. ., Cockrell, A. . and Du Plessis, S. . (2017) 'Ultraviolet light induced generation of reactive osxygen species.', in *Ultraviolet light in human, diseases and environment*. Springer, Cham.

Jahn, R. and Scheller, R. H. (2006) 'SNAREs - Engines for membrane fusion', *Nature Reviews Molecular Cell Biology*. doi: 10.1038/nrm2002.

Jaikishan, S. and Slotte, J. P. (2013) 'Stabilization of sphingomyelin interactions by interfacial hydroxyls - A study of phytosphingomyelin properties', *Biochimica et Biophysica Acta - Biomembranes*. Elsevier B.V., 1828(2), pp. 391–397. doi: 10.1016/j.bbamem.2012.08.029.

Jeon, H. *et al.* (2013) 'Ion concentration polarization-based continuous separation

device using electrical repulsion in the depletion region', *Scientific Reports*, 3, pp. 1–7. doi: 10.1038/srep03483.

Jeon, H., Kim, Y. and Lim, G. (2016) 'Continuous particle separation using pressure-driven flow-induced miniaturizing free-flow electrophoresis (PDF-induced μ-FFE)', *Scientific Reports*. Nature Publishing Group, 6(December 2015), pp. 1–9. doi: 10.1038/srep19911.

Joffre, O. P. *et al.* (2012) 'Cross-presentation by dendritic cells', *Nature Reviews Immunology*. Nature Publishing Group, 12(8), pp. 557–569. doi: 10.1038/nri3254.

Johnstone, R. M. *et al.* (1987) 'Vesicle formation during reticulocyte maturation. Association of plasma membrane activities with released vesicles (exosomes).', *Journal of Biological Chemistry*.

Kahlert, C. *et al.* (2014) 'Identification of doublestranded genomic dna spanning all chromosomes with mutated KRAS and P53 DNA in the serum exosomes of patients with pancreatic cancer', *Journal of Biological Chemistry*. doi: 10.1074/jbc.C113.532267.

Kajimoto, T. *et al.* (2013) 'Ongoing activation of sphingosine 1-phosphate receptors mediates maturation of exosomal multivesicular endosomes', *Nature Communications*. doi: 10.1038/ncomms3712.

Kazemi, B. and Darabi, J. (2018) 'Numerical simulation of dielectrophoretic particle separation using slanted electrodes', *Physics of Fluids*, 30(10). doi: 10.1063/1.5047153.

Ke, F. F. S. *et al.* (2018) 'Embryogenesis and Adult Life in the Absence of Intrinsic Apoptosis Effectors BAX, BAK, and BOK', *Cell*. Elsevier Inc., 173(5), pp. 1217-1230.e17. doi: 10.1016/j.cell.2018.04.036.

Keller, S. *et al.* (2011) 'Body fluid derived exosomes as a novel template for clinical diagnostics', *Journal of Translational Medicine*. doi: 10.1186/1479-5876-9-86.

Kerr, M. C. and Teasdale, R. D. (2009) 'Defining macropinocytosis', *Traffic*. doi:

10.1111/j.1600-0854.2009.00878.x.

Kima, I. S. *et al.* (2017) 'Mechanism of membrane fusion induced by vesicular stomatitis virus G protein', *Proceedings of the National Academy of Sciences of the United States of America*. doi: 10.1073/pnas.1618883114.

Kinchen, J. M. and Ravichandran, K. S. (2008) *Phagosome maturation: Going through the acid test*, *Nature Reviews Molecular Cell Biology*. doi: 10.1038/nrm2515.

Kobayashi, T. *et al.* (1998) 'A lipid associated with the antiphospholipid syndrome regulates endosome structure and function', *Nature*. doi: 10.1038/32440.

Kohro, T. *et al.* (2004) 'A comparison of differences in the gene expression profiles of phorbol 12-myristate 13-acetate differentiated THP-1 cells and human monocyte-derived macrophage.', *Journal of atherosclerosis and thrombosis*. doi: 10.5551/jat.11.88.

Koliha, N. *et al.* (2016) 'Melanoma affects the composition of blood cell-derived extracellular vesicles', *Frontiers in Immunology*, 7(JUL), pp. 1–12. doi: 10.3389/fimmu.2016.00282.

Köröskényi, K. *et al.* (2011) ' Involvement of Adenosine A 2A Receptors in Engulfment-Dependent Apoptotic Cell Suppression of Inflammation ', *The Journal of Immunology*, 186(12), pp. 7144–7155. doi: 10.4049/jimmunol.1002284.

Kourtzelis, I., Hajishengallis, G. and Chavakis, T. (2020) 'Phagocytosis of Apoptotic Cells in Resolution of Inflammation', *Frontiers in Immunology*, 11(March), pp. 1–8. doi: 10.3389/fimmu.2020.00553.

Kowal, J. *et al.* (2016) 'Proteomic comparison defines novel markers to characterize heterogeneous populations of extracellular vesicle subtypes', *Proceedings of the National Academy of Sciences of the United States of America*. doi: 10.1073/pnas.1521230113.

Koynova, R. and Caffrey, M. (1998) 'Phases and phase transitions of the phosphatidylcholines', *Biochimica et Biophysica Acta - Reviews on Biomembranes*.

doi: 10.1016/S0304-4157(98)00006-9.

Kozlov, M. M. *et al.* (2014) 'Mechanisms shaping cell membranes', *Current Opinion in Cell Biology*. Elsevier Ltd, 29(1), pp. 53–60. doi: 10.1016/j.ceb.2014.03.006.

Krishnan, M. *et al.* (2010) 'Geometry-induced electrostatic trapping of nanometric objects in a fluid', *Nature*. Nature Publishing Group, 467(7316), pp. 692–695. doi: 10.1038/nature09404.

Kulms, D. and Schwarz, T. (2000) 'Molecular mechanisms of UV-induced apoptosis', (7), pp. 195–201.

Lai, R. C. *et al.* (2010) 'Exosome secreted by MSC reduces myocardial ischemia/reperfusion injury', *Stem Cell Research*. doi: 10.1016/j.scr.2009.12.003.

Lane, J. D., Allan, V. J. and Woodman, P. G. (2005) 'Active relocation of chromatin and endoplasmic reticulum into blebs in late apoptotic cells', *Journal of Cell Science*. doi: 10.1242/jcs.02529.

Lang, T., Halemani, N. D. and Rammner, B. (2008) 'Interplay between lipids and the proteinaceous membrane fusion machinery', *Progress in Lipid Research*. Elsevier Ltd, 47(6), pp. 461–469. doi: 10.1016/j.plipres.2008.08.002.

Lässer, C. *et al.* (2011) 'Human saliva, plasma and breast milk exosomes contain RNA: Uptake by macrophages', *Journal of Translational Medicine*. doi: 10.1186/1479-5876-9-9.

Lauber, K. *et al.* (2003) 'Apoptotic cells induce migration of phagocytes via caspase-3-mediated release of a lipid attraction signal', *Cell*. doi: 10.1016/S0092-8674(03)00422-7.

Learmonth, R. P. and Gratton, E. (2002) 'Assessment of Membrane Fluidity in Individual Yeast Cells by Laurdan Generalised Polarisation and Multi-photon Scanning Fluorescence Microscopy', pp. 241–252. doi: 10.1007/978-3-642-56067-5_14.

Lee, K. *et al.* (2015) 'Acoustic Puri fi cation of Extracellular Microvesicles', (3), pp. 2321–2327.

Lee, S. H. S., Hatton, T. A. and Khan, S. A. (2011) 'Microfluidic continuous magnetophoretic protein separation using nanoparticle aggregates', *Microfluidics and Nanofluidics*, 11(4), pp. 429–438. doi: 10.1007/s10404-011-0808-3.

Lee, S. M. *et al.* (2020) 'FABP3-mediated membrane lipid saturation alters fluidity and induces ER stress in skeletal muscle with aging', *Nature Communications*. doi: 10.1038/s41467-020-19501-6.

Leventis, P. A. and Grinstein, S. (2010) 'The distribution and function of phosphatidylserine in cellular membranes', *Annual Review of Biophysics*, 39(1), pp. 407–427. doi: 10.1146/annurev.biophys.093008.131234.

Ley, K. *et al.* (2007) 'Getting to the site of inflammation: The leukocyte adhesion cascade updated', *Nature Reviews Immunology*, 7(9), pp. 678–689. doi: 10.1038/nri2156.

Li, H. *et al.* (1998) 'Cleavage of BID by caspase 8 mediates the mitochondrial damage in the Fas pathway of apoptosis', *Cell*, 94(4), pp. 491–501. doi: 10.1016/S0092-8674(00)81590-1.

Li, P. *et al.* (1997) 'Cytochrome c and dATP-dependent formation of Apaf-1/caspase-9 complex initiates an apoptotic protease cascade', *Cell*, 91(4), pp. 479–489. doi: 10.1016/S0092-8674(00)80434-1.

Li, X. M. *et al.* (2003) 'Sterol Structure and Sphingomyelin Acyl Chain Length Modulate Lateral Packing Elasticity and Detergent Solubility in Model Membranes', *Biophysical Journal*. doi: 10.1016/S0006-3495(03)74794-8.

Liangsupree, T., Multia, E. and Riekkola, M. L. (2021) 'Modern isolation and separation techniques for extracellular vesicles', *Journal of Chromatography A*. Elsevier B.V., 1636, p. 461773. doi: 10.1016/j.chroma.2020.461773.

Lichtenberg, D., Ahyayauch, H. and Goñi, F. M. (2013) 'The mechanism of detergent solubilization of lipid bilayers', *Biophysical Journal*, 105(2), pp. 289–299. doi: 10.1016/j.bpj.2013.06.007.

Lin, F. R., Niparko, J. K. and Ferrucci, and L. (2014) '基因的改变NIH Public Access', *Bone*, 23(1), pp. 1–7. doi: 10.1038/nature13085.Nucleotide.

Llorente, A. *et al.* (2013) 'Molecular lipidomics of exosomes released by PC-3 prostate cancer cells', *Biochimica et Biophysica Acta - Molecular and Cell Biology of Lipids*, 1831(7), pp. 1302–1309. doi: 10.1016/j.bbalip.2013.04.011.

Los, D. A. and Murata, N. (2004) 'Membrane fluidity and its roles in the perception of environmental signals', *Biochimica et Biophysica Acta - Biomembranes*, 1666(1–2), pp. 142–157. doi: 10.1016/j.bbamem.2004.08.002.

Lotsberg, M. L. *et al.* (2020) 'AXL Targeting Abrogates Autophagic Flux and Induces Immunogenic Cell Death in Drug-Resistant Cancer Cells', *Journal of Thoracic Oncology*. Elsevier, 15(6), pp. 973–999. doi: 10.1016/j.jtho.2020.01.015.

Lötvall, J. *et al.* (2014) 'Minimal experimental requirements for definition of extracellular vesicles and their functions: A position statement from the International Society for Extracellular Vesicles', *Journal of Extracellular Vesicles*, 3(1), pp. 1–6. doi: 10.3402/jev.v3.26913.

M. COHEN, G. (1997) 'Caspases: the executioners of apoptosis.', *Biochem J*, 326(1), pp. 1–16. doi: https://doi.org/10.1042/bj3260001.

Maas, S. L. N. *et al.* (2015) 'Possibilities and limitations of current technologies for quantification of biological extracellular vesicles and synthetic mimics', *Journal of Controlled Release*. Elsevier B.V., 200, pp. 87–96. doi: 10.1016/j.jconrel.2014.12.041.

Maas, S. L. N., Vrij, J. De and Broekman, M. L. D. (2014) 'Quantification and size-profiling of extracellular vesicles using tunable resistive pulse sensing', *Journal of Visualized Experiments*. doi: 10.3791/51623.

MacKenzie, A. *et al.* (2001) 'Rapid secretion of interleukin-1β by microvesicle shedding', *Immunity*. doi: 10.1016/S1074-7613(01)00229-1.

Magarkar, A. *et al.* (2014) 'Cholesterol level affects surface charge of lipid membranes in saline solution', *Scientific Reports*, 4, pp. 1–5. doi: 10.1038/srep05005.

Manganelli, V. *et al.* (2015) 'Altered Traffic of Cardiolipin during Apoptosis: Exposure on the Cell Surface as a Trigger for "antiphospholipid Antibodies"', *Journal of Immunology Research*. Hindawi Publishing Corporation, 2015. doi: 10.1155/2015/847985.

Martinez, J. *et al.* (2011) 'Microtubule-associated protein 1 light chain 3 alpha (LC3)-associated phagocytosis is required for the efficient clearance of dead cells', *Proceedings of the National Academy of Sciences of the United States of America*, 108(42), pp. 17396–17401. doi: 10.1073/pnas.1113421108.

Masuda, H., Kimura, M. and Morita, A. (2019) 'Optimum wavelength characteristics for phototherapy utilizing deep ultraviolet light-emitting diodes', *Journal of Dermatological Science*. doi: 10.1016/j.jdermsci.2019.01.006.

Matsumoto, K. *et al.* (1995) 'Induction of apoptosis in human eosinophils by anti-Fas antibody treatment in vitro', *Blood*. American Society of Hematology, 86(4), pp. 1437–1443. doi: 10.1182/blood.v86.4.1437.bloodjournal8641437.

McGrath, J., Jimenez, M. and Bridle, H. (2014) 'Deterministic lateral displacement for particle separation: A review', *Lab on a Chip*. Royal Society of Chemistry, 14(21), pp. 4139–4158. doi: 10.1039/c4lc00939h.

McIntosh, T. J. and Simon, S. A. (2006) 'Roles of bilayer material properties in function and distribution of membrane proteins', *Annual Review of Biophysics and Biomolecular Structure*, 35, pp. 177–198. doi: 10.1146/annurev.biophys.35.040405.102022.

McMahon, H. T. and Boucrot, E. (2015) 'Membrane curvature at a glance', *Journal of Cell Science*, 128(6), pp. 1065–1070. doi: 10.1242/jcs.114454.

Mercer, J. and Helenius, A. (2008) 'Vaccinia virus uses macropinocytosis and apoptotic mimicry to enter host cells', *Science*. doi: 10.1126/science.1155164.

Mercer, J. and Helenius, A. (2009) 'Virus entry by macropinocytosis', *Nature Cell Biology*. doi: 10.1038/ncb0509-510.

Midekessa, G. *et al.* (2020) 'Zeta Potential of Extracellular Vesicles: Toward Understanding the Attributes that Determine Colloidal Stability', *ACS Omega*, pp. 16701–16710. doi: 10.1021/acsomega.0c01582.

Mills, C. (2012) 'M1 and M2 Macrophages: Oracles of Health and Disease', *CRI*, 32(6).

Mitoxantrone *et al.* (2009) 'Higher liposomal membrane fluidity enhances the in vitro antitumor activity of folate-targeted liposomal', *Molecular Pharmaceutics*, 6(1), pp. 98–104. doi: 10.1021/mp800069c.

Mittelbrunn, M. *et al.* (2011) 'Unidirectional transfer of microRNA-loaded exosomes from T cells to antigen-presenting cells', *Nature Communications*. doi: 10.1038/ncomms1285.

Miyanishi, M. *et al.* (2007) 'Identification of Tim4 as a phosphatidylserine receptor', *Nature*. doi: 10.1038/nature06307.

De Momi, A. and Lead, J. R. (2008) 'Behaviour of environmental aquatic nanocolloids when separated by split-flow thin-cell fractionation (SPLITT)', *Science of the Total Environment*, 405(1–3), pp. 317–323. doi: 10.1016/j.scitotenv.2008.05.032.

Montano, M. (2014) 'Model systems', *Translational Biology in Medicine*. Woodhead Publishing, pp. 9–33. doi: 10.1533/9781908818652.9.

Morelli, A. E. *et al.* (2004) 'Endocytosis, intracellular sorting, and processing of exosomes by dendritic cells', *Blood*. doi: 10.1182/blood-2004-03-0824.

Morenilla-Palao, C. *et al.* (2009) 'Lipid raft segregation modulates TRPM8 channel activity', *Journal of Biological Chemistry*, 284(14), pp. 9215–9224. doi: 10.1074/jbc.M807228200.

Morimoto, K. *et al.* (2006) 'Lovastatin Enhances Clearance of Apoptotic Cells (Efferocytosis) with Implications for Chronic Obstructive Pulmonary Disease', *The Journal of Immunology*, 176(12), pp. 7657–7665. doi: 10.4049/jimmunol.176.12.7657.

Mozos, I. *et al.* (2017) 'Inflammatory markers for arterial stiffness in cardiovascular diseases', *Frontiers in Immunology*, 8(August), pp. 1–16. doi:

10.3389/fimmu.2017.01058.

Mulcahy, L. A., Pink, R. C. and Carter, D. R. F. (2014) 'Routes and mechanisms of extracellular vesicle uptake', *Journal of Extracellular Vesicles*, 3(1), pp. 1–14. doi: 10.3402/jev.v3.24641.

Munir, A. *et al.* (2014) 'Experimental investigation of magnetically actuated separation using tangential microfluidic channels and magnetic nanoparticles', *IET Nanobiotechnology*, 8(2), pp. 102–110. doi: 10.1049/iet-nbt.2012.0023.

Muralidharan-Chari, V. *et al.* (2010) 'Microvesicles: Mediators of extracellular communication during cancer progression', *Journal of Cell Science*. doi: 10.1242/jcs.064386.

Nagaraja, S. *et al.* (2014) 'Computational Approach To Characterize Causative Factors and Molecular Indicators of Chronic Wound Inflammation', *The Journal of Immunology*, 192(4), pp. 1824–1834. doi: 10.4049/jimmunol.1302481.

Naotomo Tottori, Yasuhiko Muramoto, Hiraku Sakai, T. N. (2020) 'Nanoparticle Separation through Deterministic Lateral Displacement Arrays in Poly(dimethylsiloxane)', *JOURNAL OF CHEMICAL ENGINEERING OF JAPAN*, 53(8), pp. 414–421. doi: https://doi.org/10.1252/jcej.19we160.

Németh, A. *et al.* (2017) 'Antibiotic-induced release of small extracellular vesicles (exosomes) with surface-associated DNA', *Scientific Reports*, 7(1), pp. 1–16. doi: 10.1038/s41598-017-08392-1.

Nguyen, N. T. and Wereley, S. (2006) 'Fundamentals and applications of microfluidics', *Artech House*. doi: http://doi.wiley.com/10.1002/1521-3773%252820010316%252940%253A6%253C9823%253A%253AAID-ANIE9823%253E3.3.CO%253B2-C.

Ogden, C. A. *et al.* (2001) 'C1q and mannose binding lectin engagement of cell surface calreticulin and CD91 initiates macropinocytosis and uptake of apoptotic cells', *Journal of Experimental Medicine*, 194(6), pp. 781–795. doi: 10.1084/jem.194.6.781.

Oh, B. R. *et al.* (2016) 'Multiplexed Nanoplasmonic Temporal Profiling of T-Cell Response under Immunomodulatory Agent Exposure', *ACS Sensors*, 1(7), pp. 941–948. doi: 10.1021/acssensors.6b00240.

Oldenborg, P. A. (2000) 'Role of CD47 as a Marker of Self on Red Blood Cells', *Science*, 288(5473), pp. 2051–2054. doi: 10.1126/science.288.5473.2051.

Oldenborg, P. A., Gresham, H. D. and Lindberg, F. P. (2001) 'CD47-signal regulatory protein α (SIRPα) regulates Fcγ and complement receptor-mediated phagocytosis', *Journal of Experimental Medicine*, 193(7), pp. 855–861. doi: 10.1084/jem.193.7.855.

Ong, S. E. *et al.* (2008) 'Fundamental principles and applications of microfluidic systems', *Frontiers in Bioscience*. doi: 10.2741/2883.

OpenWetWare contributors (2022) *Critical micelle concentration (CMC)*, *OpenWetWare*. Available at: https://openwetware.org/mediawiki/index.php?title=Critical_micelle_concentration_(CMC)&oldid=1080646.

Osteikoetxea, X., Sódar, B., *et al.* (2015) 'Differential detergent sensitivity of extracellular vesicle subpopulations', *Organic and Biomolecular Chemistry*. Royal Society of Chemistry, 13(38), pp. 9775–9782. doi: 10.1039/c5ob01451d.

Osteikoetxea, X., Balogh, A., *et al.* (2015) 'Improved characterization of EV preparations based on protein to lipid ratio and lipid properties', *PLoS ONE*, 10(3), pp. 1–16. doi: 10.1371/journal.pone.0121184.

Ostrander, D. B. *et al.* (2001) 'Decreased Cardiolipin Synthesis Corresponds with Cytochrome c Release in Palmitate-induced Cardiomyocyte Apoptosis', *Journal of Biological Chemistry*. Â© 2001 ASBMB. Currently published by Elsevier Inc; originally published by American Society for Biochemistry and Molecular Biology., 276(41), pp. 38061–38067. doi: 10.1074/jbc.m107067200.

Pahwa, R., Goyal, A. and Jialal, I. (2022) *Chronic inflammation*, *StatPearls*.

Palumbo, J. *et al.* (2020) 'Lab on a rod: Size-based particle separation and sorting in

a helical channel', *Cite as: Biomicrofluidics*, 14, p. 64104. doi: 10.1063/5.0030917.

Panaretakis, T. *et al.* (2009) 'Mechanisms of pre-apoptotic calreticulin exposure in immunogenic cell death', *EMBO Journal*, 28(5), pp. 578–590. doi: 10.1038/emboj.2009.1.

Paradies, G. *et al.* (2019) 'Role of cardiolipin in mitochondrial function and dynamics in health and disease: Molecular and pharmacological aspects', *Cells*. doi: 10.3390/cells8070728.

Parasassi, T. and Gratton, E. (1995) 'Membrane lipid domains and dynamics as detected by Laurdan fluorescence', *Journal of Fluorescence*. doi: 10.1007/BF00718783.

Penberthy, K. K. and Ravichandran, K. S. (2016) 'Apoptotic cell recognition receptors and scavenger receptors', *Immunological Reviews*, 269(1), pp. 44–59. doi: 10.1111/imr.12376.

Pihán, P., Carreras-Sureda, A. and Hetz, C. (2017) 'BCL-2 family: Integrating stress responses at the ER to control cell demise', *Cell Death and Differentiation*. Nature Publishing Group, 24(9), pp. 1478–1487. doi: 10.1038/cdd.2017.82.

Pluskota, E. *et al.* (2008) 'Expression, activation, and function of integrin άMB2 (mac-1) on neutrophil-derived microparticles', *Blood*. doi: 10.1182/blood-2007-12-127183.

Pols, M. S. and Klumperman, J. (2009) 'Trafficking and function of the tetraspanin CD63', *Experimental Cell Research*. doi: 10.1016/j.yexcr.2008.09.020.

Poojari, C. *et al.* (2019) 'Behavior of the DPH fluorescence probe in membranes perturbed by drugs', *Chemistry and Physics of Lipids*, 223(January). doi: 10.1016/j.chemphyslip.2019.104784.

Poon, I. K. H. *et al.* (2019) 'Moving beyond size and phosphatidylserine exposure: evidence for a diversity of apoptotic cell-derived extracellular vesicles in vitro', *Journal of Extracellular Vesicles*. doi: 10.1080/20013078.2019.1608786.

Poon, I. K. H., Hulett, M. D. and Parish, C. R. (2010) 'Molecular mechanisms of late

apoptotic/necrotic cell clearance', *Cell Death and Differentiation*. Nature Publishing Group, 17(3), pp. 381–397. doi: 10.1038/cdd.2009.195.

Purohit, S. *et al.* (2018) 'Proteins of TNF-α and IL6 pathways are elevated in serum of type-1 diabetes patients with microalbuminuria', *Frontiers in Immunology*, 9(JAN). doi: 10.3389/fimmu.2018.00154.

Qi, H., Yang, S. and Zhang, L. (2017) 'Endothelial dysfunction in atherosclerosis and thrombosis', *Frontiers in Immunology*, 8(AUG). doi: 10.3389/fimmu.2017.00928.

Radu, C. G. *et al.* (2004) 'T cell chemotaxis to lysophosphatidylcholine through the G2A receptor', *Proceedings of the National Academy of Sciences of the United States of America*, 101(1), pp. 245–250. doi: 10.1073/pnas.2536801100.

Raposo, G. *et al.* (1996) 'B lymphocytes secrete antigen-presenting vesicles', *Journal of Experimental Medicine*. doi: 10.1084/jem.183.3.1161.

Ravichandran, K. S. (2010) 'Find-me and eat-me signals in apoptotic cell clearance: Progress and conundrums', *Journal of Experimental Medicine*. doi: 10.1084/jem.20101157.

Record, M. *et al.* (2014) 'Exosomes as new vesicular lipid transporters involved in cell-cell communication and various pathophysiologies', *Biochimica et Biophysica Acta - Molecular and Cell Biology of Lipids*. doi: 10.1016/j.bbalip.2013.10.004.

Regtmeier, J. *et al.* (2011) 'Continuous-flow separation of nanoparticles by electrostatic sieving at a micro-nanofluidic interface', *Journal of Separation Science*, 34(10), pp. 1180–1183. doi: 10.1002/jssc.201100007.

Roberts, R. L. *et al.* (2000) 'Dynamics of rab5 activation in endocytosis and phagocytosis.', *Journal of leukocyte biology*, 68(5), pp. 627–32. Available at: http://www.ncbi.nlm.nih.gov/pubmed/11073100.

Rozo, A. J. *et al.* (2020a) 'Biophysical analysis of lipidic nanoparticles', *Methods*. Elsevier, 180(May), pp. 45–55. doi: 10.1016/j.ymeth.2020.05.001.

Rozo, A. J. *et al.* (2020b) 'Biophysical analysis of lipidic nanoparticles', *Methods*.

Elsevier, (April), pp. 0–1. doi: 10.1016/j.ymeth.2020.05.001.

Salafi, T., Zeming, K. K. and Zhang, Y. (2017) 'Advancements in microfluidics for nanoparticle separation', *Lab on a Chip*. Royal Society of Chemistry, 17(1), pp. 11–33. doi: 10.1039/C6LC01045H.

Salucci, S. *et al.* (2013) 'Ultraviolet B (UVB) irradiation-induced apoptosis in various cell lineages in vitro', *International Journal of Molecular Sciences*, 14(1), pp. 532–546. doi: 10.3390/ijms14010532.

Salvador-Gallego, R. *et al.* (2016) 'Bax assembly into rings and arcs in apoptotic mitochondria is linked to membrane pores', *The EMBO Journal*, 35(4), pp. 389–401. doi: 10.15252/embj.201593384.

Saraste, A. and Pulkki, K. (2000) 'Morphologic and biochemical hallmarks of apoptosis', *Cardiovascular Research*, 45(3), pp. 528–537. doi: 10.1016/S0008-6363(99)00384-3.

Schaible, U. E. *et al.* (2003) 'Apoptosis facilitates antigen presentation to T lymphocytes through MHC-I and CD1 in tuberculosis', *Nature Medicine*. doi: 10.1038/nm906.

Segawa, K. and Nagata, S. (2015) 'An Apoptotic "Eat Me" Signal: Phosphatidylserine Exposure', *Trends in Cell Biology*. Elsevier Ltd, 25(11), pp. 639–650. doi: 10.1016/j.tcb.2015.08.003.

Segeritz, C. P. and Vallier, L. (2017) 'Cell Culture: Growing Cells as Model Systems In Vitro', *Basic Science Methods for Clinical Researchers*, (January), pp. 151–172. doi: 10.1016/B978-0-12-803077-6.00009-6.

Segundo, C. *et al.* (1999) 'Surface molecule loss and bleb formation by human germinal center B cells undergoing apoptosis: Role of apoptotic blebs in monocyte chemotaxis', *Blood*, 94(3), pp. 1012–1020. doi: 10.1182/blood.v94.3.1012.415k05_1012_1020.

Serhan, C. N., Chiang, N. and Van Dyke, T. E. (2008) 'Resolving inflammation: Dual

anti-inflammatory and pro-resolution lipid mediators', *Nature Reviews Immunology*, 8(5), pp. 349–361. doi: 10.1038/nri2294.

Serhan, C. N. and Levy, B. D. (2018) 'Resolvinas en Inflamación: Emergencia de la superfamilia de mediadores de resolución pro.', *Diario de Investigación Clínica*, 128(7), pp. 2657–2669.

Sessa, L. *et al.* (2021) 'Hydroxylated fatty acids: The role of the sphingomyelin synthase and the origin of selectivity', *Membranes*. doi: 10.3390/membranes11100787.

Sezgin, E. *et al.* (2017) 'The mystery of membrane organization: Composition, regulation and roles of lipid rafts', *Nature Reviews Molecular Cell Biology*. doi: 10.1038/nrm.2017.16.

Shamas-Din, A. *et al.* (2013) 'Mechanisms of action of Bcl-2 family proteins', *Cold Spring Harbor Perspectives in Biology*, 5(4), pp. 1–21. doi: 10.1101/cshperspect.a008714.

Sharom, F. J. (2011) 'Flipping and flopping-lipids on the move', *IUBMB Life*, 63(9), pp. 736–746. doi: 10.1002/iub.515.

Shen, S. *et al.* (2017) 'Spiral microchannel with ordered micro-obstacles for continuous and highly-efficient particle separation', *Lab on a Chip*, 17(21).

Sica, A. and Mantovani, A. (2012) 'Macrophage plasticity and polarization: In vivo veritas', *Journal of Clinical Investigation*, 122(3), pp. 787–795. doi: 10.1172/JCI59643.

Simons, K. and Sampaio, J. L. (2011) 'Membrane organization and lipid rafts', *Cold Spring Harbor Perspectives in Biology*. doi: 10.1101/cshperspect.a004697.

Singh, N. and Baby, D. (2019) 'Inflammation and cancer', *Ann Afr Med*, 18(3), pp. 121–126. doi: 10.4103/aam.aam_56_18.

Singh, R., Letai, A. and Sarosiek, K. (2020) 'BCL-2 Family Protein', *Definitions*, 20(3), pp. 175–193. doi: 10.32388/j9r853.

Skog, J. *et al.* (2008) 'Glioblastoma microvesicles transport RNA and proteins that promote tumour growth and provide diagnostic biomarkers', *Nature Cell Biology*. doi: 10.1038/ncb1800.

Skotland, T. *et al.* (2020) 'An emerging focus on lipids in extracellular vesicles', *Advanced Drug Delivery Reviews*. The Authors, 159, pp. 308–321. doi: 10.1016/j.addr.2020.03.002.

Sola, M. *et al.* (2020) 'Tau affects P53 function and cell fate during the DNA damage response', *Communications Biology*. Springer US, 3(1), pp. 1–15. doi: 10.1038/s42003-020-0975-4.

SOTELO, J. R. and PORTER, K. R. (1959) 'An electron microscope study of the rat ovum.', *The Journal of biophysical and biochemical cytology*. doi: 10.1083/jcb.5.2.327.

Statsenko, A., Inami, W. and Kawata, Y. (2017) 'Measurement of viscosity of liquids using optical tweezers', *Optics Communications*. Elsevier Ltd., 402(March), pp. 9–13. doi: 10.1016/j.optcom.2017.05.034.

van Steen, A. C. I. *et al.* (2020) 'Actin remodelling of the endothelium during transendothelial migration of leukocytes', *Atherosclerosis*. Elsevier, 315(May), pp. 102–110. doi: 10.1016/j.atherosclerosis.2020.06.004.

Streets, A. M. and Huang, Y. (2013) 'Chip in a lab: Microfluidics for next generation life science research', *Biomicrofluidics*. doi: 10.1063/1.4789751.

Subczynski, W. K. *et al.* (2017) 'High Cholesterol/Low Cholesterol: Effects in Biological Membranes: A Review', *Cell Biochemistry and Biophysics*. doi: 10.1007/s12013-017-0792-7.

Suh, S. B., Traore, M. A. and Behkam, B. (2016) 'Bacterial chemotaxis-enabled autonomous sorting of nanoparticles of comparable sizes', *Lab on a Chip*. Royal Society of Chemistry, 16(7), pp. 1254–1260. doi: 10.1039/c6lc00059b.

Suzuki, J. *et al.* (2010) 'Calcium-dependent phospholipid scrambling by TMEM16F', *Nature*. Nature Publishing Group, 468(7325), pp. 834–840. doi: 10.1038/nature09583.

Svensson, K. J. *et al.* (2013) ‘Exosome uptake depends on ERK1/2-heat shock protein 27 signaling and lipid raft-mediated endocytosis negatively regulated by caveolin-1’, *Journal of Biological Chemistry*. doi: 10.1074/jbc.M112.445403.

Szalontai, B. *et al.* (2000) ‘Membrane dynamics as seen by Fourier transform infrared spectroscopy in a cyanobacterium, Synechocystis PCC 6803 - The effects of lipid unsaturation and the protein-to-lipid ratio’, *Biochimica et Biophysica Acta - Biomembranes*, 1509(1–2), pp. 409–419. doi: 10.1016/S0005-2736(00)00323-0.

Szoke, É. *et al.* (2010) ‘Effect of lipid raft disruption on TRPV1 receptor activation of trigeminal sensory neurons and transfected cell line’, *European Journal of Pharmacology*, 628(1–3), pp. 67–74. doi: 10.1016/j.ejphar.2009.11.052.

Takeuchi, O. and Akira, S. (2010) ‘Pattern Recognition Receptors and Inflammation’, *Cell*. Elsevier Inc., 140(6), pp. 805–820. doi: 10.1016/j.cell.2010.01.022.

Tanaka, H. *et al.* (1982) ‘1α,25-Dihydroxycholecalciferol and a human myeloid leukaemia cell line (HL-60)’, *Biochemical Journal*, 204(3), pp. 713–719. doi: 10.1042/bj2040713.

Taylor, D. D. and Shah, S. (2015) ‘Methods of isolating extracellular vesicles impact down-stream analyses of their cargoes’, *Methods*. doi: 10.1016/j.ymeth.2015.02.019.

Thakur, A. *et al.* (2020) ‘Inhibition of Glioma Cells’ proliferation by doxorubicin-loaded Exosomes via microfluidics’, *International Journal of Nanomedicine*, 15, pp. 8331–8343. doi: 10.2147/IJN.S263956.

Thakur, B. K. *et al.* (2014) ‘Double-stranded DNA in exosomes: A novel biomarker in cancer detection’, *Cell Research*. doi: 10.1038/cr.2014.44.

Théry, C. *et al.* (2006) ‘Isolation and Characterization of Exosomes from Cell Culture Supernatants and Biological Fluids’, *Current Protocols in Cell Biology*. doi: 10.1002/0471143030.cb0322s30.

Théry, C. *et al.* (2018) ‘Minimal information for studies of extracellular vesicles 2018 (MISEV2018): a position statement of the International Society for Extracellular

Vesicles and update of the MISEV2014 guidelines', *Journal of Extracellular Vesicles*, 7(1). doi: 10.1080/20013078.2018.1535750.

Théry, C., Ostrowski, M. and Segura, E. (2009) 'Membrane vesicles as conveyors of immune responses', *Nature Reviews Immunology*. doi: 10.1038/nri2567.

Tian, Y. *et al.* (2014) 'A doxorubicin delivery platform using engineered natural membrane vesicle exosomes for targeted tumor therapy', *Biomaterials*. doi: 10.1016/j.biomaterials.2013.11.083.

Torr, E. E. *et al.* (2012) 'Apoptotic cell-derived ICAM-3 promotes both macrophage chemoattraction to and tethering of apoptotic cells', *Cell Death and Differentiation*. doi: 10.1038/cdd.2011.167.

Tottori, N., Hatsuzawa, T. and Nisisako, T. (2017) 'Separation of main and satellite droplets in a deterministic lateral displacement microfluidic device', *RSC Advances*. Royal Society of Chemistry, 7(56), pp. 35516–35524. doi: 10.1039/c7ra05852g.

Trajkovic, K. *et al.* (2008) 'Ceramide triggers budding of exosome vesicles into multivesicular endosomes', *Science*. doi: 10.1126/science.1153124.

Traore, M. A. and Behkam, B. (2013) 'A PEG-DA microfluidic device for chemotaxis studies', *Journal of Micromechanics and Microengineering*, 23(8). doi: 10.1088/0960-1317/23/8/085014.

Truman, L. A. *et al.* (2008) 'CX3CL 1/fractalkine is released from apoptotic lymphocytes to stimulate macrophage chemotaxis', *Blood*, 112(13), pp. 5026–5036. doi: 10.1182/blood-2008-06-162404.

Tucher, C. *et al.* (2018) 'Extracellular vesicle subtypes released from activated or apoptotic T-lymphocytes carry a specific and stimulus-dependent protein cargo', *Frontiers in Immunology*, 9(MAR), pp. 1–13. doi: 10.3389/fimmu.2018.00534.

Ulmer, C. Z. *et al.* (2021) 'A Review of Efforts to Improve Lipid Stability during Sample Preparation and Standardization Efforts to Ensure Accuracy in the Reporting of Lipid Measurements', 56(1), pp. 3–16. doi: 10.1002/lipd.12263.A.

Vader, P. *et al.* (2016) 'Extracellular vesicles for drug delivery', *Advanced Drug Delivery Reviews*. doi: 10.1016/j.addr.2016.02.006.

Valadi, H. *et al.* (2007) 'Exosome-mediated transfer of mRNAs and microRNAs is a novel mechanism of genetic exchange between cells', *Nature Cell Biology*. doi: 10.1038/ncb1596.

Vogel, A. *et al.* (2022) 'Lipid scavenging macrophages and inflammation', *Biochimica et Biophysica Acta - Molecular and Cell Biology of Lipids*. Elsevier B.V., 1867(1), p. 159066. doi: 10.1016/j.bbalip.2021.159066.

Vogel, R. *et al.* (2016) 'A standardized method to determine the concentration of extracellular vesicles using tunable resistive pulse sensing', *Journal of Extracellular Vesicles*, 5(1). doi: 10.3402/jev.v5.31242.

Vogt, C. and Vogt, K. C. (1842) 'Untersuchungen über die Entwicklungsgeschichte der Geburtshelferkröte (Alytes obstetricans)', *Jent & Gassmann*.

Vroman, H., Hendriks, R. W. and Kool, M. (2017) 'Dendritic cell subsets in asthma: Impaired Tolerance or exaggerated inflammation?', *Frontiers in Immunology*, 8(AUG), pp. 1–11. doi: 10.3389/fimmu.2017.00941.

Waldenström, A. *et al.* (2012) 'Cardiomyocyte microvesicles contain DNA/RNA and convey biological messages to target cells', *PLoS ONE*. doi: 10.1371/journal.pone.0034653.

Wan, J. (2020) 'LC3-associated phagocytosis protects against inflammation and liver fibrosis via immunoreceptor inhibitory signaling', *Science Translational Medicine*, 12(539).

Watanabe, S. *et al.* (2019) 'The role of macrophages in the resolution of inflammation', *Journal of Clinical Investigation*, 129(7), pp. 2619–2628. doi: 10.1172/JCI124615.

Webber, J. and Clayton, A. (2013) 'How pure are your vesicles?', *Journal of Extracellular Vesicles*. doi: 10.3402/jev.v2i0.19861.

Wickman, G. R. *et al.* (2013a) 'Blebs produced by actin-myosin contraction during

apoptosis release damage-associated molecular pattern proteins before secondary necrosis occurs', *Cell Death and Differentiation*. Nature Publishing Group, 20(10), pp. 1293–1305. doi: 10.1038/cdd.2013.69.

Wickman, G. R. *et al.* (2013b) 'Blebs produced by actin-myosin contraction during apoptosis release damage-associated molecular pattern proteins before secondary necrosis occurs', *Cell Death and Differentiation*. Nature Publishing Group, 20(10), pp. 1293–1305. doi: 10.1038/cdd.2013.69.

Willmott, G. R. *et al.* (2014) 'Actuation of Tunable Elastomeric Pores: Resistance Measurements and Finite Element Modelling', *Experimental Mechanics*, 54(2), pp. 153–163. doi: 10.1007/s11340-013-9795-5.

Willms, E. *et al.* (2018) 'Extracellular vesicle heterogeneity: Subpopulations, isolation techniques, and diverse functions in cancer progression', *Frontiers in Immunology*. Frontiers Media S.A., 9(APR). doi: 10.3389/fimmu.2018.00738.

Windvoel, T. *et al.* (2010) 'Surface analysis of Polydimethylsiloxane fouled with bovine serum albumin', *World Academy of Science, Engineering and Technology*, 61, pp. 354–356.

Wolbers, F. *et al.* (2004) 'Apoptotic cell death kinetics in vitro depend on the cell types and the inducers used', *Apoptosis*, 9(3), pp. 385–392. doi: 10.1023/B:APPT.0000025816.16399.7a.

Wolf, P. (1967) 'The nature and significance of platelet products in human plasma.', *British journal of haematology*. doi: 10.1111/j.1365-2141.1967.tb08741.x.

Wollert, T. and Hurley, J. H. (2010) 'Molecular mechanism of multivesicular body biogenesis by ESCRT complexes', *Nature*. doi: 10.1038/nature08849.

Xie, D. *et al.* (2021) 'Ultraviolet light-emitting diode irradiation induces reactive oxygen species production and mitochondrial membrane potential reduction in HL-60 cells', *Journal of International Medical Research*, 49(5), pp. 0–9. doi: 10.1177/03000605211016623.

Xu, X., Lai, Y. and Hua, Z. C. (2019) 'Apoptosis and apoptotic body: Disease message and therapeutic target potentials', *Bioscience Reports*, 39(1), pp. 1–17. doi: 10.1042/BSR20180992.

Xue, J. *et al.* (2014) *Supplemental Information Transcriptome-Based Network Analysis Reveals a Spectrum Model of Human Macrophage Activation*, *Immunity*.

Xue, M. and Jackson, C. J. (2015) 'Extracellular Matrix Reorganization During Wound Healing and Its Impact on Abnormal Scarring', *Advances in Wound Care*, 4(3), pp. 119–136. doi: 10.1089/wound.2013.0485.

Yáñez-Mó, M. *et al.* (2015) 'Biological properties of extracellular vesicles and their physiological functions', *Journal of Extracellular Vesicles*. doi: 10.3402/jev.v4.27066.

Yang, J. *et al.* (2014) 'Monocyte and macrophage differentiation: Circulation inflammatory monocyte as biomarker for inflammatory diseases', *Biomarker Research*, 2(1), pp. 1–9. doi: 10.1186/2050-7771-2-1.

Yang, P. L. (2016) 'Metabolomics and Lipidomics: Yet More Ways Your Health is Influenced by Fat', in *Viral Pathogenesis: From Basics to Systems Biology: Third Edition*. doi: 10.1016/B978-0-12-800964-2.00014-8.

Yang, Y. *et al.* (2015) 'Programmed cell death and its role in inflammation', *Military Medical Research*. ???, 2(1), pp. 1–12. doi: 10.1186/s40779-015-0039-0.

Yi, F. H. *et al.* (2000) 'In vitro induction of neuronal apoptosis by anti-Fas antibody-containing sera from amyotrophic lateral sclerosis patients', *Journal of Neuroimmunology*, 109(2), pp. 211–220. doi: 10.1016/S0165-5728(00)00288-5.

Yin, C. *et al.* (2016) 'Rab17 mediates differential antigen sorting following efferocytosis and phagocytosis', *Cell Death and Disease*. Nature Publishing Group, 7(12), pp. 1–12. doi: 10.1038/cddis.2016.431.

Yin, C. and Heit, B. (2021) 'Cellular Responses to the Efferocytosis of Apoptotic Cells', *Frontiers in Immunology*, 12(April), pp. 1–12. doi: 10.3389/fimmu.2021.631714.

Yuyama, K. *et al.* (2012) 'Sphingolipid-modulated exosome secretion promotes

clearance of amyloid-β by microglia', *Journal of Biological Chemistry*. Â© 2012 ASBMB. Currently published by Elsevier Inc; originally published by American Society for Biochemistry and Molecular Biology., 287(14), pp. 10977–10989. doi: 10.1074/jbc.M111.324616.

Zhang, J. *et al.* (2016) 'Fundamentals and applications of inertial microfluidics: A review', *Lab on a Chip*. Royal Society of Chemistry, 16(1), pp. 10–34. doi: 10.1039/c5lc01159k.

Zhang, J. and An, J. (2007) 'Cytokines, Inflammation, and Pain', *International Anesthesiology Clinics*, 45(2), pp. 27–37. doi: 10.1097/AIA.0b013e318034194e.

Zhukovsky, M. A. *et al.* (2019) 'Phosphatidic acid in membrane rearrangements', *FEBS Letters*, 593(17), pp. 2428–2451. doi: 10.1002/1873-3468.13563.